CWP-434
September 2002

Selective-correlation Velocity Analysis

Valmore Celis

— Master's Thesis —
Geophysics

Center for Wave Phenomena
Colorado School of Mines
Golden, Colorado 80401
303 273-3557

ABSTRACT

Resolution in velocity spectra depends primarily on cable length, reflector depth, stacking velocity, and dominant frequency of the data. Velocity spectra often fail to separate interfering events, particularly those at late times and with high velocities. The need for increased resolution in velocity spectra is clear when one wishes to distinguish two neighboring primary events from reflectors with conflicting dips, or to identify weak primaries in the presence of nearby multiples.

Velocity spectrum methods transform data from the offset and two-way traveltime domain to the stacking velocity and zero-offset, two-way traveltime domain. This transformation can be achieved using any of several coherence measures based on the zero-lag crosscorrelation of the traces; the more commonly used ones are semblance coefficient, unnormalized crosscorrelation sum, and statistically normalized crosscorrelation sum. All these measures involve crosscorrelations between traces in a collection such as a common-midpoint (CMP) gather or common-image gather (CIG). One might think that, for a given number of data traces, the sum of all possible crosscorrelations should be a more reliable measure than the sum of only a subset of the crosscorrelations. I show, however, that use of selected subsets of crosscorrelations can preserve the reliability while improving the resolution of velocity analysis. Such subsets are formed by including in the summation only those crosscorrelations for whose pair of traces the relative differential moveout of reflections exceeds some threshold established *a priori,* and discarding those crosscorrelations for which the associated differential moveout is relatively small. I have called this process *selective-correlation* velocity analysis.

Here, for a variety of synthetic CMP gathers, I compare the performances in velocity analyses of selective-correlation sum and conventional crosscorrelation-sum measures. These comparisons show that the use of selective-correlation sum considerably enhances the resolving power of velocity spectra over that of conventional crosscorrelation sum in the presence of statics distortions and random noise, at no sacrifice in the quality of results. For closely interfering reflections under these perturbing conditions, selective-correlation velocity analysis retains its greater resolving power. Moreover, this improvement in performance is achieved at a computational cost that is comparable to that for conventional velocity analysis.

Beyond the implementation of the selective-correlation method itself, I also discuss issues related to velocity analysis. I give estimates of the uncertainties in the velocity as a function of the errors in the reflection traveltimes. These traveltime errors can be caused, for instance, by static distortions and random noise. I derive approximate expressions for the standard deviation in velocity estimates, and the bias (difference between the velocity estimate using the data with errors and the zero-error velocity) of those estimates. These

expressions allow us to estimate the relative contribution of each trace pair to the uncertainty in the velocity estimate. They also support the use of selective-correlation sum in velocity analysis since these estimates of standard deviation and bias for velocity decrease with increasing differential moveout.

A cross-section of the velocity spectra for a fixed normal-incidence time, equal to that of a reflection of interest, is what I have called a *coherence curve*. These curves reach local maxima, or peaks, for velocity values in which the coherence along a hyperbola is relatively large. The coherence curves also allow us to compare the behavior of the different coherence measures in the presence of random noise, static distortions, and interfering events. Here, for interfering events, I study the bias in the positions of peaks of the coherence curves as a function of the breadth of the peaks of the curves as it relates to the difference between primary and multiple velocities.

Finally, through applications to field marine and land CMP gathers, I demonstrate that selective-correlation sum, which I have implemented in the Seismic Un*x (SU) data processing system in both normalized and unnormalized forms, not only increases stacking-velocity resolution, but it also can reduce uncertainty in the velocity picking by uncovering primary peaks in the presence of strong multiples.

TABLE OF CONTENTS

ACKNOWLEDGMENTS

The work presented in this thesis could not have been realized without the help of several individuals. I would like to formally acknowledge them.

First, I would like to thank my thesis advisor, Dr. Ken Larner, for his great energy and motivation. He was always pushing things forward and getting new insights into the problem. He made of my work an enjoyable experience adding to it lots of knowledge. I would also like to acknowledge my other committee members for their support: Dr. Thomas Boyd and Dr. John Scales. I also thank PDVSA-Intevep for its funding support of my studies at Colorado School of Mines.

Special thanks to the following people: Dr. Terry Young and his wife Nadine Young for their kindness and support in difficult times. To all my fellow CWP students, especially Kasper Van Wijk, who helped me with LATEX and Matlab, and Reynaldo Cardona for his comments on the manuscript.

Finally, I would like to thank my wife, Minarca, for the patience and support she has shown me during my graduate studies.

Chapter 1

INTRODUCTION

1.1 Background

Estimation of seismic velocities in the subsurface is one of the important tasks in exploration seismology. Velocity is the connection between the time domain, where recorded seismic data reside, and depth domain, where the ultimate goals of explorationists are pursued. Much of the information about the velocity distribution in the subsurface is derived from stacking velocities obtained from common-midpoint (CMP) gathers of traces recorded in surface reflection seismology. These stacking velocities are often used for estimating root-mean-square (rms) velocities, which may be used to estimate interval velocities. Each type of velocity has its importance in differents steps of processing; for instance, stacking velocities are used to perform CMP stacking, rms velocities can be used for time migration, and interval velocities for depth migration and depth conversion. For example, the more accurate the estimate of stacking velocity, the more effective will be processing that aligns primary reflections and stacks them, while at the same time attenuating undesirable events such as multiples.

Velocity estimation requires that reflection data be recorded at nonzero offsets between sources and receivers. Recorded traces obtained at these separations produce a variation in reflection time with offset, for a given reflection event, known as *normal moveout* (NMO). For most practical applications, NMO for a single event can be approximately described by a hyperbola that depends on the two-way zero-offset traveltime, the distance between source and receiver positions, and the velocity distribution of the medium above the reflecting interface. Velocity analysis takes advantage of this hyperbolic moveout characteristic to obtain from surface seismic data the stacking-velocity variation with reflector depth or zero-offset reflection time. The goal of velocity analysis is to obtain interpreted velocity values that correspond to the best coherency of the signal along hyperbolic trajectories over the spreadlength of the CMP gather. Velocity analysis can be divided into two stages: (1) computation of velocity spectra, which is carried out through some statistical coherence measure, and (2) velocity picking, where interpretation comes into play. Our interest here, however, is centered on the first stage of velocity analysis, the spectra computation.

The conventional approach to estimating stacking velocities is to pick maxima of the velocity spectra (Taner and Koehler, 1970). For a given CMP gather, the spectrum at a given time is computed by fixing a zero-offset reference time $t_{0,i}$ and then sweeping over a predetermined range of trial velocities $(v_1, v_2, ..., v_m)$ usually at a regular velocity interval

Δv. Each pair of $t_{0,i}$ and v_n will produce a particular hyperbolic moveout pattern. Then, the velocity spectrum, for fixed time $t_{0,i}$, is obtained by a correlation process along those hyperbolas. A peak in the spectrum indicates the velocity corresponding to the hyperbola that best fits the data at a given $t_{0,i}$. This procedure is repeated for different uniformly incremented zero-offset times $(t_{0,1}, t_{0,2}, \ldots)$ until the end of the seismic record or a specified maximum time is reached. The computed velocity spectra are displayed as a function of zero-offset traveltime and trial velocity. Then, the picking process begins. As mentioned above, here the focus is on the computation of velocity spectra.

Several good properties of the stacking velocity spectra can be mentioned: (1) they provide maximum-likelihood estimates for stacking velocity of well-separated reflections in the presence of additive uncorrelated noise with Gaussian statistics (Kirling et al., 1984; Biondi and Kostov, 1989); (2) they are robust with respect to deviations of the noise from being Gaussian; (3) implementation is relatively simple and computationally much less intensive than, for example, eigenvalue methods (e.g., Biondi and Kostov, 1989; Key et al., 1987); and (4) when two or more events have close arrival times at zero offset but their corresponding moveouts are sufficiently different, conventional velocity spectra can still produce good estimates. When, however, a pair of events are too close to one another and have little moveout difference relative to the dominant period in the data, the estimates can be biased and, even worse, the spectra may show only one maximum for a given $t_{0,i}$.

Resolution in velocity spectra depends primarily on cable length, depth of the reflecting interface, magnitude of the overburden velocity (more specifically, stacking velocity), and the dominant frequency of the data. Stacking velocity spectra often fail to separate interfering events at late times and high velocities, as well as for relatively shallow events that are dominated by low frequencies and have relatively small moveout difference. The need for higher-resolution velocity spectra is clear when one wishes to distinguish two neighboring primary events coming from reflectors with conflicting dips, or to identify weak primaries in the presence of strong multiples.

De Vries and Berkhout (1984) addressed the resolution problem using an alternative tool for velocity analysis based on minimum entropy. This approach analyzed the spectral content of data as a function of moveout parameters such as stacking velocity for a CMP gather and migration velocity for a common-reflection-point (CRP) gather. To obtain an estimate of the stacking velocity using minimum-entropy velocity analysis, one must specify a window around the zero-offset time of a targeted reflection. This method can be applied in either the space-frequency domain or the space-time domain; higher velocity resolution is obtained in the space-frequency domain, whereas the approach is computationally more attractive in the space-time domain.

Gelchinsky et al. (1985) considered algorithms of phase and group correlation based on the concept of analytic signal (Taner et al, 1979). These correlation algorithms require the construction of functionals that must be analyzed in order to estimate the parameters (e.g., velocity) of the detected signal. Such analysis is performed using a system of inequalities that depend on parameters whose determination and influence on velocity analysis is unclear. Another resolution-enhancement method for seismic velocity analysis, based on

the eigenstructure decomposition of the covariance matrix of the data, was developed by Biondi and Kostov (1989). Their method can be powerful in resolving closely interfering reflections; unlike conventional velocity spectra, however, the number of events in conflict must be estimated *a priori* at each time level, which is impractical for field data. Furthermore, the influence of noise in data on their method is not well understood, and the method is computationally more costly than other commonly-used velocity-analysis procedures.

A convenient alternative approach for increasing resolution in conventional velocity analysis is through use of optimum stacking weights. Schoenberger (1996) developed a method for multiple suppression, called *optimum weighted stack*, that requires knowledge of the residual moveout of a targeted multiple and its frequency content. The weights produced in Schoenberger's method are used to improve velocity resolution by applying them directly to the traces in the CMP gather prior to performing conventional velocity analysis. This approach shares some of the philosophy that underlies the selective-correlation method studied here.

Several other authors have dealt with the problem of optimizing the velocity-estimation process or improving the resolution of stacking velocity analysis (e.g., Kirling et al., 1984; Toldi, 1989). All these methods constitute a suite of approaches with advantages and limitations: where one method fails, another may succeed, and vice versa. As a result, tradeoffs have to be made, for instance between resolution and robustness.

Here, I present a method for increasing the resolution of stacking velocity analysis that allows the analyst to distinguish more clearly between primary and multiple reflections, or between neighboring primary events. This approach preserves the good properties of conventional semblance mentioned above, while entailing only a relatively minor modification (at comparable computation effort) of the conventional velocity-spectra calculation.

1.2 Approach

In the approach developed and evaluated here, I use a *selective-correlation sum* that excludes from the spectrum computation crosscorrelations of pairs of traces based on differential moveout of reflections. Neidell and Taner (1971) used the sum of crosscorrelations of traces in computing velocity spectra. In their approach, they sum all possible crosscorrelations among the traces of a CMP gather along hyperbolic trajectories governed by a range of trial velocities, giving the same weight to each contributing correlation independent of the differential moveout between crosscorrelated traces. If the differential moveout is small, however, as occurs for short-offset traces, the traces will be approximately in phase for a relatively wide range of velocities, giving a broad semblance response as a function of trial velocity (Sherwood and Poe, 1972). In contrast, crosscorrelation of a pair of traces with large differential moveout offers more resolving power for the velocity spectra than does that of traces with small differential moveout. Hence, the idea behind the approach in this thesis is to allow into the summation only those crosscorrelations whose pair of traces have a relatively large differential moveout. This discrimination process allows one to increase

the resolution of the velocity analysis, preserving the character and features of conventional semblance at comparable computational cost.

The methodology for this work is based on the sum of crosscorrelations described by Neidell and Taner (1971). The new feature of the present approach is that, instead of summing over the set of all possible crosscorrelations, the summation is performed over selected subsets of crosscorrelations based on moveout in the data traces in a CMP or CRP gather. In order to do the selection, I first assign a numerical *significance* value to each pair of crosscorrelated traces using a parabolic trajectory as an approximation of differential moveout. These significance values are related to the judged importance of the contribution of each crosscorrelation to the resolution in the velocity spectrum, which depends on the normal moveout of the events. For instance, if the offsets of two traces are close to one another or their offsets are relatively close to zero, the differential moveout will be small and the contribution of their associated crosscorrelations to resolution will be represented by a smaller significance value than that of those trace pairs for which the differential moveout is larger. Each possible crosscorrelation pair is assigned a significance value that is normalized to have values ranging from zero to one. For identical traces, as in autocorrelations, the differential moveout is zero, so the significance value is zero. A value of unity is associated with the maximum differential moveout possible, produced by the crosscorrelation between traces recorded at the shortest and longest offsets.

I then specify a threshold for these values; all crosscorrelations with significance values below this threshold are discarded, and the rest of crosscorrelations, with values above the threshold are included in the spectra computation. Therefore, I sum only crosscorrelations whose contribution have comparatively large associated significance values, thus helping better constrain the estimate of stacking velocity.

Based on the significance values, one might choose to include in the summation only a relatively small percentage (e.g., 30%) of all possible crosscorrelations, but those with the most resolving power. This process should improve the velocity resolution of the spectra-computation process and thus possibly reduce uncertainty in the velocity picking.

One might think that a disadvantage of the new approach with respect to conventional ones is that with fewer crosscorrelations included in the summation the effectiveness in attenuating random noise and dealing with statics distortions will be somewhat diminished. Tests on synthetic data, however, show that accuracy of selective-correlation velocity analysis is comparable to that achieved by conventional crosscorrelation sum in the presence of statics distortions and random noise; specifically, the peak of the spectra for both methods is governed strongly by crosscorrelations for pairs of traces with relatively large differential moveout, the very ones we include in the selective-correlation approach. Thus if the velocity peak is biased, due to either statics or random noise, the bias will be about the same in both velocity estimation methods, even where reflections are closely interfering.

Using synthetic CMP gathers, I compare the performance of selective correlation sum, both unnormalized and normalized, with those of unnormalized crosscorrelation sum and conventional semblance, as well as with conventional velocity analysis applied to traces with

weights designed for optimum suppression of multiples in stacking. This comparative study uses synthetic data in the presence of correlated and uncorrelated noise, statics distortions, and other factors that influence the accuracy and resolution of velocity analysis such as spreadlength, relative strength of reflections, and bandwidth of data. I also show that reducing the fold of a CMP gather (e.g., by discarding every other trace), in order to reduce the number of crosscorrelations in the spectra computation, by no means is equivalent to selective-correlation sum.

Applications to field data, both marine and land, exemplify features of the selective-correlation sum method seen in the synthetic data examples. Additionally, I present analyses aimed at understanding the performance of the selective-correlation approach exhibited in the results of applications to synthetic data.

1.3 Thesis content

Chapter 2 is devoted to understanding the fundamentals of velocity analysis based on selective-correlation sum and how this approach can improve velocity resolution. There, I review the more commonly used coherence measures for spectra computation and their various relationships. Also, I discuss the rationale and characteristics of a parabolic approximation of differential moveout used to assign numerical significance values to each crosscorrelation involved in the spectra calculation; I then use these values in a criterion for discarding crosscorrelations. In addition, I describe the use of optimum stacking weights in velocity estimation as an alternative method for improving velocity resolution. Although the use of optimum stacking weights differs in some key respects from the selective-correlation sum, these two methods have the most similar philosophy and performance of the various approaches for enhancing resolution. Here, I also show an implementation of the selective-correlation approach such that its computation cost is comparable to that of the conventional approach.

In Chapter 3, I use synthetic CMP gathers to study factors that can influence the estimation of stacking velocity: spreadlength, bandwidth of data, random- and coherent-noise contamination, statics distortions, and relative strength of interfering reflections. For each of these factors, I present comparisons between conventional velocity analysis and selective-correlation sum.

In Chapter 4, I discuss issues in velocity analysis exemplified in the tests with synthetic data. Here, I study how traveltime errors propagate to the velocity estimates using approximate expressions for the variance and bias of the velocity as a function of errors in data. These expressions have implications for the expected performance of the conventional and selective-correlation velocity analysis. I also analyze the bias of the locations of the peaks in the coherence curves as a function of the breadth of the peaks of the curves as it relates to the difference between primary and multiple velocities. These analyses use superposition of Gaussians to model coherence curves. Although, this modeling involves the approximations of superposition and use of Gaussian shapes, it accounts well for features present in

coherence curves obtained using selective-correlation sum.

The field-data examples in Chapter 5 show the enhanced resolution and robustness of the selective-correlation-sum method. Finally, in Chapter 6, I summarize highlights of the work and also offer lessons learned in stacking velocity estimation. In addition, I give my thoughts about possible extensions of the work presented here.

Chapter 2

SELECTIVE-CORRELATION VELOCITY ANALYSIS

Various choices of coherency measure can be used in computing velocity spectra. Most of these coherence measures are based on zero-lag crosscorrelations between the traces along hyperbolic moveout trajectories in CMP gathers (Neidell and Taner, 1971). The more commonly used are semblance coefficient, unnormalized and normalized crosscorrelation sum, and stacked amplitude. In this thesis, I take advantage of the structure of the crosscorrelation-sum coherence measure, both unnormalized and statistically normalized, to select crosscorrelations whose pair of traces have a differential moveout that exceeds a minimum pre-established threshold value. These crosscorrelations, with relatively large differential moveout, are included in the sum while the rest, with associated differential moveout less than the specified threshold, are excluded. The approach followed here, however, does not use the exact differential moveout as a selection criterion; instead, for convenience I use a parabolic approximation of differential moveout in the selection.

First, in this chapter, I give a review of the coherence measures more commonly used in velocity estimation, and how they relate to one another. I also discuss the form in which these coherence measures can be written to facilitate the implementation of the selective-correlation sum method. Second, I derive the parabolic approximation of differential moveout used in the crosscorrelation-discarding process, and discuss its characteristics. Finally, I give a formal definition of selective-correlation sum and show examples of applying this method to synthetic CMP gathers. I also compare these results against those obtained by applying several other coherence measures to the same synthetic data. In addition, I discuss and compare the velocity-resolution enhancement of the selective-correlation approach with that of a method based on use of optimum trace weights.

2.1 Coherence measures

Throughout this entire section, I will follow the notation given in Yilmaz (2001). The simplest form of coherence measure is the *stacked amplitude* (Garotta and Michon, 1967), consisting of the sum of the trace amplitudes along a certain moveout path. The stacked amplitude (SA) at two-way zero-offset travel time t_0 is defined as

$$SA(v_{trial}, t_0) = \sum_{j=1}^{M} f_{j,t(j)}, \tag{2.1.1}$$

where M is the number of traces in the CMP gather, $f_{j,t(j)}$ is the amplitude on the jth trace along a reflection-time trajectory $t(j)$. In stacking-velocity computation, this trajectory $t(j)$ is the two-way traveltime along a hyperbola governed by a trial velocity v_{trial} :

$$t(j) = \sqrt{t_0^2 + \frac{x_j^2}{v_{trial}^2}}, \tag{2.1.2}$$

where x_j is the offset from the source to detector j.

The simplicity of the stacked amplitude makes it computationally inexpensive. For this reason, Sherwood and Poe (1972) used it as the basis of their approach for analyzing constant-velocity stacks (CVS) in picking stacking velocities.

The *unnormalized crosscorrelation sum CC* (Neidell and Taner, 1971) is the sum of all crosscorrelations between any two traces in a CMP gather within a time window. It is given, as a function of trial velocity v_{trial} and two-way zero-offset travel time t_0, by

$$CC(v_{trial}, t_0) = \sum_{j=2}^{M} \sum_{k=1}^{j-1} \sum_{w} f_{j,t(j)}\ f_{k,t(k)}, \tag{2.1.3}$$

where the window w, for the lth trace, is determined by the expression

$$w(l) = t(l) + i\Delta t, \qquad i = -N/2, \ldots, 0, \ldots, N/2, \tag{2.1.4}$$

where the length of the time window is $N+1$ samples. Here, $t(l)$ is given by the hyperbola (2.1.2), Δt is the data sampling interval, and i takes integer values. The window $w(l)$ is symmetrically positioned about the reflection-time $t(l)$ on the lth trace. Moreover, the boundaries of the time window (2.1.4) are parallel to the hyperbolic trajectory (2.1.2) over the entire spreadlength. This is not the case for all algorithms in practice, but the difference for our purposes is immaterial.

The hyperbolic trajectory (2.1.2) and time window (2.1.4), defined for the unnormalized crosscorrelation sum, will also be used for all subsequent coherence measures. Henceforth, the time window (2.1.4) will be referred simply as w.

Reordering the sums in expression (2.1.3), we can write it as

$$CC(v_{trial}, t_0) = \sum_{w} \sum_{j=2}^{M} \sum_{k=1}^{j-1} f_{j,t(j)}\ f_{k,t(k)}. \tag{2.1.5}$$

Equation (2.1.5) can be written as an energy difference by using the identity

$$\left\{ \sum_{j=1}^{M} f_{j,t(j)} \right\}^2 \equiv \sum_{j=1}^{M} f_{j,t(j)}^2 + 2 \sum_{j=2}^{M} \sum_{k=1}^{j-1} f_{j,t(j)}\ f_{k,t(k)}.$$

Solving for the double summation factor,

$$\sum_{j=2}^{M}\sum_{k=1}^{j-1} f_{j,t(j)}\ f_{k,t(k)} = \frac{1}{2}\left\{\left\{\sum_{j=1}^{M} f_{j,t(j)}\right\}^2 - \sum_{j=1}^{M} f_{j,t(j)}^2\right\},$$

and inserting this into expression (2.1.5), gives

$$CC(v_{trial}, t_0) = \frac{1}{2}\sum_{w}\left\{\left\{\sum_{j=1}^{M} f_{j,t(j)}\right\}^2 - \sum_{j=1}^{M} f_{j,t(j)}^2\right\}. \tag{2.1.6}$$

Equation (2.1.6) represents the unnormalized crosscorrelation sum as half the difference between the output stacked-trace energy and the input energy computed over the window w. This is an efficient way to implement velocity analysis because of the relatively small number of operations involved (order MN, where N is the number of samples in the time window w for each set of values of t_0 and v_{trial}). Although, this form of an energy difference looks computationally attractive, is not amenable to selection of individual crosscorrelations, as is allowed by expression (2.1.5). This latter expression, on the other hand, apparently needs order M^2N operations. However, we can achieve the smaller number of multiplications by writing the unnormalized crosscorrelation sum (2.1.5) as

$$CC(v_{trial}, t_0) = \sum_{w}\left\{\sum_{j=2}^{M} f_{j,t(j)}\left\{\sum_{k=1}^{j-1} f_{k,t(k)}\right\}\right\}. \tag{2.1.7}$$

The inner bracket becomes just a constant after the summation, leaving only order M multiplications times N, the number of samples inside the window w.

If all $f_{j,t(j)}$ were equal, from either equation (2.1.6) or (2.1.7) the unnormalized crosscorrelation sum would be equal to

$$N_c = \frac{M(M-1)}{2} \tag{2.1.8}$$

times the common trace energy inside the window w. Here, N_c is the number of all possible crosscorrelations involved in the calculation.

The normalized version of equation (2.1.5), known as *normalized crosscorrelation sum* NCC (Neidell and Taner, 1971), is obtained dividing expression (2.1.5) by the geometric mean of the energy in the two channels involved in any crosscorrelation over the window w, and introducing a constant to produce a maximum amplitude equal to unity. The normalized crosscorrelation sum is given by

$$NCC(v_{trial}, t_0) = \frac{2}{M(M-1)} \sum_w \sum_{j=2}^{M} \sum_{k=1}^{j-1} \frac{f_{j,t(j)}\ f_{k,t(k)}}{\sqrt{\sum_w f_{j,t(j)}^2 \sum_w f_{k,t(k)}^2}}. \tag{2.1.9}$$

In expression (2.1.9), the terms $\sum_w f_{j,t(j)}^2$ and $\sum_w f_{k,t(k)}^2$ represent the trace energy, for the jth and kth traces inside the window w centered at reflection times $t(j)$ and $t(k)$, respectively.

To normalize expression (2.1.6), we divide it by the average energy of the traces inside the window w, getting

$$\frac{\frac{1}{2} \sum_w \left\{ \left\{ \sum_{j=1}^{M} f_{j,t(j)} \right\}^2 - \sum_{j=1}^{M} f_{j,t(j)}^2 \right\}}{\frac{1}{M} \sum_w \sum_{j=1}^{M} f_{j,t(j)}^2}.$$

Introducing a constant to produce maximum amplitude equal to one,

$$\frac{\frac{2}{M(M-1)} \frac{1}{2} \sum_w \left\{ \left\{ \sum_{j=1}^{M} f_{j,t(j)} \right\}^2 - \sum_{j=1}^{M} f_{j,t(j)}^2 \right\}}{\frac{1}{M} \sum_w \sum_{j=1}^{M} f_{j,t(j)}^2},$$

and simplifying this expression, we get

$$ECC(v_{trial}, t_0) = \frac{\sum_w \left\{ \left\{ \sum_{j=1}^{M} f_{j,t(j)} \right\}^2 - \sum_{j=1}^{M} f_{j,t(j)}^2 \right\}}{(M-1) \sum_w \sum_{j=1}^{M} f_{j,t(j)}^2}. \tag{2.1.10}$$

Expression (2.1.10), known as the *energy-normalized crosscorrelation sum* (ECC), again looks computationally attractive with only MN operations. Nevertheless, as in the unnormalized crosscorrelation sum (2.1.5), we can achieve the same order of multiplications by writing the normalized crosscorrelation sum (2.1.9) as

$$NCC(v_{trial}, t_0) = \frac{2}{M(M-1)} \sum_w \left\{ \sum_{j=2}^{M} \frac{f_{j,t(j)}}{\sqrt{\sum_w f_{j,t(j)}^2}} \left\{ \sum_{k=1}^{j-1} \frac{f_{k,t(k)}}{\sqrt{\sum_w f_{k,t(k)}^2}} \right\} \right\}. \tag{2.1.11}$$

Expressions (2.1.7) and (2.1.11) favor our goal of selecting crosscorrelations, something that is not possible when CC and NCC are written in the forms (2.1.6) and (2.1.10), with a computational effort that is similar to that achieved for these two latter expressions.

Finally, a widely used coherency measure is the normalized output-to-input energy ratio (Neidell and Taner, 1971), or *semblance coefficient* SC, given by

$$SC(v_{trial}, t_0) = \frac{\sum_w \left\{ \sum_{j=1}^{M} f_{j,t(j)} \right\}^2}{M \sum_w \sum_{j=1}^{M} f_{j,t(j)}^2}. \tag{2.1.12}$$

The semblance coefficient is related to the normalized crosscorrelation, in its energy-normalized form (2.1.10), by

$$ECC = \frac{M \times SC - 1}{M - 1}. \tag{2.1.13}$$

This expression shows that the semblance coefficient SC and the energy-normalized cross-correlation sum ECC are simply biased versions of one another.

Several observations can be made about these coherence measures. First, they all are based on the implicit assumption that amplitude does not change with offset. Sarkar et al. (2000) have shown that the coherence measure can degrade in the presence of large amplitude variations, particularly where the wavelet polarity changes with offset; however, the simplicity of this model of constant amplitude with offset makes these coherence measures robust against noise. Second, selective-correlation velocity analysis is based on expressions (2.1.3) and (2.1.9) because it allows us to select the individual crosscorrelations that we wish to include in the sum. From the energy-difference based expressions (2.1.6) and (2.1.10), in contrast, the selection of crosscorrelations is not possible. Finally, below I compare the performance of selective-correlation sum to that of several coherence measures, especially with that of semblance coefficient. According to resolution tests made by Neidell and Taner (1971) with noise-free synthetic data, the semblance performed better than the crosscorrelation sum. It should be pointed out, however, that since the semblance coefficient is proportional to the energy-normalized crosscorrelation sum [expression (2.1.13)], the resolution for both coherence measures cannot be significantly different. In fact, the only difference between expressions (2.1.10) and (2.1.12) is the term $\sum_{j=1}^{M} f_{j,t(j)}^2$ in the numerator of energy-normalized crosscorrelation sum. Thus, the semblance coefficient includes autocorrelations, whose contribution to the spectrum is nothing but a DC term, which gives no information about velocity.

Now, I proceed to describe the method of selecting the crosscorrelations that are included in the summation.

2.2 Parabolic approximation

To select crosscorrelations based on the differential moveout of events, we first assign a numerical significance value to each pair of traces to be crosscorrelated. As explained in the previous section, the total number of crosscorrelations in a CMP gather with M traces, for each trial velocity v_i and time t_0, is $M(M-1)/2$. We will assign a significance value to each of these crosscorrelations. The procedure should assign values close to zero for pairs of traces with relatively small differential moveout, and large values for those with larger differential moveout. Such values need only characterize moveout sufficiently well for our purpose of selection of crosscorrelations.

For several reasons, the selection process uses a parabolic approximation to the hyperbolic differential moveout rather than the hyperbolic expression itself. First, at best any

choice of hyperbolic moveout can be exact only if moveout is exactly hyperbolic (which it never is). Moreover, since the hyperbolic moveout varies with the zero-offset time and stacking velocity, any parameters that specify hyperbolic moveout can apply to just one event and would not hold for the others. The parabolic approximation, in contrast, while not exactly representative of the moveout, describes a trend in moveout from short to long offset that is unchanged for all zero-offset times and quadratic parameters. Furthermore, the parabolic description of differential moveout is simpler than the hyperbolic one — no square roots need be computed.

Starting with the normal moveout equation,

$$t_j^2 = t_0^2 + \frac{x_j^2}{v^2}, \tag{2.2.14}$$

where t_j is the two-way arrival time associated with receiver j, t_0 is two-way normal-incidence time, x_j is offset from source to receiver j, and v is the stacking velocity. This expression can be also written as

$$t_j = t_0 \left(1 + \frac{x_j^2}{v^2 t_0^2}\right)^{1/2}. \tag{2.2.15}$$

Then, for small offset, approximation using a truncated Taylor series of first order gives

$$t_j \approx t_0 \left(1 + \frac{x_j^2}{2v^2 t_0^2}\right) = t_0 + \frac{x_j^2}{2v^2 t_0}, \tag{2.2.16}$$

which is a parabola in x_j. For the jth and kth traces, with $j \geq k$, the parabolic approximation for differential moveout, Δt_{jk}, is

$$\Delta t_{jk} = t_j - t_k \approx t_0 + \frac{x_j^2}{2v^2 t_0} - \left(t_0 + \frac{x_k^2}{2v^2 t_0}\right),$$

or

$$\Delta t_{jk} \approx \frac{x_j^2 - x_k^2}{2v^2 t_0}. \tag{2.2.17}$$

Approximation (2.2.17) for differential moveout is zero when $j = k$ and reaches its maximum when the offset between traces j and k is maximum, that is, when x_k is the shortest offset x_0, and x_j is the maximum offset $x_{\max}$. Since we are interested in a set of relative values to compare against a predetermined threshold, let us normalize these values over the range zero to one. To do so, we divide expression (2.2.17) by

$$\frac{(x_{\max}^2 - x_0^2)}{2v^2 t_0},$$

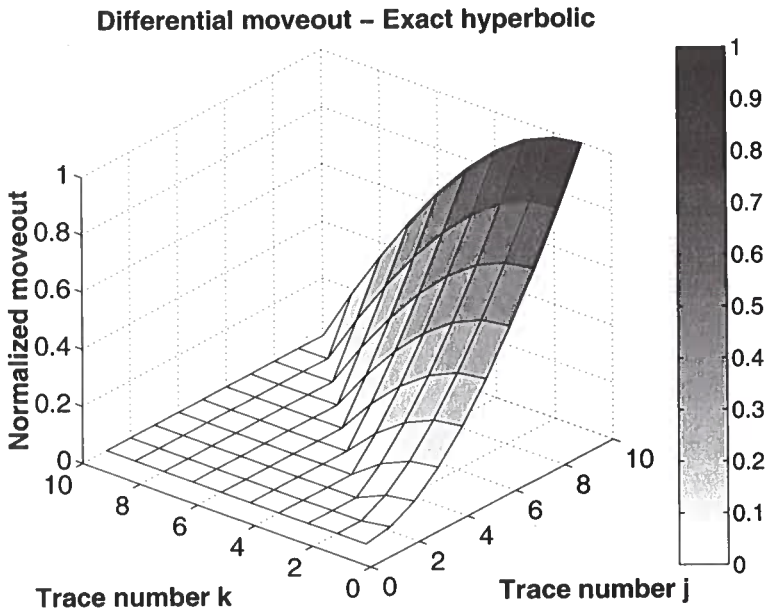

FIG. 2.1. Normalized values of the exact hyperbolic differential moveout for a hypothetical reflection in a CMP gather.

giving

$$S_{jk} \equiv \frac{x_j^2 - x_k^2}{x_{\max}^2 - x_0^2}. \tag{2.2.18}$$

The quantity S_{jk}, which ranges from zero to one, is proportional to the approximated differential moveout. Let us define this dimensionless quantity, for traces j and k, as the *significance value.*

Expression (2.2.18) is independent of velocity and normal incidence time, a significant advantage over the expression we would have obtained if we had computed moveout from the hyperbolic equation. It also characterizes sufficiently well, for the purpose of discarding crosscorrelations, the relative moveout of reflections, between any pair of traces in a CMP gather.

We can use simple numerical calculation to compare the exact differential moveout and that approximated by expression (2.2.18). Consider the moveout for reflection from a single horizontal reflector below a homogeneous layer with velocity 2 km/s and layer thickness 1 km. The modeled acquisition parameters are: cable length 2250 m, ten receivers, and distance between receivers 250 m. Figure 2.1 shows the exact differential moveout of the reflection, for a normalized range zero to one, as a function of the two trace indices j and k. The horizontal plane of the figure depicts all possible two-trace combinations. Since, zero-lag crosscorrelations (along the moveout trajectory) between traces j and k, and between k and j are the same, only crosscorrelations with $j > k$ considered. The vertical dimension shows the normalized values of differential moveout. A similar plot for

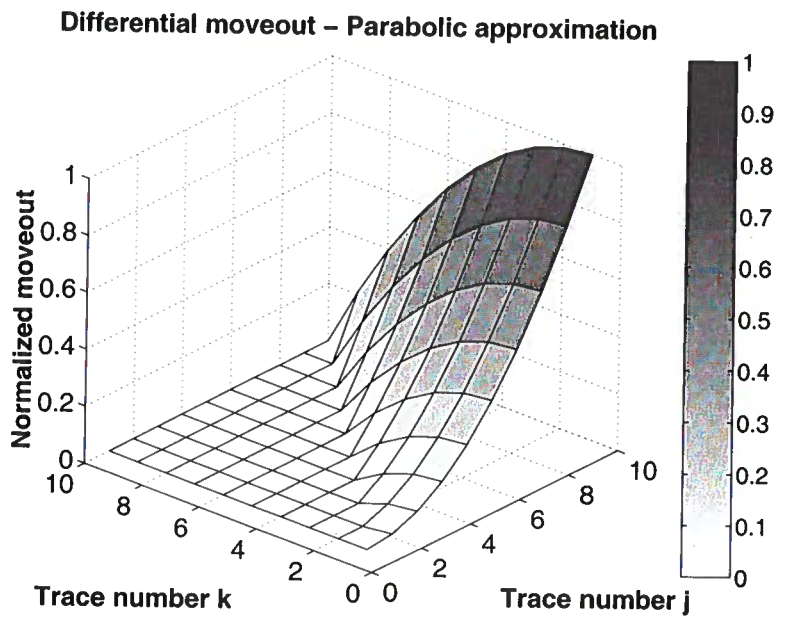

FIG. 2.2. Normalized values of the parabolic approximation to differential moveout (i.e., significance value) for *any* reflection in a CMP gather.

the parabolic approximation is presented in Figure 2.2. Based on how well the moveout of the parabolic trajectory approximates that of the hyperbolic trajectory, we expect that expression (2.2.18) provides a convenient approach to attaching relative importance to each crosscorrelation through the assigned significance value S_{jk}. Although it is suboptimal as compared with using hyperbolic moveout for any specific event, it is preferable in that it accomplishes generally what one wishes at low cost, independent of details of zero-offset time and stacking velocity, for every reflection in a CMP gather.

Although, I have chosen a parabolic approximation of differential moveout as a tool in selecting crosscorrelations, any other method that somehow describes the differential moveout could be used. The choice of selection method is just a detail toward our goal of excluding certain crosscorrelations from the calculation of the velocity spectra.

2.3 Selective-correlation sum

2.3.1 Method

Figure 2.3 is a schematic representation showing all trace pairs used in conventional crosscorrelation sum, in which all crosscorrelations are summed. The ordinate in the figure represents trace number k, and the abscissa trace number j for trace pairs that might be crosscorrelated. Since only trace pairs with indices $k < j$ are considered, the triangular re-

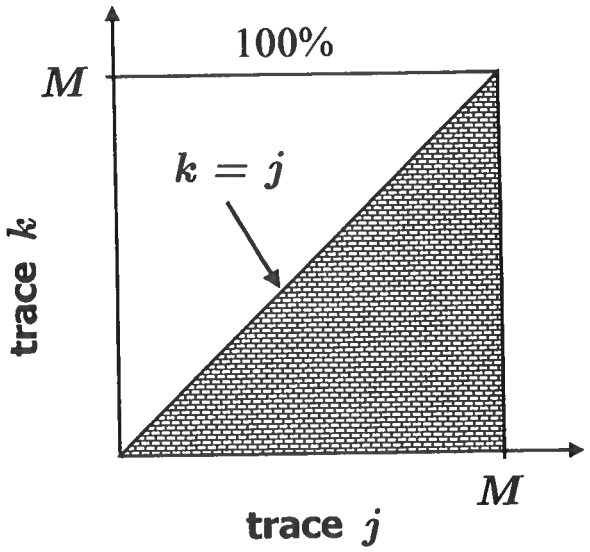

FIG. 2.3. Cartoon indicating those combination of traces j and k whose crosscorrelations are used in the conventional crosscorrelation-sum method (shown in brick pattern). The trace combinations of all possible crosscorrelations (100%) will be used in the sum.

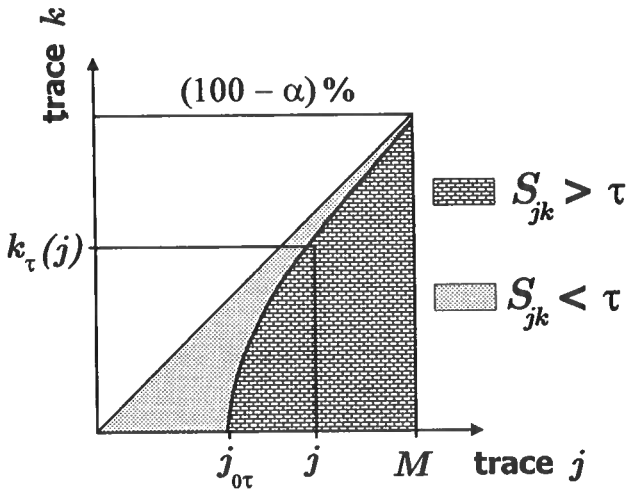

FIG. 2.4. Cartoon indicating those combination of traces j and k whose crosscorrelations are used in the selective-correlation sum method (shown in brick pattern) and those combinations that are excluded from the sum (shown in dotted pattern). (100-α)% of the crosscorrelations are summed.

gion shown by the brick pattern of shading depicts that all the trace pairs whose crosscorrelations are included in the sum. For conventional crosscorrelation sum, as shown here, 100% of the crosscorrelations are included. In a similar schematic for the selective-correlation sum (Figure 2.4), the brick-pattern region occupies a smaller portion of the lower triangular region for which $k < j$; the smaller the percentage of crosscorrelations used, the smaller the region showing trace pairs included in the computation. As depicted in (Figure 2.4), only those trace pairs with trace indices such that the associated offsets satisfy the inequality $S_{jk} > \tau$ are used in the summation. Here, τ is a user-specified threshold. The larger the threshold value τ, the larger the percentage α of crosscorrelations that are excluded from the computation of coherence. Discarding α percent of the crosscorrelation leaves (100-α)% of the crosscorrelations in the summation. Thus, for the selective-correlation sum method, the lower bound of the trace index j has been increased from 2 to $j_{0\tau} > 2$ in conventional crosscorrelation sum [expression (2.1.5)], and the upper bound of trace index k is now the function $k_\tau(j)$ of the trace index j. Therefore, the only difference between formula (2.1.3) and the one for selective-correlation sum will be in the lower limit for the sum over j and the upper limit for the sum over k.

The selective-correlation sum CC_{sc} is then given by

$$CC_{sc}(v_{trial}, t_0) = \sum_{w} \sum_{j=j_{0\tau}}^{M} \sum_{k=1}^{k_\tau(j)} f_{j,t(j)}\, f_{k,t(k)}, \tag{2.3.19}$$

where the summation limits $j_{0\tau}$ and $k_\tau(j)$ are those depicted in Figure 2.4. In the appendix, I derive expressions for these limits, for a given threshold value τ, under the assumption of equidistant offsets in a CMP gather.

Analogously, for the normalized version of selective-correlation sum, the only change from expression (2.1.9) is in the limits on the sums over j and k. Those new limits are the same values $j_{0\tau}$ and $k_\tau(j)$ as in expression (2.3.19).

Now, I exemplify, with synthetic model data, the features seen in the schematic representations of Figures 2.3 and 2.4. Figure 2.5a shows a ten-trace synthetic CMP gather for the same subsurface model parameters used to generate Figure 2.1. The significance values for the offsets used here are plotted on the two-dimensional contour plot in Figure 2.5b. Figure 2.5b depicts a matrix of trace number k versus trace number j, where the asterisks (*) indicate the trace combinations that yield the 45 crosscorrelations involved in the calculation of the velocity spectra. The shading indicates the significance value assigned by the parabolic approximation to each of these crosscorrelations. As seen in this plot, larger significance values (darker shades) are associated with larger differential moveout. For example, the crosscorrelation between traces 1 and 2, has an assigned value of $S_{jk} = 0.01$; between traces 1 and 5, it is $S_{jk} = 0.19$; and between traces 1 and 10, which corresponds to the largest differential moveout, S_{jk} is unity. Now, suppose we discard crosscorrelations for which the associated significance values are smaller than a specified threshold. For instance, if we wished to use only those crosscorrelations with associated S_{jk} values larger than, say 0.44, only 18 crosscorrelations out of the 45 will be considered (Figure 2.6b), which represents the 40% percent of the total number of crosscorrelations.

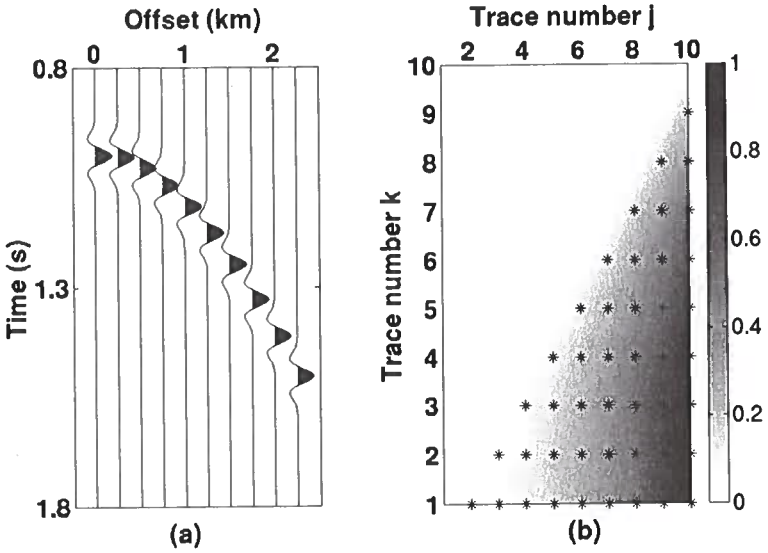

FIG. 2.5. (a) Synthetic CMP gather with ten traces; (b) trace number-versus-trace number plot indicating with asterisks (*) the trace combinations of all possible cross-correlations (i.e., all those for which $j > k$). The shading indicates the significance value S_{ij} assigned by the parabolic approximation.

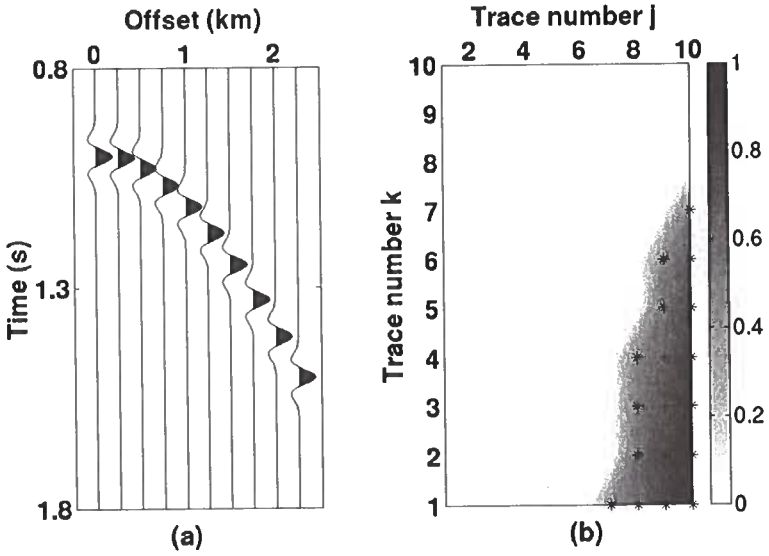

FIG. 2.6. (a) The same CMP gather as in Figure 2.5; (b) selected crosscorrelations for values of $S_{ij} > 0.44$, leaving only 40% of crosscorrelations to be used in the computation of coherence.

2.3.2 Computational effort and implementation

A common way of implementing the unnormalized crosscorrelation sum is through use of expression (2.1.6) instead of expression (2.1.5) because of the small number of operations involved. Although expression (2.1.5) seems to need order M^2N operations, when written as in expression (2.1.7) the same order of operations as in expression (2.1.6), MN, is required. In this form, as traces are read into memory they are multiplied with an accumulating sum of traces that had previously been read into memory. The velocity spectra computation using conventional unnormalized crosscorrelation sum, in the form of expression (2.1.7), may be summarized in the following pseudo code:

For $v = v_1, \ldots, v_n$
    GNMO(t, x) = apply NMO correction to the CMP gather with velocity v
    For $it = 1, \ldots, ntout$ $\%ntout$ = number of output time windows.
        F_{sum} =GNMO$(it, 1)$;
        $F_{acc} = 0$;
        For $j = 2, \ldots, M$ $\%M$ = number of traces in the CMP.
            F = GNMO(it, j);
            $F_{acc} = F_{acc} + F * F_{sum}$;
            $F_{sum} = F_{sum} + F$;
        end
        SPECTRA$(it, v) = F_{acc}$;
    end
end

Selective correlation sum can be implemented in much the same way using expression (2.3.19). The following pseudo code shows an implementation of the selective-correlation sum approach using the indices $j_{0\tau}$ and $k_\tau\,(j)$,

Compute $j_{0\tau}$ for the given threshold τ
For $v = v_1, \ldots, v_n$
    GNMO(t, x) = apply NMO correction to the CMP gather with velocity v
    For $it = 1, \ldots, ntout$ $\%ntout$ = number of output time windows.
        $F_{sum} = sum\{\text{GNMO}(it, 1 : k_\tau\,(j_{0\tau}))\}$;
        $F_{acc} = 0$;
        For $j = j_{0\tau}, \ldots, M-1$ $\%M$ = number of traces in the CMP.
            F = GNMO(it, j);
            $F_{acc} = F_{acc} + F * F_{sum}$;
            $F_{sum} = F_{sum} + sum\{\text{GNMO}(it, k_\tau(j)+1 : k_\tau(j+1))\}$;
        end

SPECTRA$(it, v) = F_{acc}$;
end
end

2.4 Velocity resolution

2.4.1 Single, noiseless reflection

Let us now illustrate, with noise-free synthetic data, how this velocity-spectra process alters the resolving power of velocity estimation. The first model considered consists of a single horizontal reflector below a homogeneous layer with velocity of 4.5 km/s and layer thickness of 6.75 km. Figure 2.7a shows a CMP gather for cable length 3150 m, 64 receivers, and distance between receivers of 50 m. The peak frequency of the Ricker wavelet in the data is 12.5 Hz. (All tests with synthetic model data presented in this thesis are modeled using a Ricker wavelet. I employ the value of dominant or peak frequency of the Ricker wavelet to characterize the frequency content of the data). Figure 2.7b shows the corresponding velocity panel computed using the conventional unnormalized crosscorrelation sum for all possible crosscorrelations. Notice the spread of strong spectral amplitude across the velocity panel, from 3.5 km/s all the way to the right end of the velocity panel at 6.5 km/s. The smearing, here, is produced by a combinations factors: relatively low frequency, high velocity, and large depth of the layer relative to the spreadlength. This smearing suggests large uncertainty in the velocity picking.

Figure 2.8a is the same velocity panel as in Figure 2.7b, with 100% of the crosscorrelations included (henceforth, 100% of crosscorrelations means the conventional crosscorrelation sum with all crosscorrelations included in the sum; any reduced percentage means that the approach of selective-crosscorrelation sum is used with that percentage of crosscorrelations summed). The remaining velocity plots were obtained using 50% of the crosscorrelations (Figure 2.8b), 25% of them (Figure 2.8c), and 10% of them (Figure 2.8d). As percentage of crosscorrelations summed decreases, the apparent resolution in picking a velocity for the reflection event of Figure 2.7a improves.

Although the same shaded contour scale is used for all four plots, the choice of shading scale can often bias one's interpretation. To better see the dependence of coherence on the percentage of crosscorrelations used, Figure 2.9 shows plots of coherence curves – plots of UC_{sc} as a function of trial velocity v_{trial} – at fixed incidence time t_0, in particular the time of the modeled reflection. Shown in Figure 2.9 are coherence curves at $t_0 = 3$ s, extracted from Figure 2.8, with each curve normalized to a peak amplitude of unity. We can make two observations from this plot: First, the lower the percentage of summed crosscorrelations, the sharper the peak of the curve, and, second, percentages lower than 100% yield (undesirable) side lobes with negative values. For trial velocities that depart significantly from the correct one, the trial moveout trajectory can cross from, for example, the peak of the event's wavelet at small offset to a trough at large offset. Thus some contributing crosscorrelations will have negative values. This also happens for the conventional approach of summing

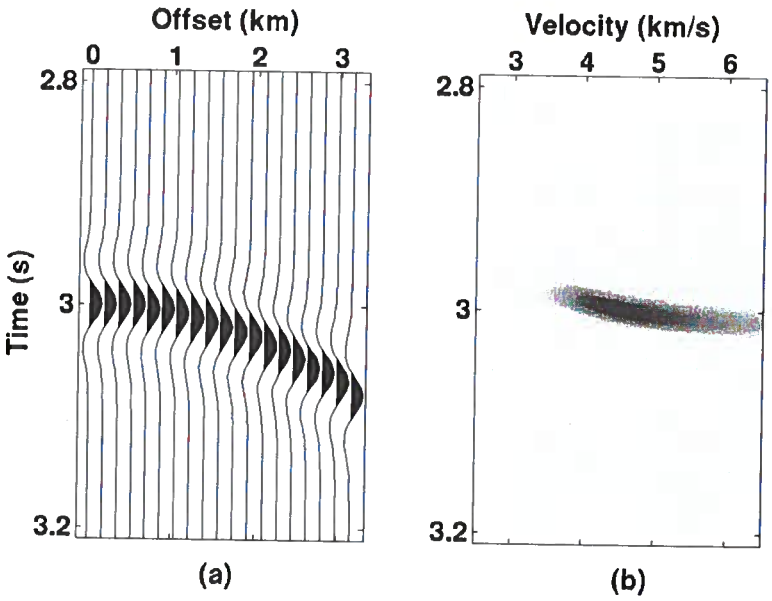

FIG. 2.7. (a) Synthetic CMP gather with a reflection single event; (b) velocity panel for the synthetic data, computed using a conventional method. The broad region of large computed coherence (i.e., dark shading) indicates potential for large uncertainty in picking stacking velocity.

all possible crosscorrelations, but in the conventional approach positive values dominate in the crosscorrelations of traces with small differential moveout that we would have excluded in the selective-correlation method. Later, we will consider implications of these negative coherence values for velocities away from the correct ones.

2.4.2 Two noiseless interfering events

Because of this improvement in velocity resolution, the selective-correlation sum method can aid in separating closely interfering events, as occurs with neighboring primaries and multiples. Figure 2.10a shows a CMP gather containing two events with the same zero-offset arrival time of 2 s, but different moveout velocities of 4.5 km/s and 3.5 km/s, respectively. Only at offsets larger than 2 km, is the difference in NMO of the two events observable. In this example, the peak frequency of the Ricker wavelet is again 12.5 Hz. Figure 2.10b shows the velocity panel associated with these data, computed using the conventional crosscorrelation sum method. Looking only at the velocity plot is impossible to distinguish the two events present in the data, and the most probable velocity pick would be around a value of 4 km/s. The selective-crosscorrelation sum (25%) allows separation of the two maxima, yielding good estimates of the velocity for each reflection (Figure 2.11b).

Perhaps, however, this improvement is only apparent, dependent on the choice of shad-

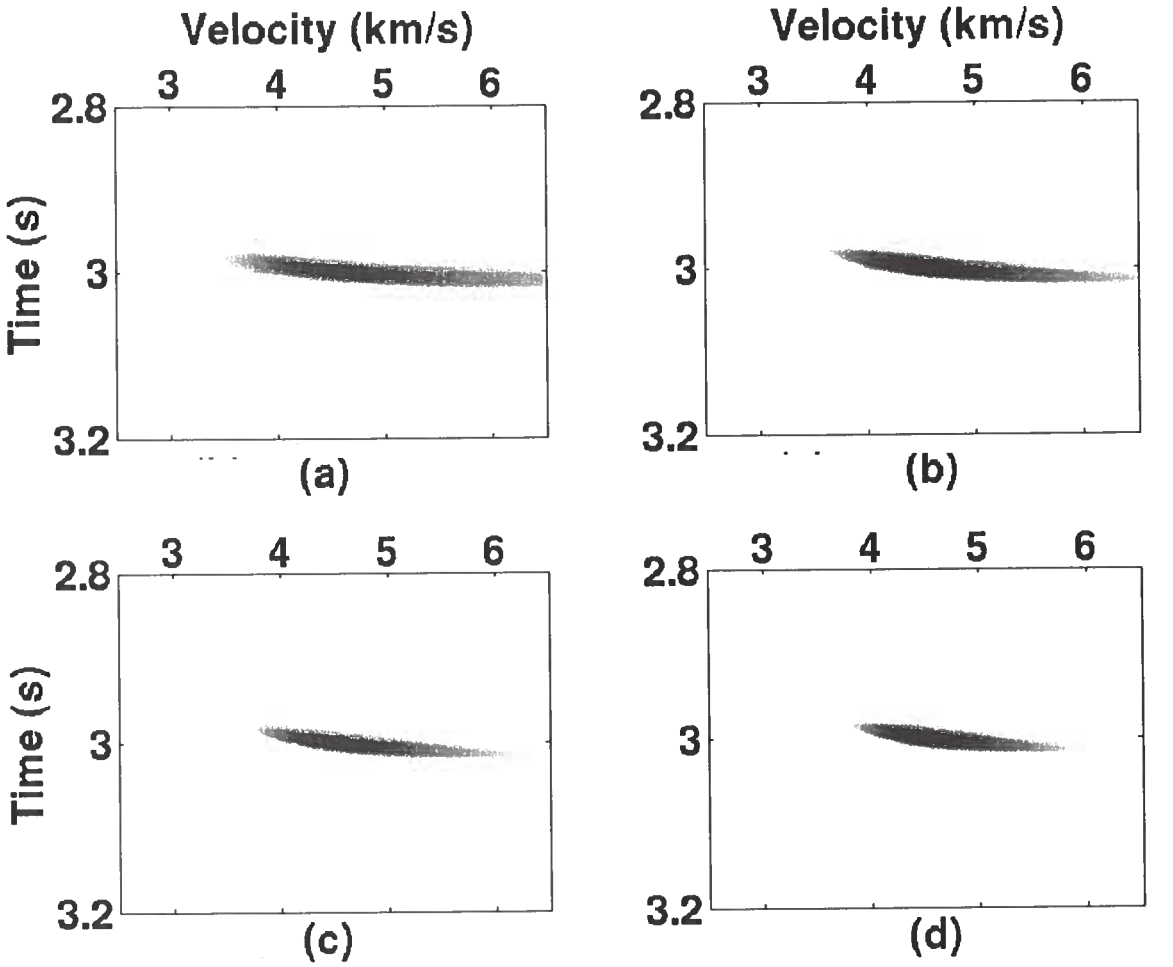

FIG. 2.8. Velocity panels computed using:(a) conventional crosscorrelation sum (100 % of crosscorrelations included) and using selective-correlation sum with the percentages (b) 50%, (c) 25%, (d) 10%. All four plots use the same contour-shading scale, with darker shading for higher coherence amplitude.

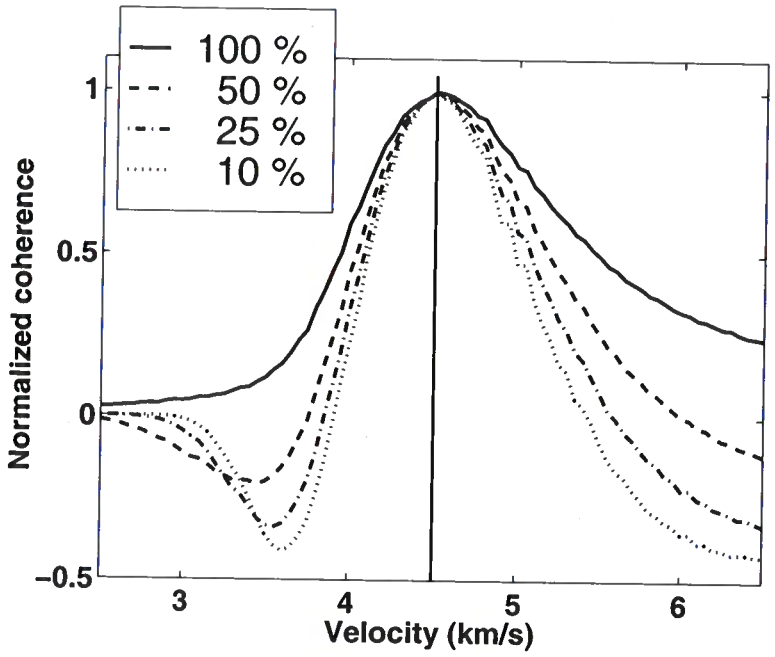

FIG. 2.9. Coherence curves for the conventional crosscorrelation sum (100%), and selective-correlation sum for the percentages 50%, 25%, and 10%. The vertical line indicates the correct stacking velocity.

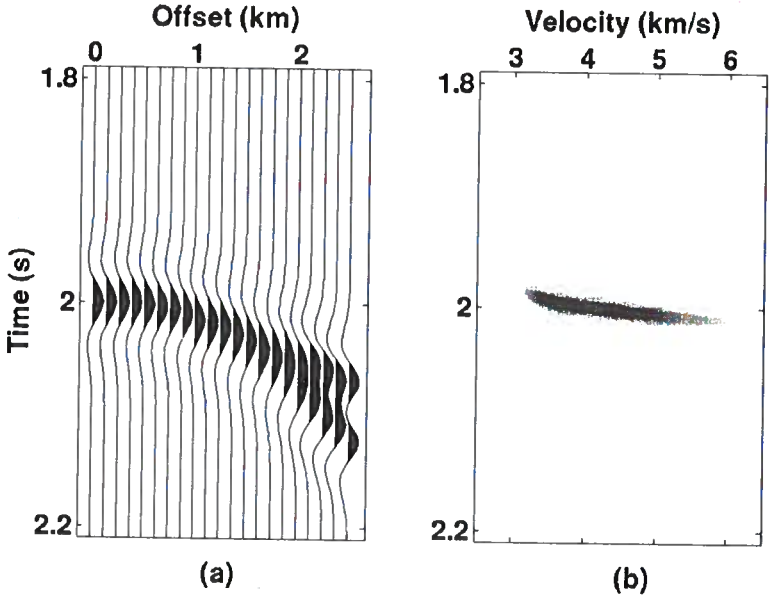

FIG. 2.10. (a) Synthetic gather with two interfering events, and (b) velocity panel for the data computed using the conventional unnormalized crosscorrelation sum method. From this velocity panel, it is impossible to identify the presence of two events (in fact, as shown in Figure 2.12, the data have only a single peak).

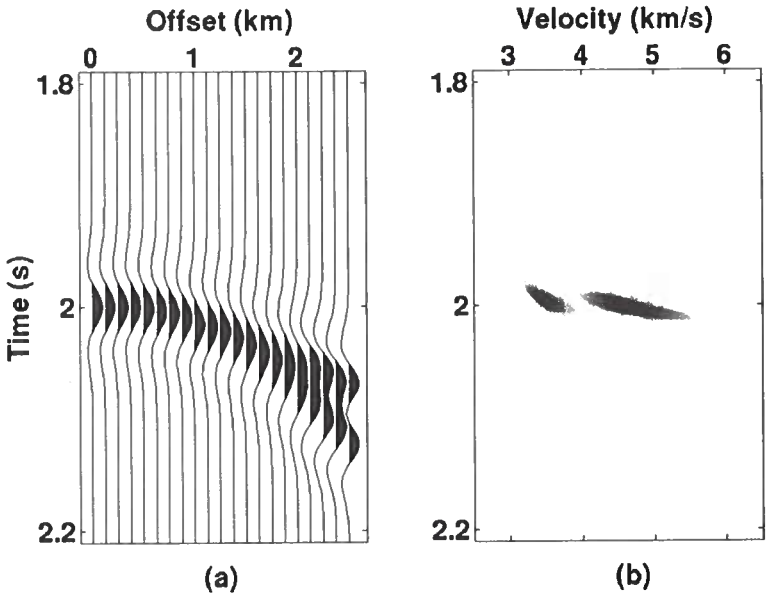

FIG. 2.11. (a) Same CMP gather as in Figure 2.10a; (b) velocity panel computed using selective-correlation sum using a 25% of crosscorrelations.

ing scale used for the contour plots. The coherence curves for zero-offset time of 2 s, in Figure 2.12, reveal the substantial improvement in resolution when just the 25% of the crosscorrelations with largest associated differential moveouts are used in the sum. The standout of the two peaks is greater yet when only 15% of the crosscorrelations, with large differential moveout, are used in the sum (Figure 2.13). Any percentage between 100% and 15% yields intermediate shapes between those of the two curves. Based on many tests with synthetic data, significant improvement is achieved for percentages of 50% or less.

2.4.3 Comparison with other coherence measures

As mentioned above, Neidell and Taner (1971) suggest that the semblance coefficient, expression (2.1.12), offers better resolution than do other coherence measures. Figure 2.14 shows coherence curves generated using the conventional crosscorrelation sum (solid line), the selective-correlation sum for 25% of crosscorrelations (dashed-dotted line), and the semblance coefficient (dashed line). The semblance coefficient detected the existence of two events, giving a better result than that of the conventional crosscorrelation sum, yet its peak locations are biased; that is, the velocities at the peak locations differ from the correct values. This improvement in velocity resolution achieved by the semblance coefficient is small when compared to that of the selective-correlation sum, for which the peak locations are unbiased.

Another way to increase velocity resolution is through use of optimum trace weights

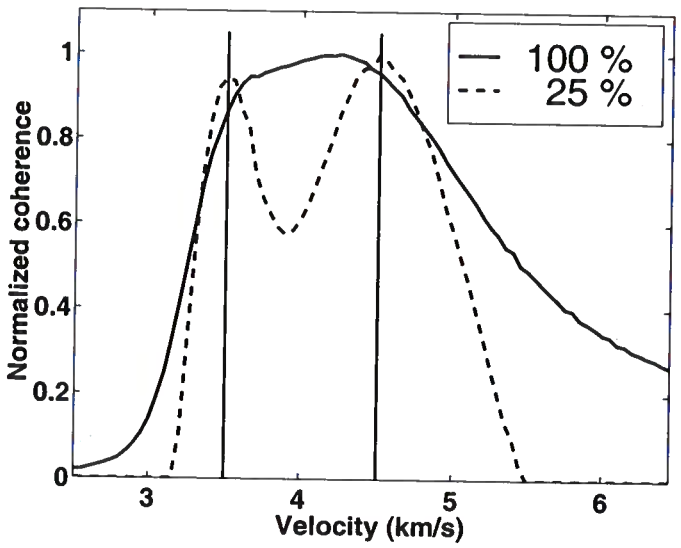

FIG. 2.12. Coherence curves for two interfering events. Conventional crosscorrelation sum (100%) and selective-correlation sum (25%). The vertical lines indicate the correct velocities for the two events.

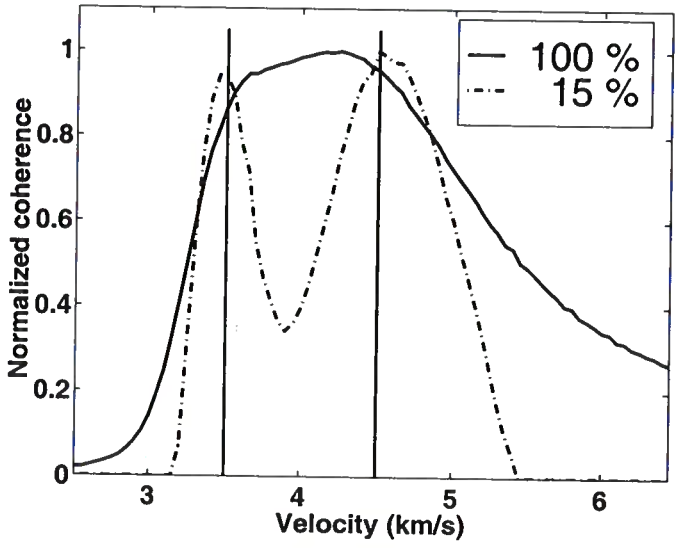

FIG. 2.13. Coherence curves for two interfering events. Conventional crosscorrelation sum (100%) and selective-correlation sum (15%). The vertical lines indicate the correct velocities for the two events.

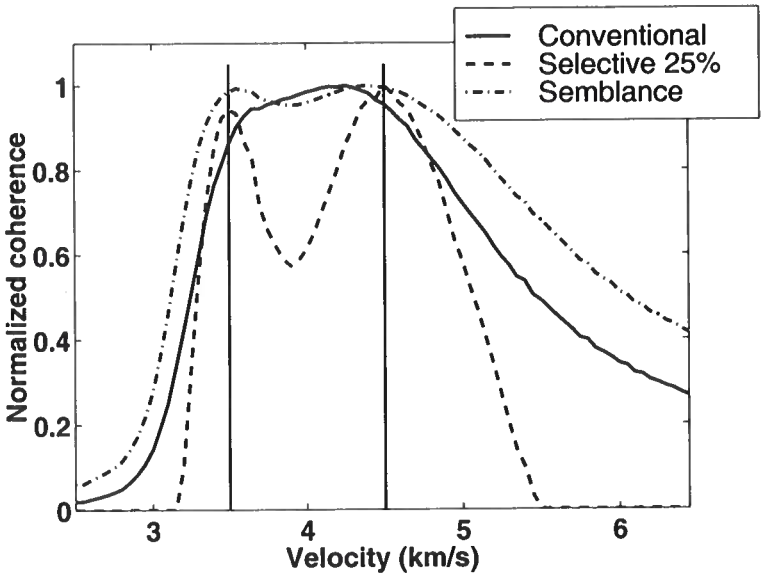

FIG. 2.14. Coherence curves for two interfering events using conventional crosscorrelation sum, selective-correlation sum (25%), and semblance. The vertical lines indicate the correct velocities for the two events.

such as those produced by Schoenberger's multiple-suppression method. In his method, a weight is assigned to each data trace, prior to stacking, based on least-squares optimization. CMP stacking with these weights constitutes a stacking filter designed to minimize the energy in stacked multiples, based on their frequency content and residual moveout, after data have been NMO-corrected to align primaries. This results in better multiple attenuation than does the conventional stack, in which traces are equally weighted. For improving resolution in velocity analysis, the weights produced in Schoenberger's method are applied directly to the traces in the CMP gather prior to performing conventional (i.e., 100%) velocity analysis.

The weights designed for optimum rejection of the interfering event with larger moveout in Figure 2.10a, and preservation of the other, are shown in Figure 2.15. These weights are optimum for the following set of parameters: Ricker-wavelet peak frequency 12.5 Hz, primary velocity 4.5 km/s, multiple velocity 3.5 km/s, zero-offset reflection time 2 s, ratio of rms amplitude of random noise to peak amplitude of multiple 0.3, maximum offset 2.5 km, offset increment 50 m, and 50 receivers. As seen in this figure, the procedure gives relatively more importance to long-offset traces than to short- and intermediate-offset ones. Applying the weights to the traces in the CMP gather of Figure 2.10a, and then performing velocity analysis using conventional crosscorrelation sum produced the coherence curve shown as the dashed line in Figure 2.16. The solid line pertains to the conventional velocity-analysis method applied to traces with uniform weights. Indeed, with the use of optimum weights, resolution is improved when compared with that of either conventional crosscorrelation sum or semblance coefficient (Figure 2.14), but still selective-correlation sum (Figures 2.12 and

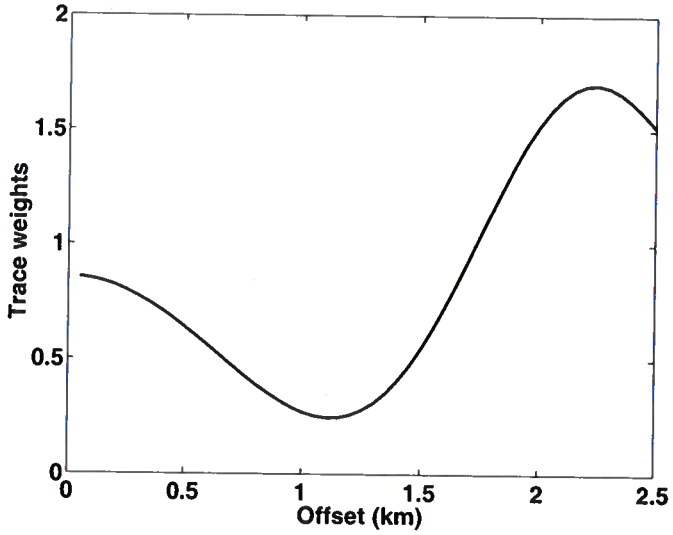

FIG. 2.15. Optimum stacking weights used prior to conventional velocity estimation for the synthetic CMP gather with interfering events, shown in Figure 2.10a.

2.13) shows more standout of the two maxima. Note, as in the result using semblance coefficient (Figure 2.14), the small bias in velocity associated with the peaks in the dashed coherence curve in Figure 2.16.

The velocity-resolution enhancement method of selective-correlation sum and that based on optimum trace weights are similar in that both apply weights to crosscorrelations. These crosscorrelation weights in selective-correlation sum are zeros and ones, whereas in the optimum-weights approach they are the result of multiplying the stacking weights of individual traces involved in each crosscorrelation. A difference between these two approaches is that because the weights are optimized for a specific set of problem parameters, the result for optimum weights is fixed by the weights used. Although the selective-correlation-sum approach is not based on an optimization scheme, it provides us with a knob that we can fully open (100 % of crosscorrelations, equivalent to conventional crosscorrelation sum) or close until a desired percentage of crosscorrelations is reached (e.g., 50%, 30%). Also, its resolution performance is mantained for a wide range of primary reflection times and stacking velocities. Aside from a scale-factor change in the coherence curves, the change as the knob is turned is that the lower the percentage used, the higher the resolution. In principle, one could go from including all crosscorrelations to the extreme of including only one, that being the correlation between the shortest and longest offset traces. For field data, however, the extreme of including only one crosscorrelation is unacceptable. In the next chapter, I show that in order to maintain the stability of selective-correlation velocity analysis in presence of random noise and static distortions, 20% or more of crosscorrelations should be included in the sum. Also in that chapter, through further tests with synthetic data I examine factors that influence velocity estimation by the conventional and the selective approaches.

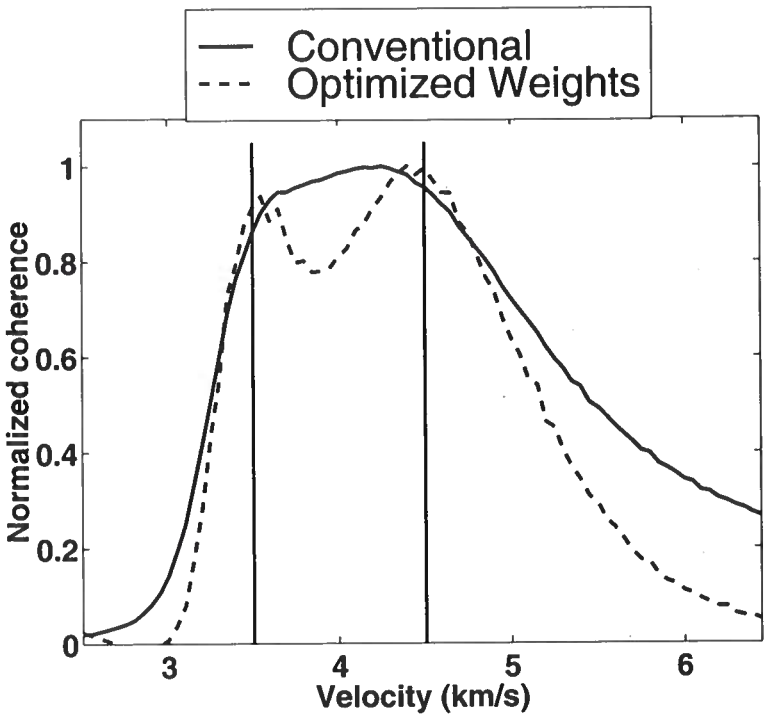

FIG. 2.16. Coherence curves, for conventional crosscorrelation sum with use of uniform and optimum weights, for the interfering-event data in Figure 2.10a. The vertical lines indicate the correct velocities.

Chapter 3

FACTORS THAT INFLUENCE VELOCITY ESTIMATES

The quality of velocity estimation from reflection seismic data is influenced by many factors. Among the most important are spreadlength as it relates to the moveout and bandwidth of the data, random and coherent noise contamination, statics distortions, interfering primary events, and relative strength of primaries and multiples. Here, I compare the performance of velocity analysis, using a conventional method and the selective-correlation sum, applied to synthetic CMP data in presence of these factors. In addition, I show that reducing the fold of a CMP gather (by, say deleting every other offset), in order to reduce the number of crosscorrelations, is inferior to use of selective-correlation sum.

3.1 Spreadlength

As is well recognized in practice, for given reflector depth and moveout velocity, resolution in velocity analysis increases with spreadlength. The relationship between velocity resolution and offset can be established by starting with the NMO equation

$$t^2 = t_0^2 + x^2/v^2, \tag{3.1.1}$$

where t is the hyperbolic traveltime, t_0 is the zero-offset traveltime, x is offset, and v is velocity. Taking the partial derivative with respect to velocity in expression (3.1.1), we get

$$2t\frac{\partial t}{\partial v} = -\frac{2x^2}{v^3}.$$

From this, the velocity variation δv can be expressed as function of time, time variation δt, velocity, and offset by

$$\delta v \approx -\frac{v^3 t}{x^2}\delta t. \tag{3.1.2}$$

Expression (3.1.2) implies that, for given time error δt on, say, the far-offset trace, the longer the offset the better the velocity resolution. (This expression also supports the familiar behavior that velocity resolution decreases with increasing NMO velocity and reflector depth because, at fixed x, t increases with reflector depth). Practical issues, however, typically

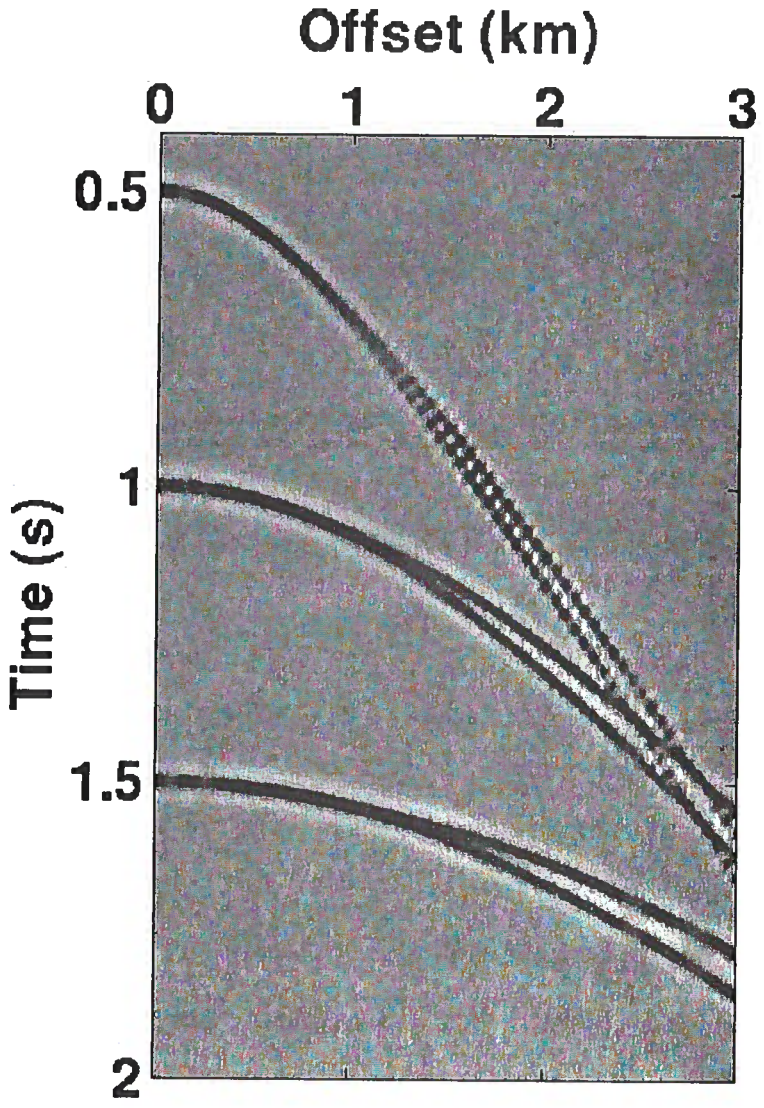

FIG. 3.1. Synthetic CMP gather with three primary reflections and neighboring multiples.

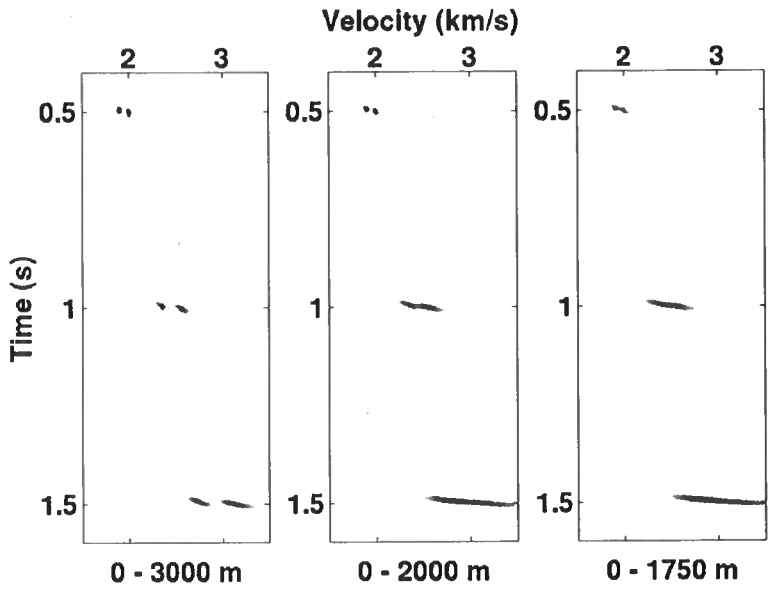

FIG. 3.2. Velocity panels for the CMP gather in Figure 3.1 with different spreadlengths, using conventional crosscorrelation sum.

limit the ratio of spreadlength-to-reflector depth before the assumption of hyperbolic reflections breaks down, thus further complicating the velocity-estimation problem.

The following example shows the influence of spreadlength on velocity estimation in the presence of closely interfering events. Figure 3.1 contains a synthetic CMP gather with three pairs of primary and multiple reflections at the same zero-offset two-way traveltimes of the primaries (0.5, 1.0, and 1.5 s). The Ricker wavelet in the data has peak frequency of 20 Hz, and the maximum offset is 3000 m. Figures 3.2 and 3.3 show velocity panels computed using a conventional method and the selective method (both unnormalized) for 25% of crosscorrelations, respectively, for spreadlengths of 3000, 2000, and 1750 m. Although for spreadlength of 3000 m the maxima are sharper for the selective method (Figure 3.3), both methods resolve the two maxima corresponding to primaries and multiples at the three zero-offset times. For the range 0 - 2000 m, the two coherence maxima produced by conventional method (Figure 3.2) start to join one another at 1 s, and are completely indistinguishable at 1.5 s, while the selective method (Figure 3.3) still generates two separate maxima even for the deeper events. For the shortest spreadlength shown here (0 -1750 m), the conventional method (Figure 3.2) fails to separate the primaries and multiples reflections, even for the shallower ones at 0.5 s. For this spreadlength, the selective method (Figure 3.3) produces separate maxima except for the events at 1.5 s, for which differential moveout is so small that the events practically overlap over the entire spreadlength.

This example demonstrates the loss of velocity resolution for smaller spreadlengths and later reflections. That loss of resolution can reach the point of showing only one maximum for two closely interfering events. This resolution loss and biasing of the maxima, however,

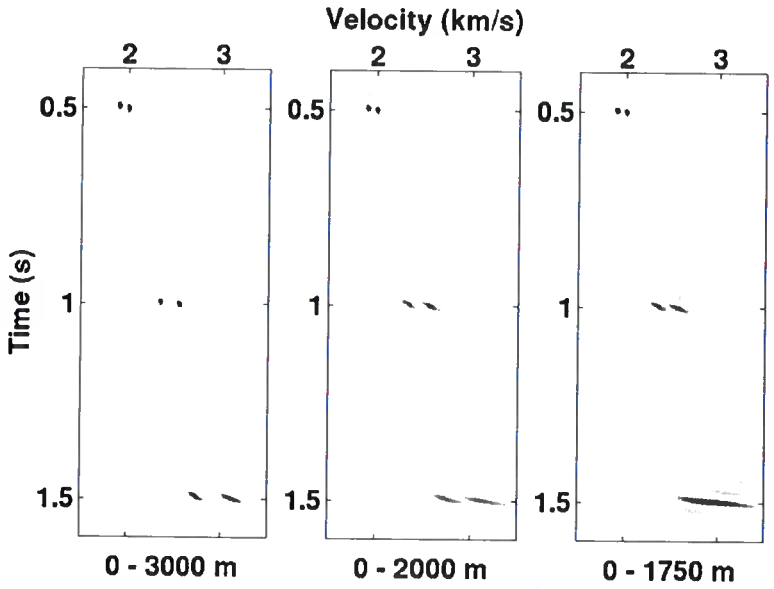

FIG. 3.3. Velocity panels for the CMP gather in Figure 3.1 with different spreadlengths, using selective-correlation sum (25%).

can be substantially reduced by using the selective-correlation sum method for computation of the velocity panel.

3.2 Frequency content

Expression (3.1.2) indicates how the dependence of velocity errors on errors in reflection times varies with spreadlength, NMO velocity, and reflection time. Even when the reflection times have no error, however, the bandlimited wavelet in the seismic data for fixed t_0, maps differential moveout into a coherence function of some breadth as a function of trial velocity. The breadth of that coherence function, for fixed spreadlength, is larger the lower the dominant frequency of the data wavelet. Equivalently, velocity resolution is better for high- than for low-frequency data.

As mentioned in Chapter 2, we can use the dominant or peak frequency of the Ricker wavelet used in the modeling of the synthetic data to characterize the frequency content in the data.

Figures 3.4 through 3.7 are plots of coherence curves at $t_0 = 2$ s, for the same two interfering events (e.g., primary and multiple) simulated in the CMP gather shown in Figure 2.10a, but for dominant frequency in the wavelet of 12.5, 14, 18, and 25 Hz, respectively. The bias in the coherence curve for the conventional method (100%) is so large when the peak frequency in the modeled data is 12.5 Hz that only one peak is identifiable, but located at a

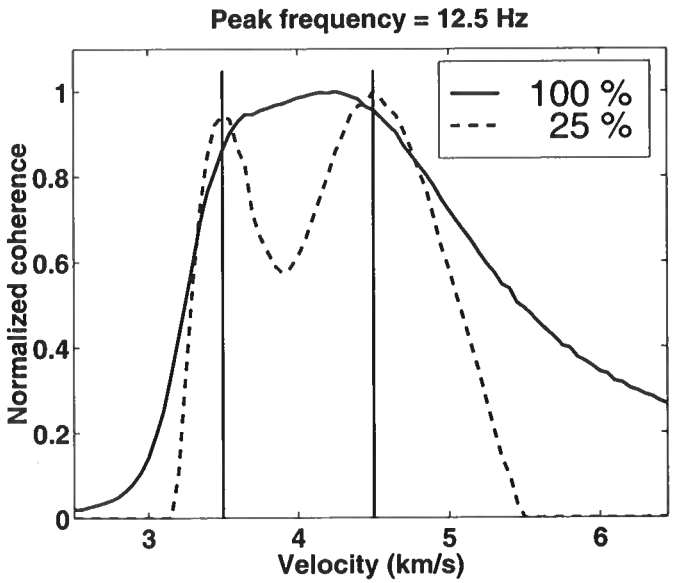

FIG. 3.4. Coherence curves for interfering events of Figure 2.10a with peak frequency of 12.5 Hz.

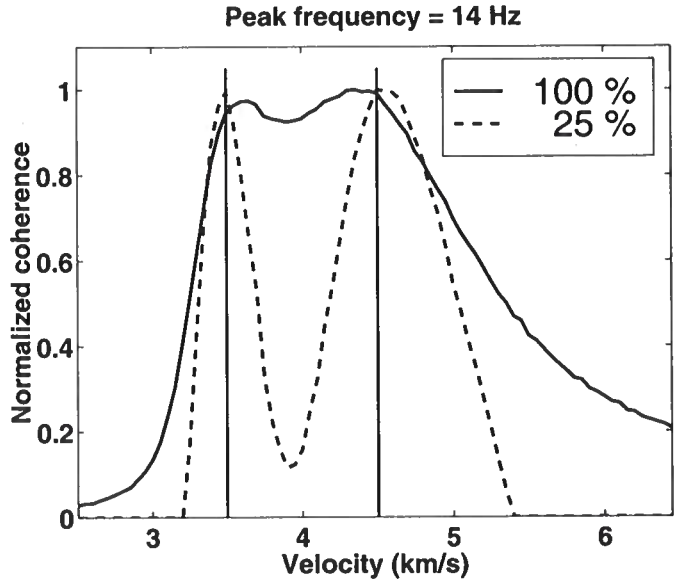

FIG. 3.5. Coherence curves for interfering events of Figure 2.10a with peak frequency of 14 Hz.

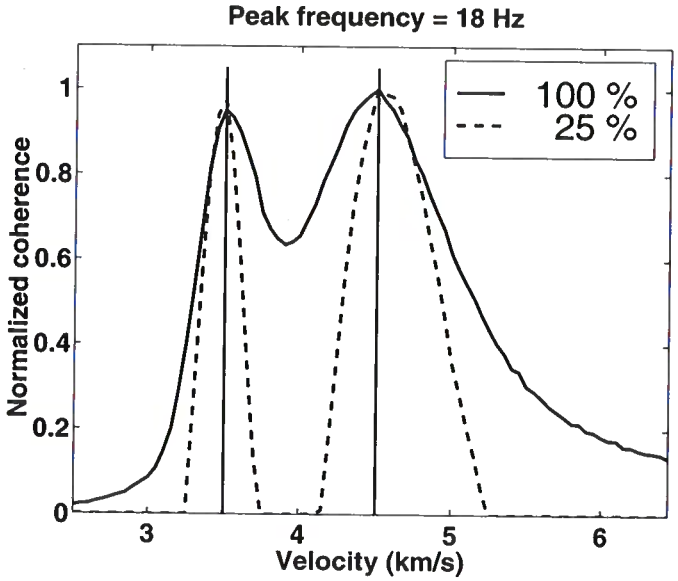

FIG. 3.6. Coherence curves for interfering events of Figure 2.10a with peak frequency of 18 Hz.

wrong velocity. For this same peak frequency, the selective-correlation method (25%) yields unbiased peaks for the primary and multiple with good standout. Two different peaks, although at biased locations, start to show up in the coherence curve corresponding to the conventional method (100%) when the peak frequency of the modeled data is increased from 12.5 to 14 Hz (Figure 3.5). At this peak frequency, the selective method, using 25% of crosscorrelations, again shows unbiased peaks but with greater standout than in the previous example. Figure 3.6 contains the coherence curves, for peak wavelet frequency of 18 Hz, in which both methods produced unbiased peaks. The selective method shows a complete separation of the peaks indicating the correct velocities for primary and multiple, while the conventional method (100%) exhibits a standout comparable to that seen for the selective method when the dominant frequency in the data is only 12.5 Hz (Figure 3.4). This suggests that the conventional approach requires higher-frequency data in order to achieve the velocity resolution of the selective-correlation sum approach.

Similar results are shown in Figure 3.7, for peak frequency in the Ricker wavelet of 25 Hz. In general, the selective-correlation sum method produces higher resolution results compared to that of conventional method, for data with the same frequency content.

3.3 Strong multiples

Primaries typically have smaller moveout than do multiples at comparable zero-offset time, implying that velocity can be used as a way to discriminate between primaries and

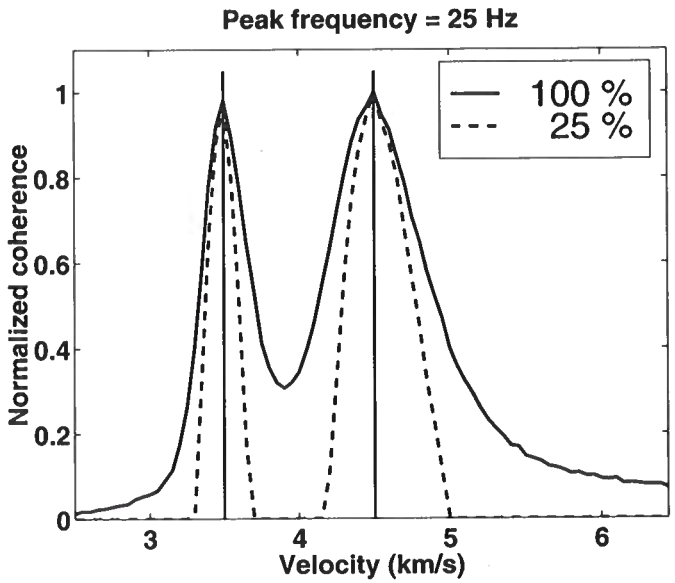

FIG. 3.7. Coherence curves for interfering events of Figure 2.10a with peak frequency of 25 Hz.

multiples. If the velocity function for primaries is used in NMO correction, that correct aligns the primaries while the multiples are undercorrected. CMP stacking will then preserve the primaries while attenuating multiples. Picking the velocity of primaries from the peaks in velocity spectra, however, can be a difficult task in the presence of multiples that interfere closely with primaries. As we have seen in examples that include multiple-like features (e.g., Figures 2.10a and 3.1), selective-correlation velocity analysis can improve the prospects for picking the velocity function corresponding to primaries because of its higher resolving power.

The examples described in Figures 2.10a and 3.1 dealt with primaries and multiples of the same signal amplitude. In coherence curves of conventional velocity estimation, however, strong-amplitude multiples can swamp nearby weaker primaries. Figure 3.8 shows three CMP gathers, each with four reflections and nearby multiples. The ratio shown beneath each CMP gather is the ratio of the amplitude of primary to that of multiple. The CMP gather on the left has primaries and multiples with the same strength. For the gather in the middle the amplitudes of multiples are twice that of nearby primaries, and for the gather on the right multiples amplitudes are three times those of primaries. The corresponding velocity spectra for the CMP gathers of Figure 3.8, computed using conventional crosscorrelation sum, are shown in Figure 3.9, and those computed using selective-correlation sum using 25% of crosscorrelations are shown in Figure 3.10. Selective-correlation sum separates primaries and multiples even when the amplitude of multiple is much stronger than that of primaries, thus aiding interpretation of primary stacking velocities. The conventional correlation sum (Figure 3.9) is so dominated by the multiples when their amplitudes are stronger than those of primaries that no peak may be identified for later primaries. Even when amplitudes of

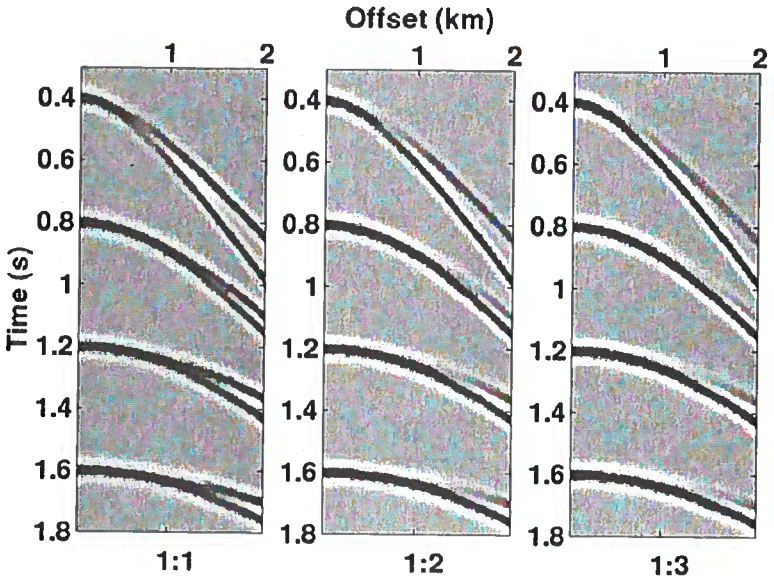

FIG. 3.8. Synthetic CMP gathers with different ratios of primary-to-multiple amplitude.

primaries and multiples are equal, no separation is evident on the deeper events.

To more closely assess these results, in Figure 3.11 are plots of velocity curves for normal incidence time $t_0 = 1.2$ s for amplitude ratio of multiple to that of primaries, 1:2. As before, the vertical lines indicates the correct stacking velocities. The coherence curve for the conventional method is dominated by the presence of the multiple to the extent that the primary event shows no evidence of a peak in the curve. The selective method, in contrast, shows two clearly defined and well separated features, the smaller one corresponding to the velocity of the primary.

3.4 Noise-contaminated data

Additive noise in data distorts the time shifts in the crosscorrelations used in computation of velocity spectra, thus reducing the stability of velocity estimates. Of particular concern for the selective-correlation approach is the possibility that by discarding many crosscorrelations we may be compromising the stability of the velocity estimates. Here, we introduce additive bandlimited random noise and compare the performances of conventional and selective-correlation methods. In Chapter 4, I will give an explanation of the results of these tests.

Figure 3.12 shows a single-event CMP gather with uncorrelated, random noise bandlimited to the same passband as the signal. For this gather SNR ≈ 0.5, where signal-to-noise

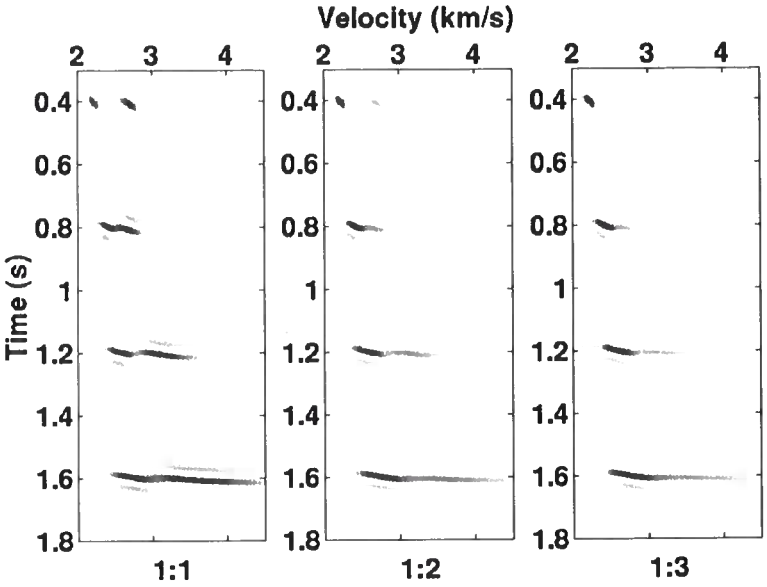

FIG. 3.9. Velocity panels, for different ratios of primary-to-multiple amplitude, using conventional crosscorrelation sum.

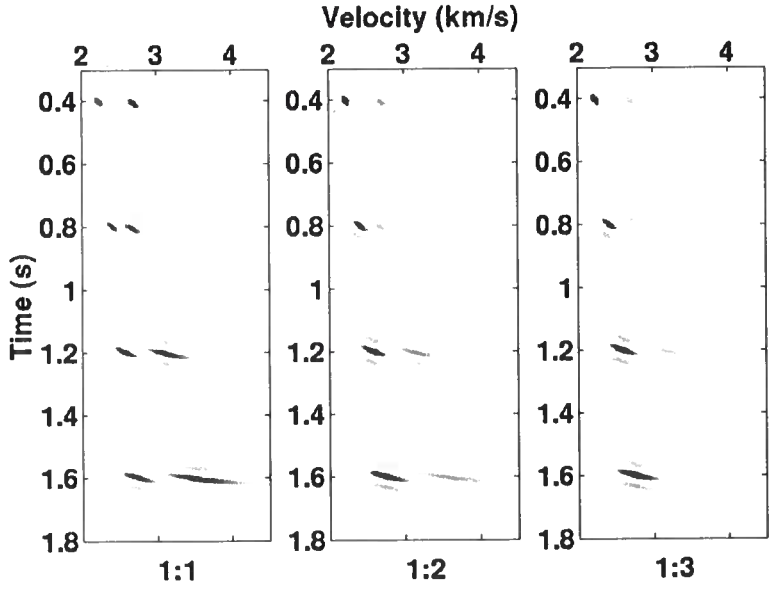

FIG. 3.10. Velocity panels, for different ratios of primary-to-multiple amplitude, using selective-correlation sum (25%).

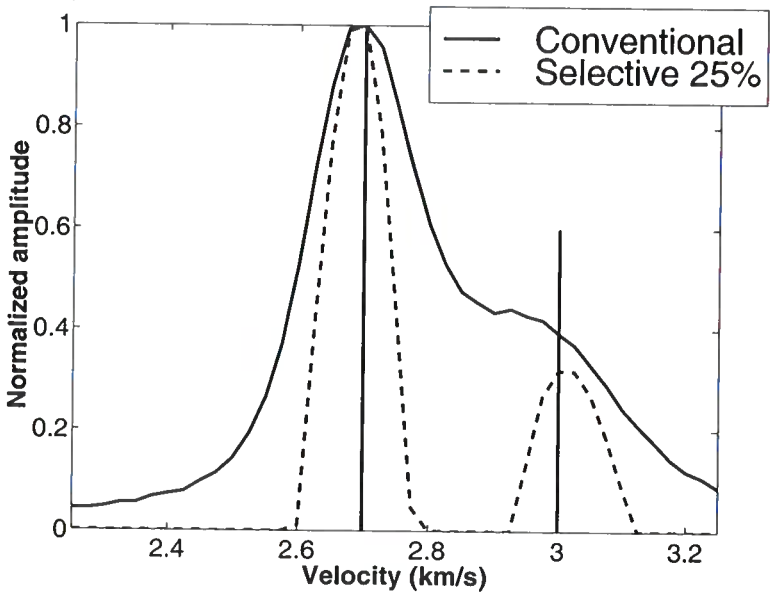

FIG. 3.11. Coherence curves at t_0 =1.2 s, extracted from Figures 3.9 and 3.10, for a ratio of primary-to-multiple amplitude of 1:2.

ratio (SNR) is computed as the ratio of the peak amplitude of the reflection signal to the root-mean-squared (rms) amplitude of the noise. The reflector model and data parameters in this example are the same as those in Figure 2.7a. Figure 3.13 shows the corresponding coherence curves for conventional crosscorrelation sum and selective-correlation sum using 25% of the crosscorrelations, and Figure 3.14 shows coherence curves for a similar CMP gather but different realization of added noise. In both figures, note that for the selective-correlation sum the peak of the curve is again sharper than that of the curve for conventional crosscorrelation sum, implying higher resolution. Note also that, in each figure, both peaks are located at about the same velocity (which, in both Figures 3.13 and 3.14, is not the correct value), suggesting that accuracy of the two methods is comparable. In the example of Figure 3.14, the velocity at peaks of both curves are far from the correct velocity, indicated by the vertical line.

In numerous other similar tests, I have observed that the peaks in the curves for both methods coincide when the percentage used in the sum is not too small (say, 20% or higher). Moreover, the location of the velocity peak is strongly governed by crosscorrelations for pairs of traces with large differential moveout. Because the selective-correlation method includes trace pairs with relatively large differential moveout, it includes those trace pairs that dominate the contributions in conventional velocity analysis. This argument supports the observation that the robustness of the selective-correlation-sum method in the presence of added uncorrelated noise is comparable to that of conventional analysis while the peaks for the selective-correlation method remain sharper than those when 100% of the crosscorrelations are used.

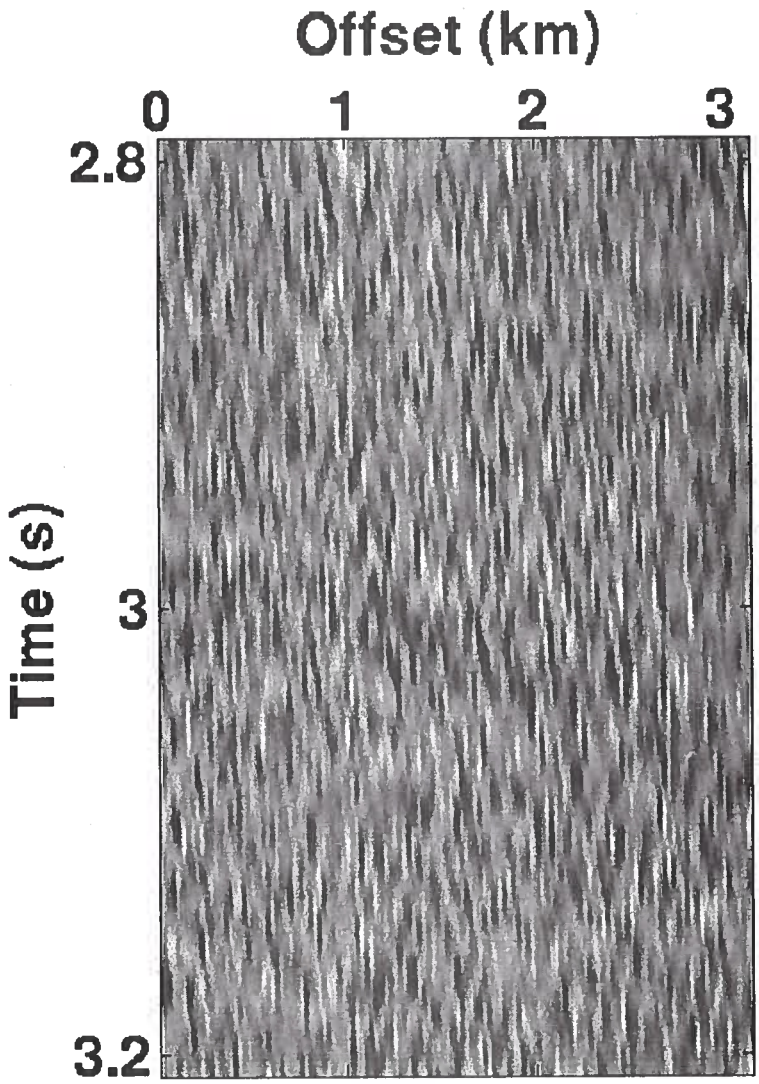

FIG. 3.12. CMP gather with the same single reflection event of Figure 2.7a, with bandlimited random noise added such that SNR ≈ 0.5, yielding poor evidence of the reflection.

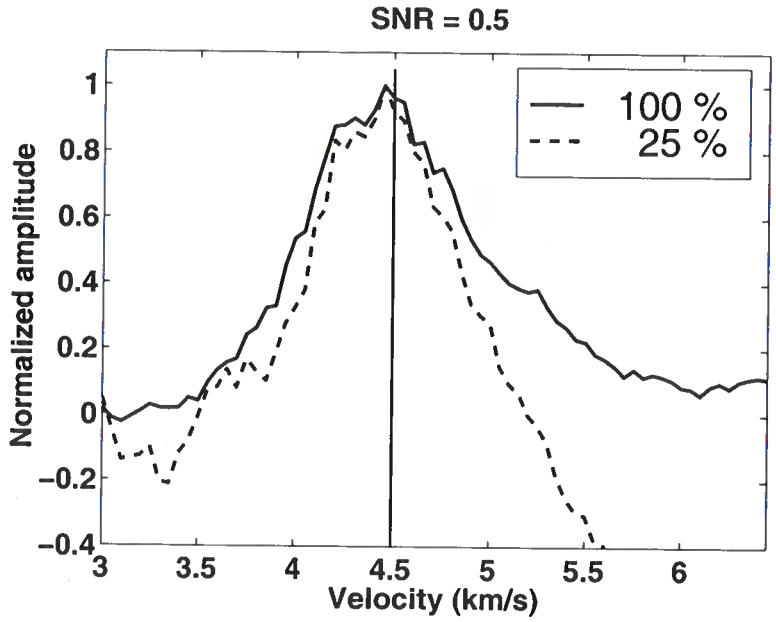

FIG. 3.13. Coherence curves, for data with SNR ≈ 0.5, using conventional crosscorrelation sum (100%) and selective-correlation sum (25%). The vertical line indicates the correct velocity.

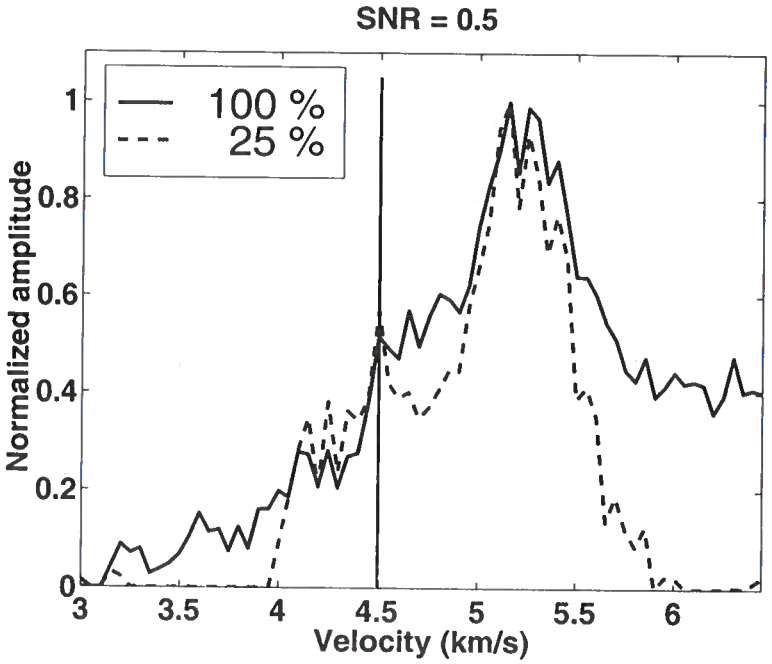

FIG. 3.14. Similar plot of coherence curves as that in Figure 3.13, but for a different realization of added random noise (again with SNR ≈ 0.5).

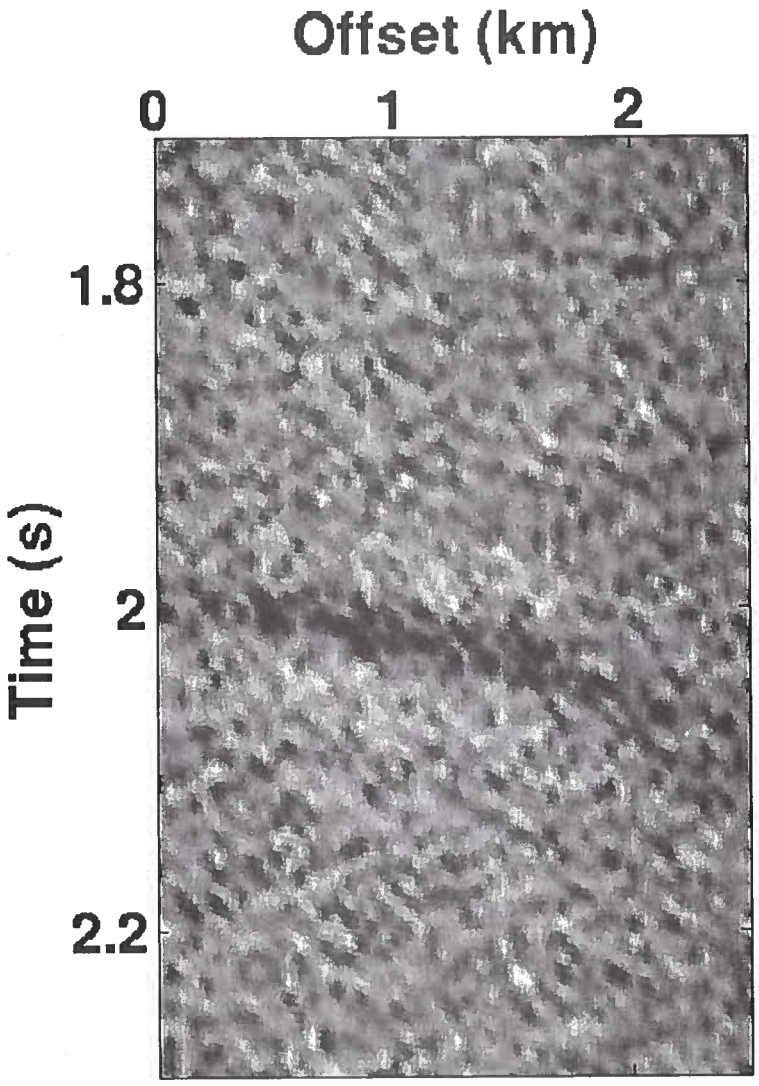

FIG. 3.15. Same CMP gather as in Figure 2.10a with interfering events, now with additive noise such that SNR ≈ 1.

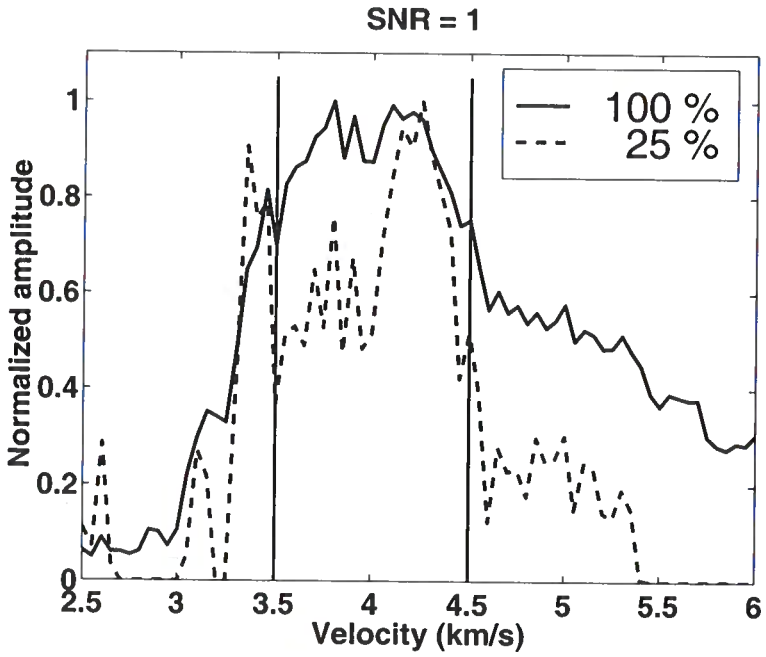

FIG. 3.16. Coherence curves for the CMP data of Figure 3.15 with two interfering events and SNR $\approx$ 1. The vertical lines indicate the correct velocities.

Figure 3.15 shows another noise-contaminated synthetic CMP gather, but now two interfering reflection events are contaminated by the added bandlimited random noise (SNR $\approx$ 1, here). Figure 3.16 shows the coherence curves for the conventional and selective-correlation methods. Although the peaks are at wrong velocity locations, the selective method indicates the presence of two events whereas the conventional method shows only one somewhat smoother peak, also at an incorrect velocity. In this example, the relative error in the primary velocity, picked from the higher velocity peak of the coherence curve computed using selective-correlation sum (25%), is about 8%. The coherence curve computed using a conventional method shows no clearly distinguishable peak associated with the primary velocity. Again the velocity errors are dominated by timing differences on crosscorrelations of trace pairs with larger differential moveout. The errors in picking both the 'primary' and 'multiple' have the same sign, with larger error for the event (primary) with the larger associated stacking velocity.

3.5 Statics-contaminated data

The errors introduced by the presence of added noise result from perceived timing errors in the crosscorrelation process. Static time distortions in data similarly distort the time shifts obtained by crosscorrelation. Figure 3.17 shows a CMP gather with a reflection event containing static distortions (Gaussian random) with a large standard deviation of

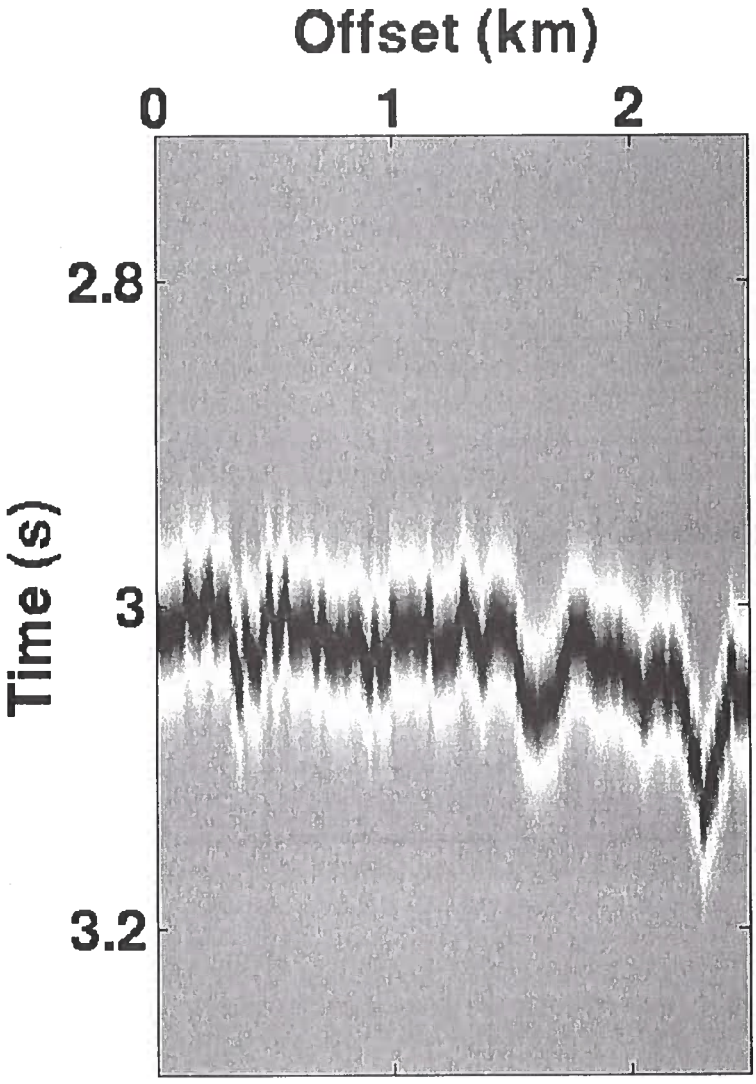

FIG. 3.17. Synthetic CMP gather containing a rflection at $t_0 = 3$ s, with random static time distortions (standard deviation = 80 ms) applied.

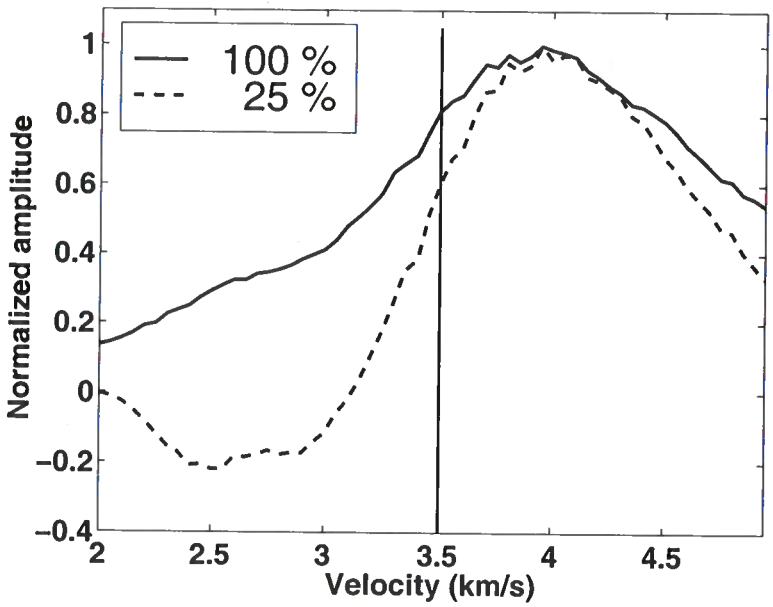

FIG. 3.18. Coherence curves, for the event in Figure 3.17, computed using conventional crosscorrelation sum (100%) and selective-correlation sum (25%).

80 ms. A 5-point lateral running average was applied to the random sequence of time distortions to introduce lateral correlation in the simulated statics. The model for this example is a single horizontal reflector below a homogeneous layer with velocity of 3.5 km/s and a layer thickness of 5.25 km. The cable length is 2500 m, group interval 50 m, number of channels 50, and peak Ricker-wavelet frequency 12.5 Hz. Figure 3.18 shows the velocity curves for the statics-distorted reflection, again using conventional crosscorrelation sum, and selective-correlation sum for 25% of crosscorrelation. For these data, NMO is comparable to the sizable statics distortions imposed. As seen in Figure 3.18, the peaks in the velocity curves are biased toward velocities that, for this realization of statics, are about 500 m/s higher than the correct velocity. Again, as happened for tests with added noise, the peaks of the coherence curves computed using both the conventional and the selective-correlation method coincide, but at this wrong velocity value. Also, as with added noise, the velocity peak for 25% is narrower than that for 100%, but both are broader than the peaks for data not contaminated by noise or statics distortions (Figure 3.19). All these observations hold for other tests with statics-contaminated data (not shown here), the only essential difference being a change of the location of the peak with each different realization.

Static distortions have action on coherence curve for CMP data with two interfering events that is similar to that seen when such data were contaminated by added random noise (Figure 3.16). The result of contaminating the data in Figure 2.10a with laterally smoothed static shifts is shown in Figure 3.20. Figure 3.21 shows the corresponding velocity curves in which, again, the solid curve is for the conventional method while the dashed one is for the selective method. The conventional method produced only one maximum near the

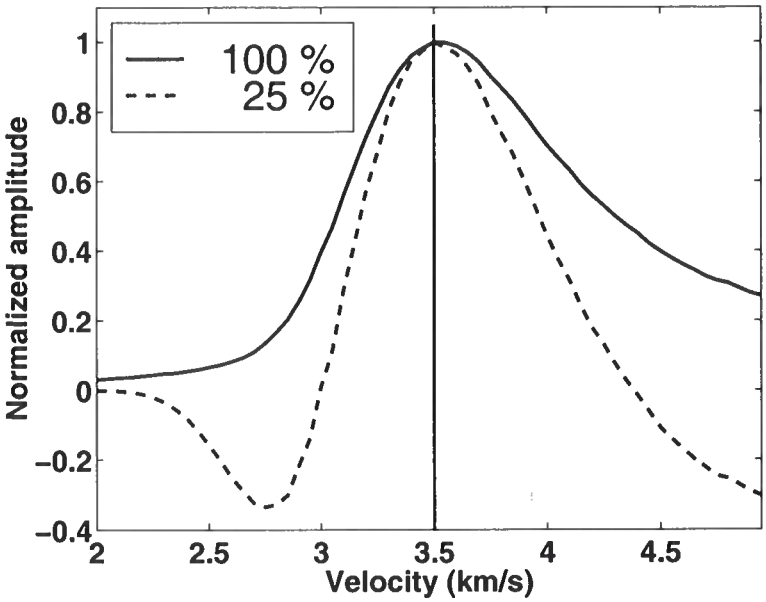

FIG. 3.19. Coherence curves, for the event in Figure 3.17, but with no contamination by noise or static distortions, computed using conventional crosscorrelation sum (100%) and selective-correlation sum (25%).

velocity of the higher velocity event (biased toward a velocity between those of the primary and of the multiple). Fortuitously this peak coincides with one of the maxima of the curve computed with the selective-correlation method, with its higher resolution power. The selective-correlation method has detected the presence of two reflection events, with the lower velocity event fortuitously showing a maximum near the correct velocity.

3.6 CMP gather with many reflections

Bringing more realism into the synthetic data examples, I generated CMP gathers with a series of 50 primary reflections and 50 multiples (both with Poisson distribution of arrival times) for the one-dimensional velocity model of Figure 3.23. The curves in that figure represent the interval and rms velocities for multiples (left) and primaries (right).

Figure 3.22 shows an 64-fold CMP gather with spreadlength of 3.15 km, trace spacing of 50 m, Ricker-wavelet peak frequency of 18 Hz, and, for now, no noise. Now, primaries are interfered with not only by multiples but also by other primaries. The velocity spectra computed using both conventional crosscorrelation sum and selective-correlation sum are shown in Figure 3.24. In both velocity spectra the dashed lines show the rms velocity of multiples (lower velocity) and that of the primaries (higher velocity). As in examples above, in the conventional method the interference between maxima corresponding to primaries and multiples makes difficult the correct identification of peaks with primary velocities,

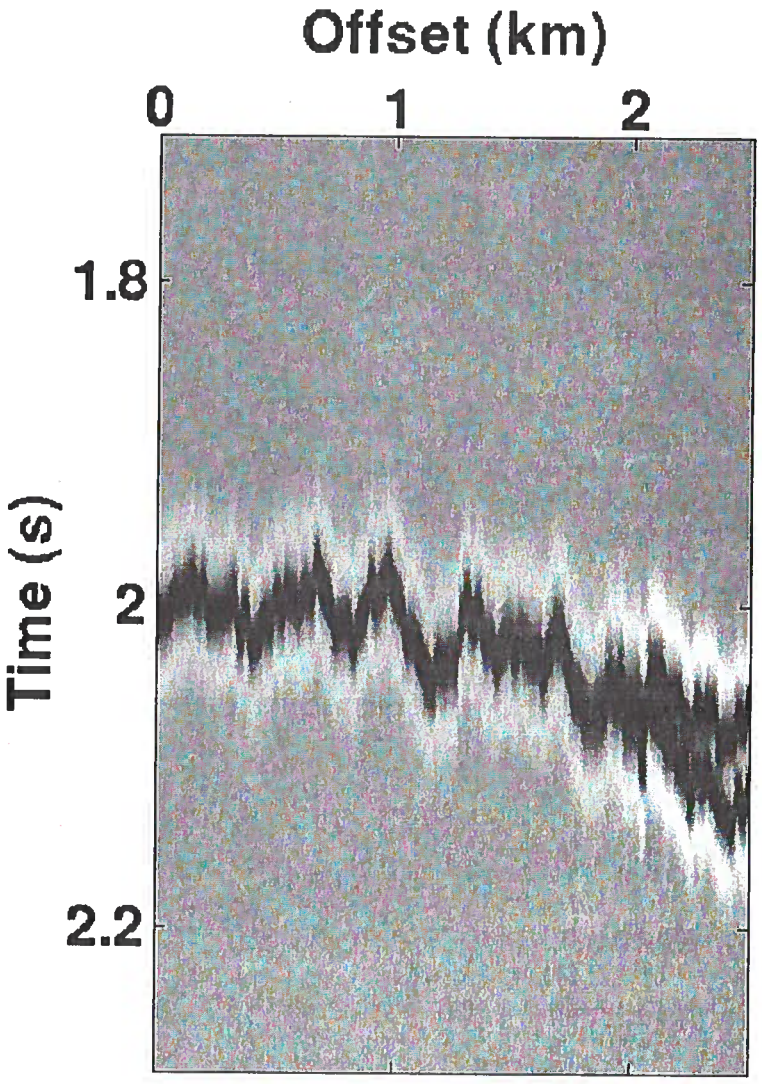

FIG. 3.20. CMP gather as in Figure 2.10a with interfering events, contaminated by randomly generated static time distortions.

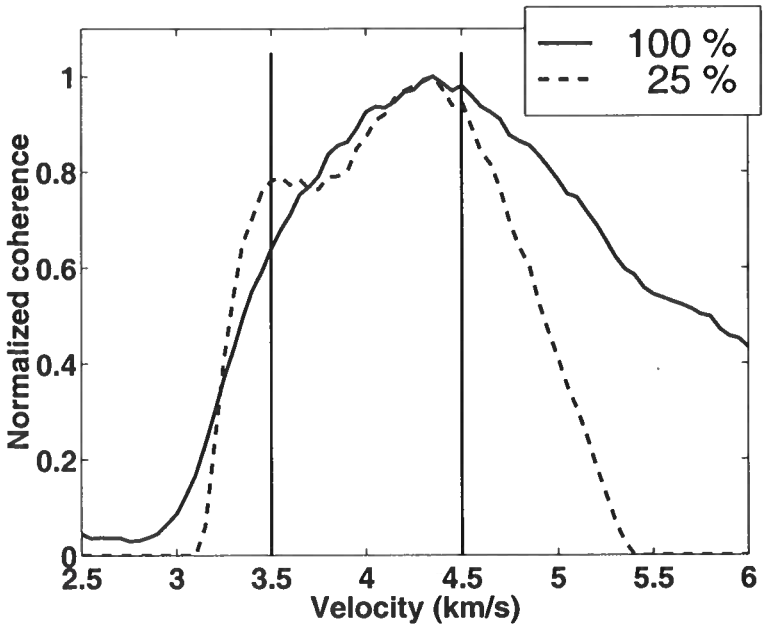

FIG. 3.21. Coherence curves at $t_0 = 2$ s for the data with interfering events of Figure 3.20.

especially below 2 s. Considerably higher resolution is achieved in the results of selective-correlation sum for 25% of crosscorrelations, allowing better identification of the primary velocity function.

Adding a bit more realism to the model, I included in the CMP gather of Figure 3.22 both static distortions and added uncorrelated noise with Gaussian statistics (Figure 3.25). These perturbed data have laterally smoothed static distortions with standard deviation of 20 ms, and added bandlimited random noise with SNR $\approx$ 2. Figure 3.26 shows the velocity spectra for these data. Higher resolution, again, is achieved with the selective method compared to that achieved by the conventional one. In this example, the results of the selective-correlation method are biased slightly toward higher velocities due to the perturbations in the data; however, the higher resolution achieved by this method still allows more accurate picks compared to those made on the velocity panel with a conventional method. Such synthetic model data are useful for testing new approaches such as selective-correlation velocity analysis, but they still lack the complexity of field data. Ahead, in Chapter 5, I show field data applications using selective-correlation velocity analysis in which velocity resolution is also improved compared to that of conventional methods.

Certainly, another way to reduce the number of crosscorrelations to 25% of the original is simply to halve the fold of the data by dropping every other trace from the CMP gather, thereby doubling the group interval. This action, however, by no means increases the resolution of stacking velocity. The total number of crosscorrelations performed in the calculation of the spectrum of a 64-fold CMP gather, for fixed trial velocity and normal-

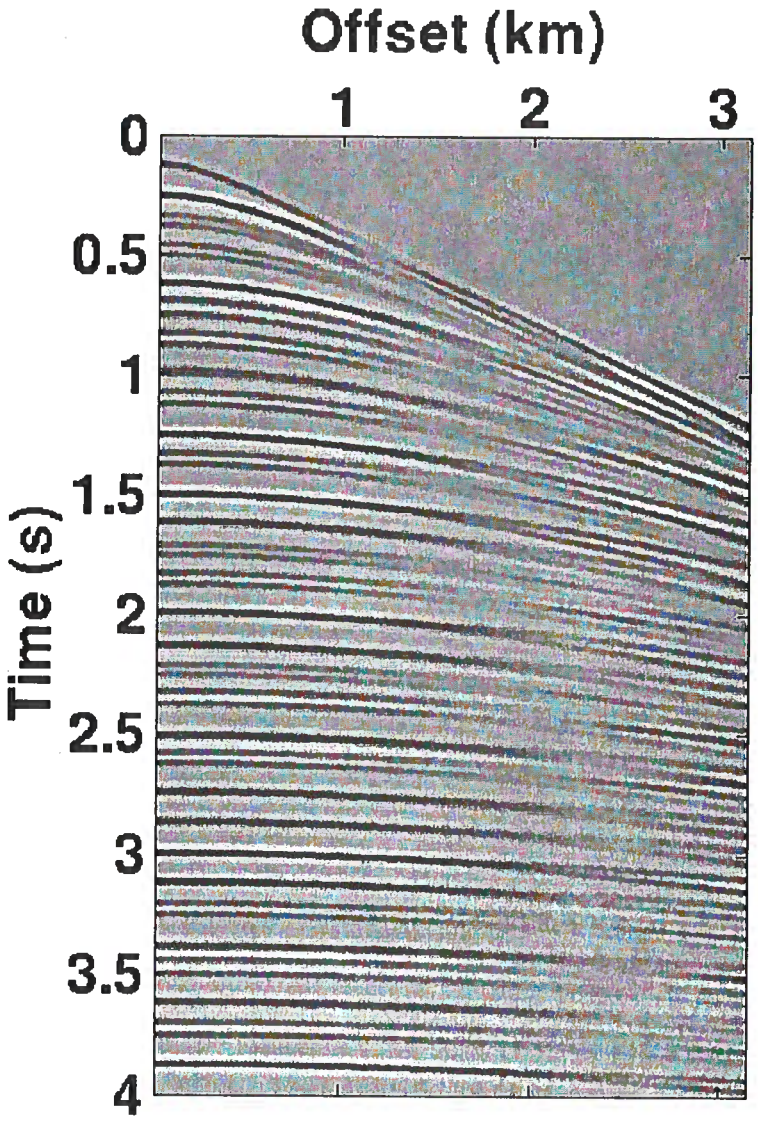

FIG. 3.22. Noiseless synthetic CMP gather with many primary reflections and associated multiples.

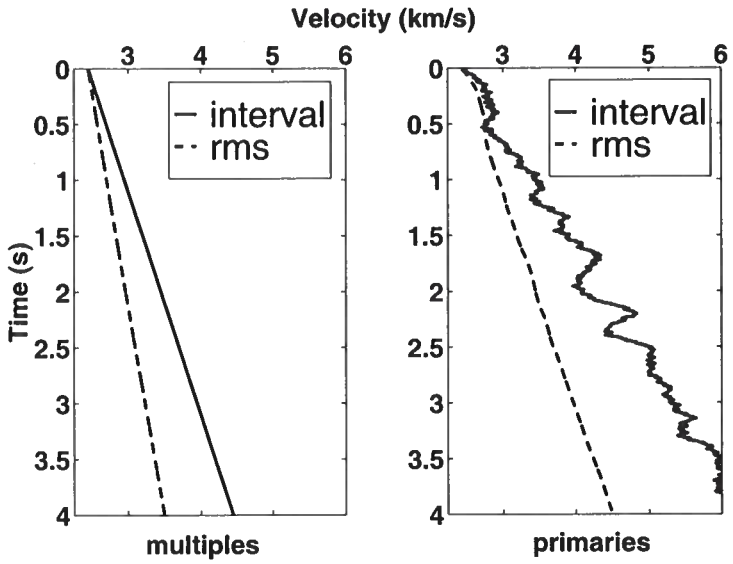

FIG. 3.23. One-dimensional velocity model for multiples (left) and primaries (right).

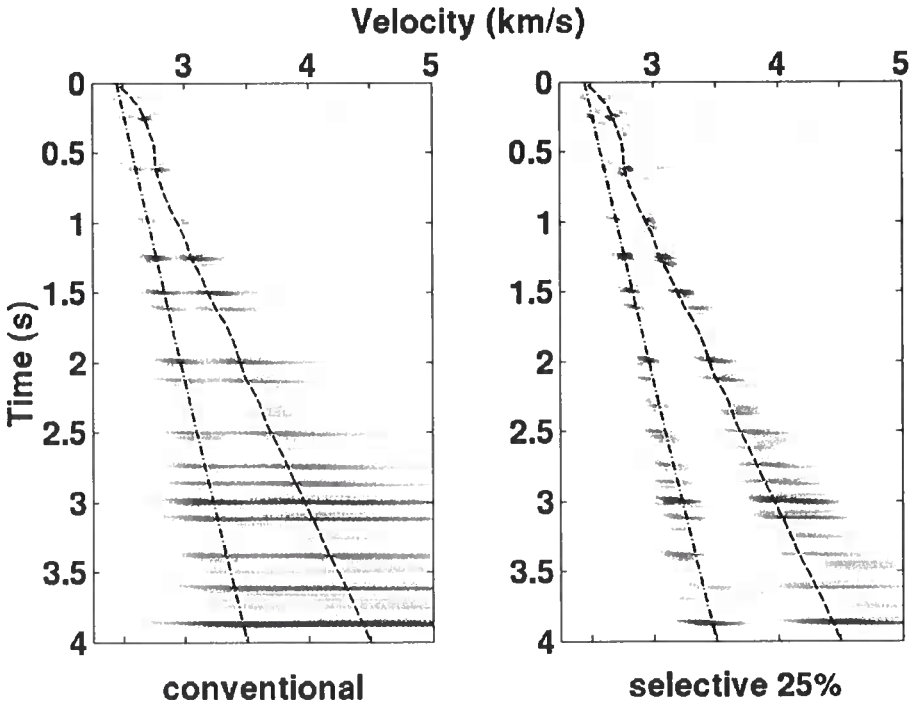

FIG. 3.24. Velocity spectra, using conventional crosscorrelation (left) and selective-correlation sum (right) for 25% of crosscorrelations, for the CMP gather with many reflections in Figure 3.22.

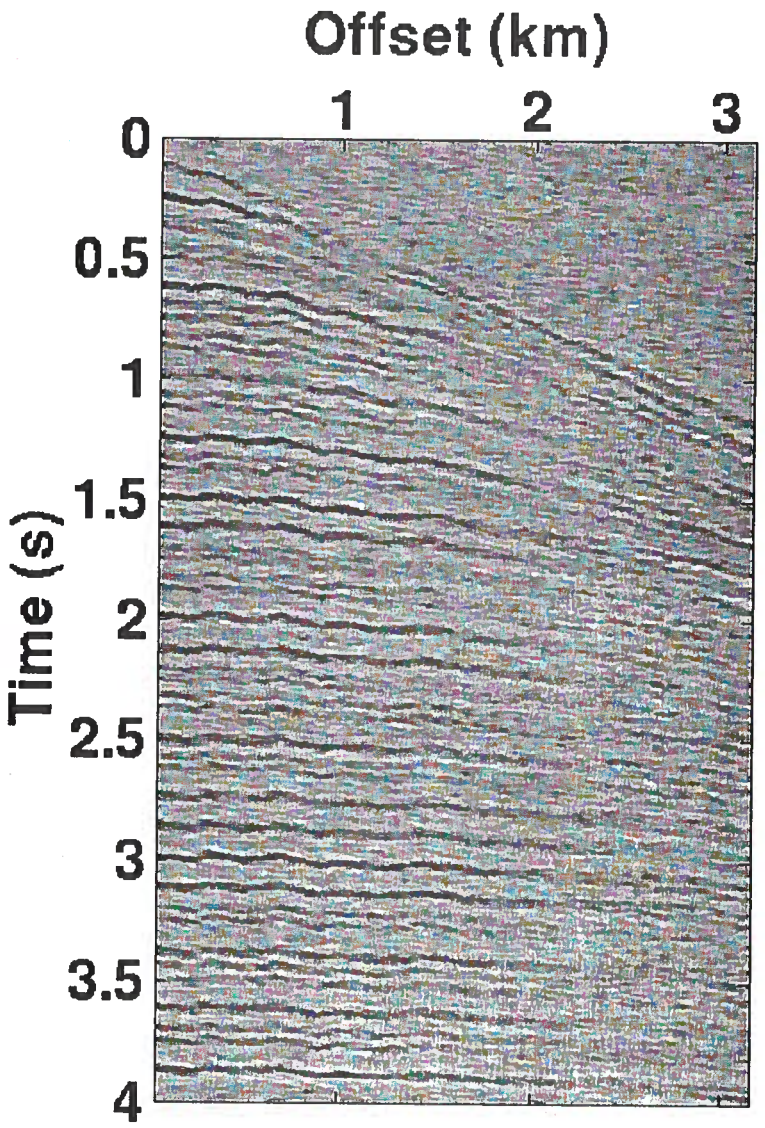

FIG. 3.25. Same synthetic CMP gather of Figure 3.22 with many reflections, now contaminated by random noise and static distortions.

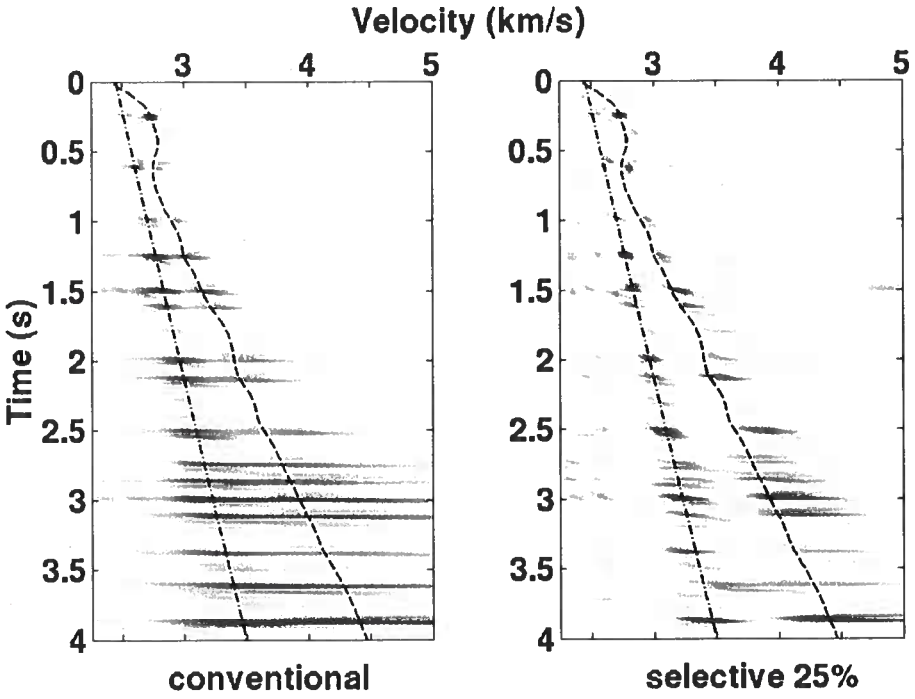

FIG. 3.26. Velocity spectra, using conventional crosscorrelation (left) and selective-correlation sum (right) for 25% of crosscorrelations, for the CMP gather (Figure 3.25) with many reflections contaminated by random noise and statics.

incidence two-way time, is around 2000. This means that, only about 500 crosscorrelations are included in the sum when 25% is chosen in the selective-correlation velocity analysis for these CMP data. The CMP gather shown in Figure 3.27 is the same as that of Figure 3.25, but with fold reduced from 64 to 32 by doubling the trace spacing. Thus, the total number of crosscorrelations in conventional crosscorrelation sum (i.e., with no deletion of crosscorrelations based on differential moveout) for these data is the same ($\approx$ 500) as when we applied selective-correlation sum using 25% of crosscorrelations to the 64-fold data. Figure 3.28 shows the velocity panels for the 64- and 32-fold data using conventional crosscorrelation sum. This demonstrates that reducing fold and performing conventional velocity analysis fails to change velocity resolution. Besides some spurious peaks at about 1.5 s, no significant differences on the character of the velocity spectra are seen between the velocity panels of the 64- and 32-fold data.

By lowering the fold even more, from 32- to 16-fold, again by increasing the group interval, the conventional crosscorrelation sum uses only 120 crosscorrelations. To achieve the same number of crosscorrelations using the selective approach for the 64-fold CMP gather (Figure 3.25), only 6% of all crosscorrelations would be included in the sum. Figure 3.29 shows the velocity panel computed using the selective-correlation sum (6%) and that of conventional crosscorrelation sum for the 16-fold CMP gather. Although somewhat noisier, the velocity panel for the 16-fold CMP gather is essentially the same in character as those for the 32- and 64-fold CMP gathers. The panel computed using selective-correlation sum (6%), however, shows serious problems with extraneous peaks (artifacts) because of the extremely low percentage of crosscorrelations included in the sum. Nevertheless, the good separation of primary and multiple velocities remains.

Figure 3.29 exemplify two extreme cases: (1) in the velocity panel computed using a conventional method the fold in the CMP gather is considerably low compared to the fold in data acquire in modern acquisition, and (2) in the panel using the selective approach the percentage of crosscorrelations that are included in the sum is so low that spurious peaks complicate the interpretation. For such low percentage, the selective approach lacks the contributions from trace pairs with intermediate as well as small differential moveout. This leaves only those crosscorrelations with rapid variation as a function of velocity. Tests on synthetic data (not shown here) show that in presence of additive random noise and statics distortions for percentages of 20% or higher, the selective-correaltion sum has stability that is comparable to that of conventional methods.

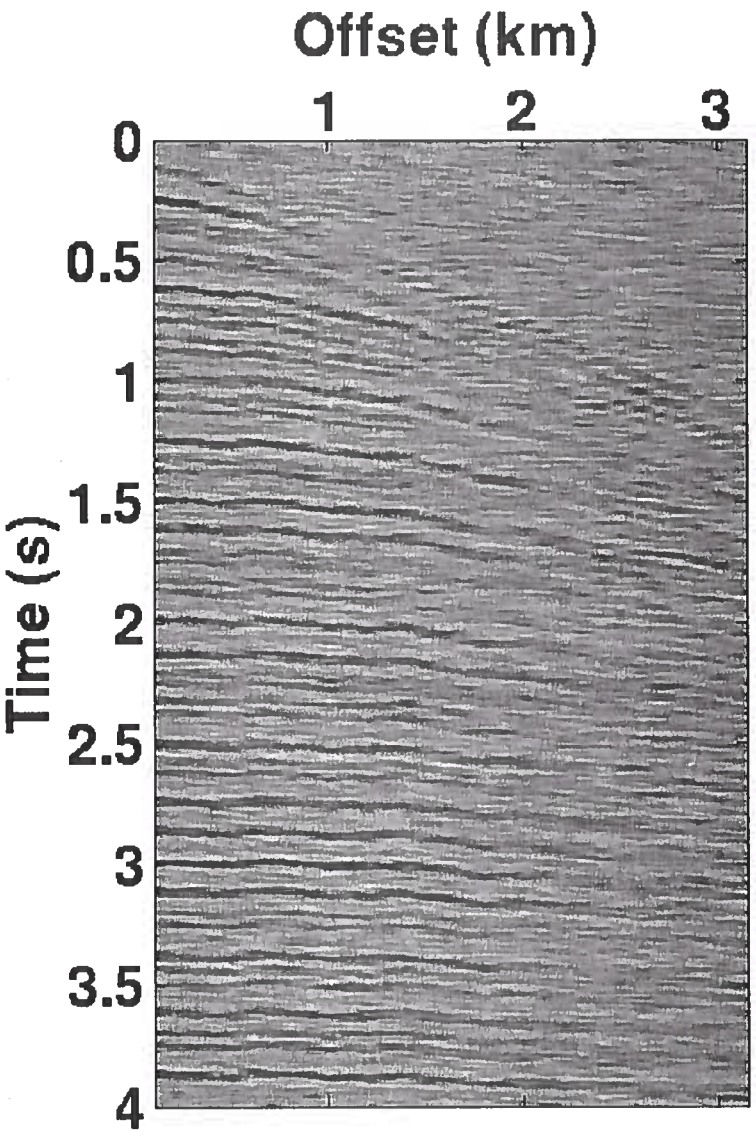

FIG. 3.27. Same synthetic CMP gather of Figure 3.25, with fold reduced from 64 to 32, while maintaining the full spreadlength.

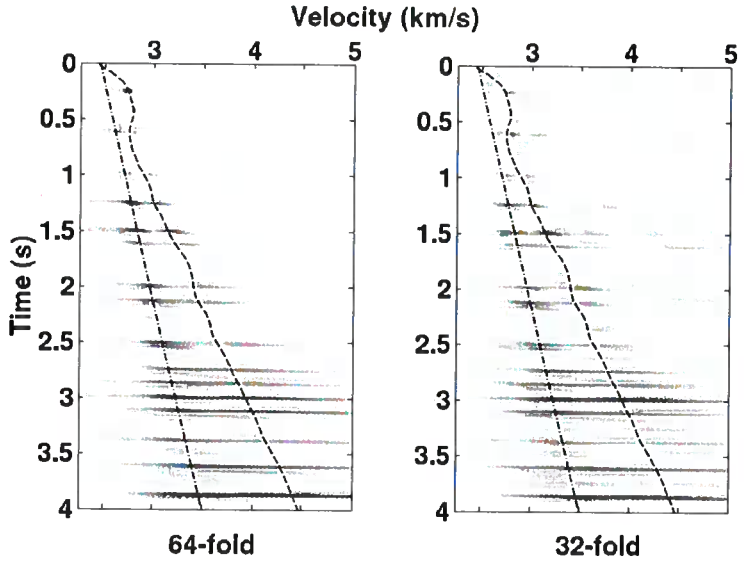

FIG. 3.28. Velocity panels computed using conventional crosscorrelation sum for the 64-fold CMP gather (Figure 3.25) and the 32-fold CMP gather (Figure 3.27).

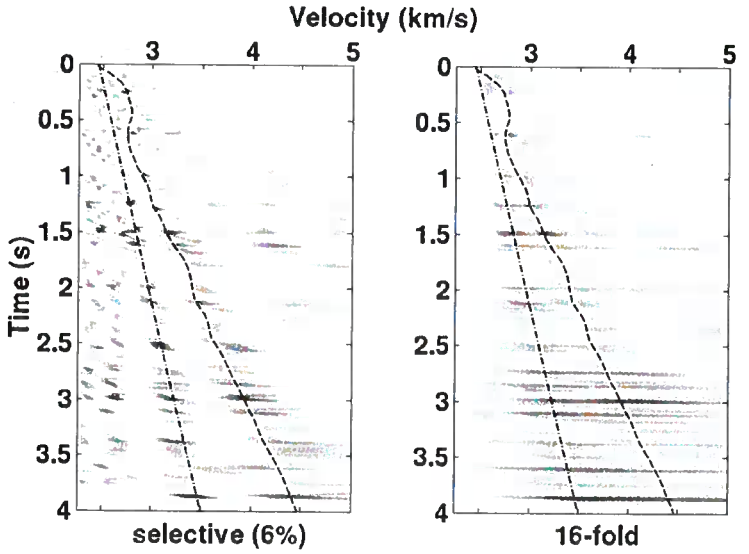

FIG. 3.29. Velocity panels computed using selective-correlation sum (6%) for the 64-fold CMP gather (Figure 3.25) and conventional crosscorrelation sum for the same CMP gather with a reduced fold of 16-fold (not shown) by increasing the group interval.

Chapter 4

ISSUES

The examples shown in Chapter 3 illustrate familiar issues of resolution limitations and uncertainty in velocity analysis for data contaminated by added noise, static distortions, and interfering events. They also show improved resolution with preserved stability when the selective-correlation is used. In this chapter, I first analyze uncertainties in velocity estimation introduced by traveltime errors that may have been caused by either static distortions or random noise. To do so, I use error-propagation analysis to express the variance in the velocity, and the bias (difference between the expected velocity estimate using the data with errors and the true velocity) in terms of the errors in the reflection traveltimes. We will see traveltime errors magnify into velocity-estimation errors least for trace pairs with relatively large differential moveout. We will also see that these trace pairs have the largest influence on velocity errors and resolution.

Also, I model coherence curves as the superposition of asymmetric Gaussian functions to address issues related to the biasing or shifting of the coherence curve peaks in the presence interfering events. This modeling allows us to study the bias as a function of the breadth of the curves as it relates to the difference between primary and multiple velocities. Comparisons between the curves of velocity bias obtained by modeling and those obtained from velocity analysis using the conventional and selective methods show similarity in the shapes of the curves, aiding in the understanding of loss of resolution and biasing of velocity estimates when multiples interfere with primaries. The understanding gained holds despite the facts that coherence curves for individual events are not Gaussian-shaped and that superposition of the coherence curves of primary and multiple is only an approximation to the resultant curve when both events are present in the data. We find again that, all other factors held fixed, the biasing is smaller for the selective-correlation method.

4.1 Traveltime errors

For a reflection with hyperbolic moveout, rms velocity v, and zero-offset two-way traveltime t_0, the reflection time on traces j and k are given by

$$t_k^2 = t_0^2 + \frac{x_k^2}{v^2}, \tag{4.1.1}$$

and

$$t_j^2 = t_0^2 + \frac{x_j^2}{v^2}, \tag{4.1.2}$$

where x_j and x_k are the offsets for traces j and k. Solving for v, we get

$$v = \left(\frac{x_j^2 - x_k^2}{t_j^2 - t_k^2} \right)^{1/2} . \tag{4.1.3}$$

Now, let us introduce perturbations in just t_j, which can be due any combination of static distortions and random noise. Let d be the time perturbations, a random variable normally distributed with zero mean and variance σ_d^2. The perturbed traveltimes are $\widetilde{t_j} = t_j + d$, where the mean, or expected value is the zero-error traveltime, $E\left[\widetilde{t_j}\right] = t_j$. When we introduce $\widetilde{t_j}$ in expression (4.1.3), v also becomes a random variable $\widetilde{v}$

$$\widetilde{v} = \left(\frac{x_j^2 - x_k^2}{\widetilde{t_j}^2 - t_k^2} \right)^{1/2} . \tag{4.1.4}$$

Analysis of propagation of errors (Davidson et al., 1997) in expression (4.1.4) gives estimates of the variability and bias (difference between the expected velocity estimate using the data with errors and the true velocity) in the velocity, as a function of the variability in the traveltimes. The variance of $\widetilde{v}$, σ_v^2, is given by

$$\sigma_v^2 \approx \left(\frac{\partial \widetilde{v}}{\partial \widetilde{t_j}} \right)^2_{\widetilde{t_j}=t_j} \sigma_d^2 \qquad = \frac{v^2 t_j^2}{\left(t_j^2 - t_k^2\right)^2} \sigma_d^2, \tag{4.1.5}$$

and the velocity bias, b_v, is

$$b_v \approx \frac{1}{2} \left(\frac{\partial^2 \widetilde{v}}{\partial \widetilde{t_j}^2} \right)_{\widetilde{t_j}=t_j} \sigma_d^2 \qquad = \frac{v\left(2t_j^2 + t_k^2\right)}{2\left(t_j^2 - t_k^2\right)^2} \sigma_d^2. \tag{4.1.6}$$

These expressions are well defined when $t_j \neq t_k$, which holds for $x_j \neq x_k$, as we require. Also, the approximations in expressions (4.1.5) and (4.1.6) are valid when $\widetilde{t_j}$ is close to its mean value t_j; that is when the variance of $\widetilde{t_j}$ is relatively small. Note that the bias in velocity estimate (for timing errors with zero mean) results from the nonlinearity of the mapping from reflection time to velocity, as in equation (4.1.4). This gives a nonzero value for the second derivative in equation (4.1.6).

Figure 4.1 shows curves of velocity standard deviation, σ_v, versus the magnitude of differential moveout $|\Delta t| = |t_j - t_k|$, for values of the standard deviation in the traveltimes of $\sigma_d = 10$, 20, 30 and 40 ms. The modeled reflection has a zero-offset two-way traveltime $t_0 = 1$ s and rms velocity $v = 2.0$ km/s. In this example, x_k has been set to 0.5 km, and x_j varies from 1 to 3 km. Thus t_k is constant and t_j increases as x_j increases. From Figure 4.1, the standard deviation decreases monotonically for increasing differential moveout (or increasing separation between x_k and x_j). Note that the sign of the differential moveout

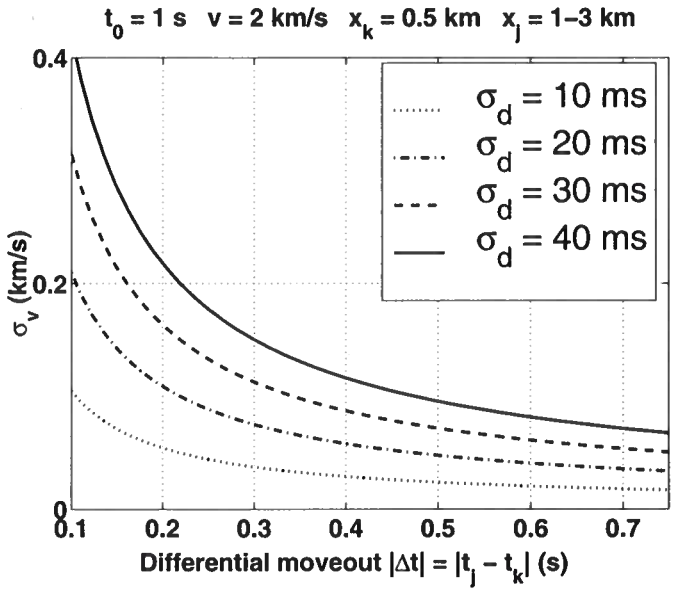

FIG. 4.1. Curves of standard deviation in velocity estimate versus differential moveout computed using formula (4.1.5), for different values of the errors σ_d in the traveltimes at offset x_j. The zero-offset two-way traveltime of this reflection is $t_0 = 2$ s.

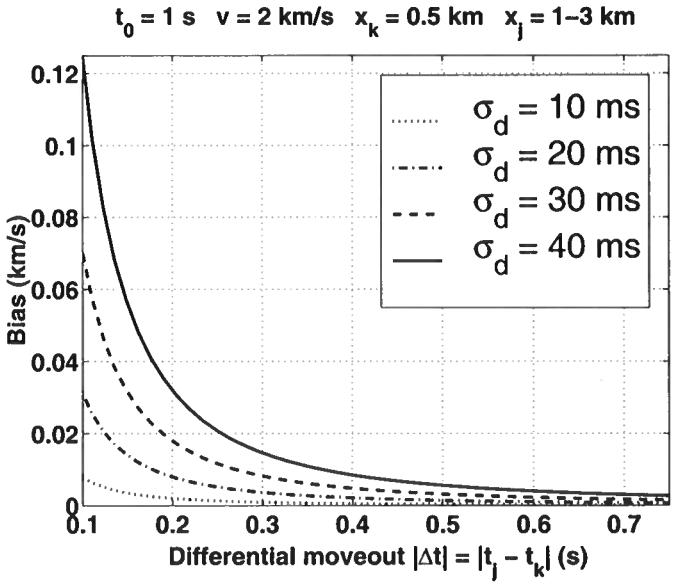

FIG. 4.2. Curves of bias in velocity estimate versus differential moveout computed using formula (4.1.6), for different values of the errors σ_d in the traveltimes at offset x_j. The zero-offset two-way traveltime of this reflection is $t_0 = 1$ s.

$t_j - t_k$ can be positive or negative depending on the relative positions of offsets x_k and x_j; still these two characteristics hold as long as $x_j \neq x_k$.

The proportionality of the standard deviation of the velocity and that of traveltime is evident in Figure 4.1. Also, as mentioned above, for large differential moveouts all the curves converge to zero error. This confirms intuition that selecting crosscorrelation pairs with relatively large differential moveout, as in selective-correlation sum, can improve the resolution of velocity estimates.

At zero-offset time equal to that of a single-reflection event with traveltime errors, the standard deviation of the velocity estimate in a coherence curve may be identified with the breadth of the curve, and the bias with the location of its peak. Therefore, ignoring factors such as frequency content in the data and interfering events, the standard deviation of the velocity would be associated with resolution and bias with accuracy. The bias given by approximation (4.1.6) thus represents by how far the expected velocity estimated using erroneous traveltimes differs from the correct value.

Figure 4.2 shows curves of bias versus differential moveout with the same parameters as in the example of Figure 4.1. The observations made for the variance are also valid for the bias. Specifically, the larger the standard deviation in the traveltimes the larger the velocity bias estimate; also, all curves of bias tend to zero for large differential moveout for fixed standard deviation in the traveltimes. This implies that constraining the summation to those crosscorrelation pairs with large differential moveout will reduce the bias relative to that when we sum over all possible crosscorrelations.

Note also that the bias b_v is always positive. The explanation for this is the following: Assume that $\{t\}_j$ is the traveltime of a hyperbolic reflection on trace j. If we add errors d with zero mean and standard deviation σ_d to the traveltime, the traveltime with errors $\{t+d\}_j$ will fall within the time interval $I = [t-\Delta t, t+\Delta t]_j$, which is centered on the zero-error traveltimes $\{t\}_j$. Assume also that any traveltime in the interval I is equally likely, and we wish to estimate stacking velocity for the reflection event using only the zero-offset trace, with no errors, and the trace j, with errors. Let us then analyze what happens at the extremes of the interval I. Using the traveltime $t+\Delta t$ to estimate stacking velocity, implying larger NMO, will result in the lower bound (underestimate) of the velocity estimates in the time interval I. In contrast, use of the traveltime $t-\Delta t$, implying smaller NMO, will result in the upper bound (overestimate) of the velocity estimates in the interval I. Now, the range of velocities that overestimate the true velocity in the upper half of the interval I, $(t, t-\Delta t]$, is much larger than the range of velocities that underestimate the true velocity in the lower half of interval I, $[t+\Delta t, t)$. This implies that the mean value of the velocity estimates, within the entire interval I, will produce a velocity that overestimates the true velocity. Bias, as I've defined it here, is the expected value of the estimator minus the true value; therefore, the bias is always positive. This positive velocity bias holds also when the reflections on all traces in a CMP gather have error with zero mean.

The velocity-estimation process using coherence measures, however, is more complex than the simple approximated formulas for variance (4.1.5) and bias (4.1.6), and cannot

be fully explained by them. As shown in Chapters 2 and 3, in the presence of static distortions or random noise, the peak of coherence curves of conventional crosscorrelation sum and selective-correlation sum coincide when the percentage of crosscorrelations included in the sum, whose pair of traces have large differential moveout, exceeds 20%. That means that the bias of the peak in the coherence curve, which indicates the expected velocity estimated based on the data with errors in the traveltimes, is dominated by the cumulative bias of the crosscorrelation pairs with large differential moveout. To exemplify the error accumulation when using coherence measures, consider the simplistic case of a 3-fold CMP gather with a hypothetical reflection at 1 s and velocity of 2 km/s, and with three traces located at offsets 0, 1 and 2 km. If the middle trace (and only that trace) has an error in the traveltime with a standard deviation of 20 ms, the standard deviation and bias in the velocity estimated using only the first two traces will be 180 m/s and will be 22 m/s, respectively; in contrast, using only the second two the standard deviation will be 60 m/s and bias will be 4 m/s. Since the trace combination 1-3 (offsets 0 and 2 km) produce no errors, the velocity uncertainties are determined by the uncertainties in trace combinations 1-2 and 2-3. The standard deviation of the velocity estimate, which is the sum in quadrature of the individual standard deviations, would be 190 m/s; also, the resultant bias would be the simple sum of each bias, 26 m/s. Clearly, the largest contribution to the resultant errors is the trace combination with the smaller differential moveout. The analysis for a CMP gather with much larger fold, with each trace having some random error in traveltime, would be much more complicated, but this analysis of errors for a 3-trace gather characterizes the dominant contributions, to errors, of traces with small differential moveout.

4.2 Interfering events

Resolution may loosely be defined as the ability to distinguish two overlapping functions, usually of the same form, in a set of observations. In optics, this is called *two-point resolution*, which is the ability to distinguish the images of two closely located point sources. The classical limit to this two-point resolution is the *Rayleigh resolution limit* (Rayleigh, 1874), which is intended to define the minimum distance at which two overlapping sinc-function patterns can still be distinguished in visual observations of their sum. Although the goal here is not to give a specific resolution criterion for stacking velocity in the presence of two interfering events, the analysis below is somewhat related to that of Rayleigh resolution.

Figure 4.3 shows unnormalized coherence curves, computed using the conventional crosscorrelation sum, for the example with two interfering events of Figure 2.10a. The two dashed curves are the coherence curves for each of the reflection events separately, meaning that the velocity spectra computation used a single-reflection CMP gather as input, without interference from the other event. The solid curve is that measured one when the input to the spectra computation is a CMP gather containing both interfering events. The vertical lines indicate the correct velocity of the events. Several observations can be made from these curves: First, note how the breadth of the dashed curves vary with velocity; the curves are narrower toward lower velocities and then, after reaching their peaks, become

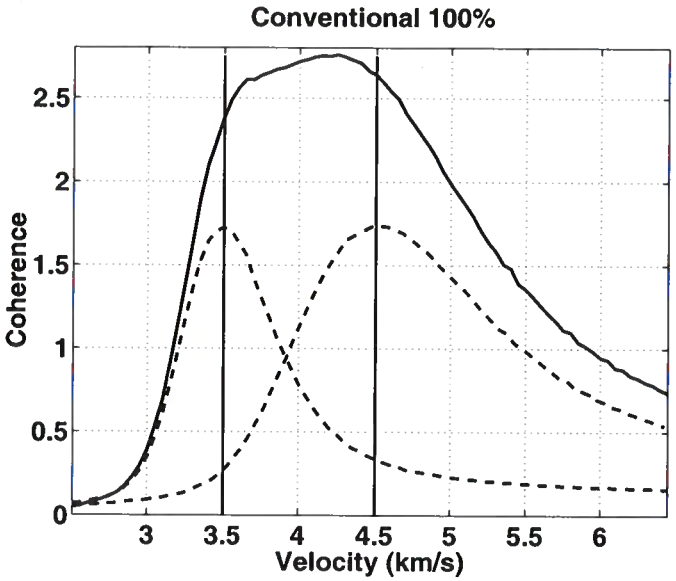

FIG. 4.3. Unnormalized coherency curves, computed using conventional crosscorrelation sum. The dashed curves pertain to isolated reflection events with the correct velocity for each indicated by the vertical lines, while the solid is that measured for a CMP gather containing both events. These curves somewhat resemble lopsided Gaussians.

broader toward higher velocities. This asymmetry has its root in the same explanation given for the positive velocity bias observed and explained in the previous section. Any time shift away from that for the peak in a trace crosscorrelation will lead to a magnified departure of the associated velocity from that of the peak, with larger magnification toward higher velocities. Second, the peak amplitudes of the coherence curves, in dashed pattern, are exactly the same because both reflection events were generated using identical wavelets, with no amplitude variation in either time or offset. Third, the coherence curves for the individual reflections resemble lopsided Gaussians, a feature that will be useful later in this section.

Even for this noiseless simplistic example, there is no complete explanation for how these two events interact to produce the coherence curve shown in the solid pattern. Features to note in the solid curve are (1) it shows just one peak, (2) it has stronger amplitude toward the higher of the two true velocities, and (3) the peak is biased from the correct primary velocity toward the velocity of the multiple.

Here, I shall model the behavior of coherence curves in the presence of interfering reflection events, paying especial attention to the biasing of locations of the peaks in absence of random noise. To do so, I assume that the coherence curves extracted from velocity spectra, computed using conventional crosscorrelation sum, can be modeled using lopsided Gaussians, as defined in equation (4.2.7). The same cannot be said for those coherence

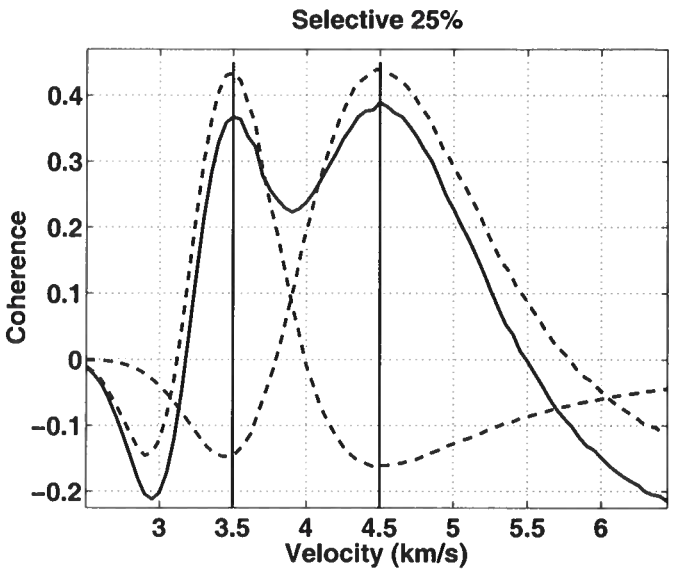

FIG. 4.4. Unnormalized coherency curves, computed using selective-correlation sum. The dashed and solid curves have the same meaning as that given in the caption for Figure 4.3. These curves no longer resemble Gaussians.

curves generated using selective-correlation sum. Figure 4.4 shows similar coherence curves to those shown in Figure 4.3, now using selective-correlation sum (25%); clearly, they no longer resemble Gaussians. Again, the dashed curves were computed for each event separately, and the solid one for both events present in the data simultaneously. The negative side lobes present in the dashed curves will pull the peaks of the solid curve down and also could potentially bias their locations, depending on the frequency content in the data. In the subsequent analyses, however, for simplicity in gaining understanding I will use Gaussians shapes to model the coherence curves.

Let us model a coherence curve C for a single reflection with stacking velocity v_0 as

$$C(v) = \begin{cases} C_L(v)/\max[C_L(v)], & \text{if } v < v_0 \\ C_R(v)/\max[C_R(v)], & \text{if } v \geq v_0 \end{cases}, \tag{4.2.7}$$

where C_L and C_R are

$$C_L(v) = \frac{1}{S_L} \exp\left[-(v - v_0)^2 / S_L^2\right] + K_L,$$

and

$$C_R(v) = \frac{1}{S_R} \exp\left[-(v - v_0)^2 / S_R^2\right] + K_R.$$

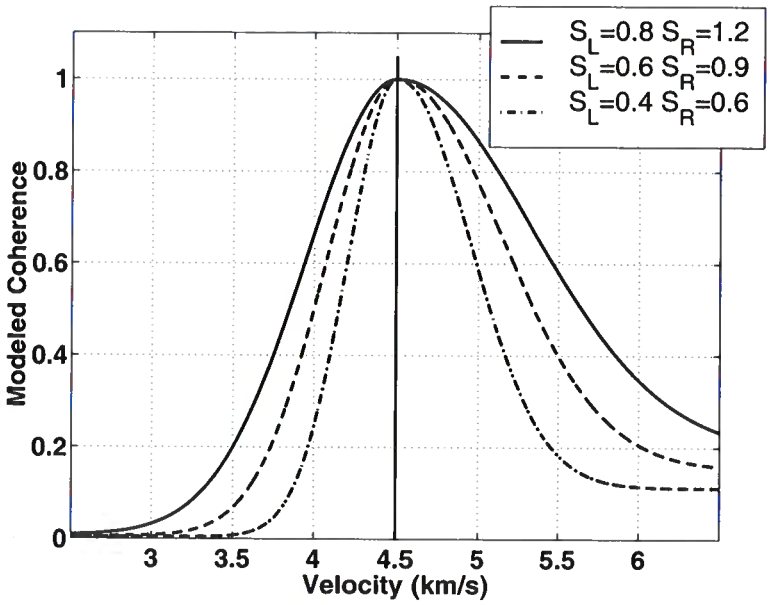

FIG. 4.5. Modeled coherence curves for $v_p = 4.5$ km/s (indicated by the vertical line) for diferent values of S_L and S_R, which control the widths of the curves.

Here, v is velocity, S_L and S_R control the breadth on the left and right sides of the curve, respectively, and K_L and K_R control the modeled coherence amplitudes for velocities much higher and much lower than v_0. Note that the peak of $C(v)$ =1 at $v = v_0$. Figure 4.5 shows modeled coherence curves for a $v_0 = 4.5$ km/s and different values of S_L and S_R, with $K_L = 0.01$ and $K_R = 0.2$; the vertical line shows the location of v_0. These parameters were chosen such that the curves are sharper toward lower velocities and broader toward higher ones, as is observed in actual coherence curves. As the values of S_L and S_R decrease, the curves become sharper, which is equivalent, for fixed t_0, to either (1) increasing the peak frequency in the data used in computing actual coherence curves, or (2) applying selective-correlation sum for a percentage of crosscorrelations used less than 100%. As we saw in examples of Chapter 3, the resolution achieved by conventional crosscorrelation sum for CMP data with a given peak frequency is comparable to that achieved by selective-correlation sum for the same dataset with lower peak frequency. Thus, the solid curve in Figure 4.5 could well represent the coherence curve corresponding to the data when using 100% of crosscorrelations, and the dashed and dashed-dot curves would represent coherence curves using smaller percentages of crosscorrelations, for instance 35% and 25%, respectively.

Expression (4.2.7) can be used to model the coherence curves of a primary C_p and a multiple C_m, with velocities v_p and v_m, respectively. Let us then assume that we can model the coherence curve in the combined presence of primary and multiple by the superposition of these two curves; we assume $C_{p+m} = C_p + C_m$. (No doubt, the superposition is only an approximate description of the process of forming the curve C_{p+m}.) Henceforth, the sub-

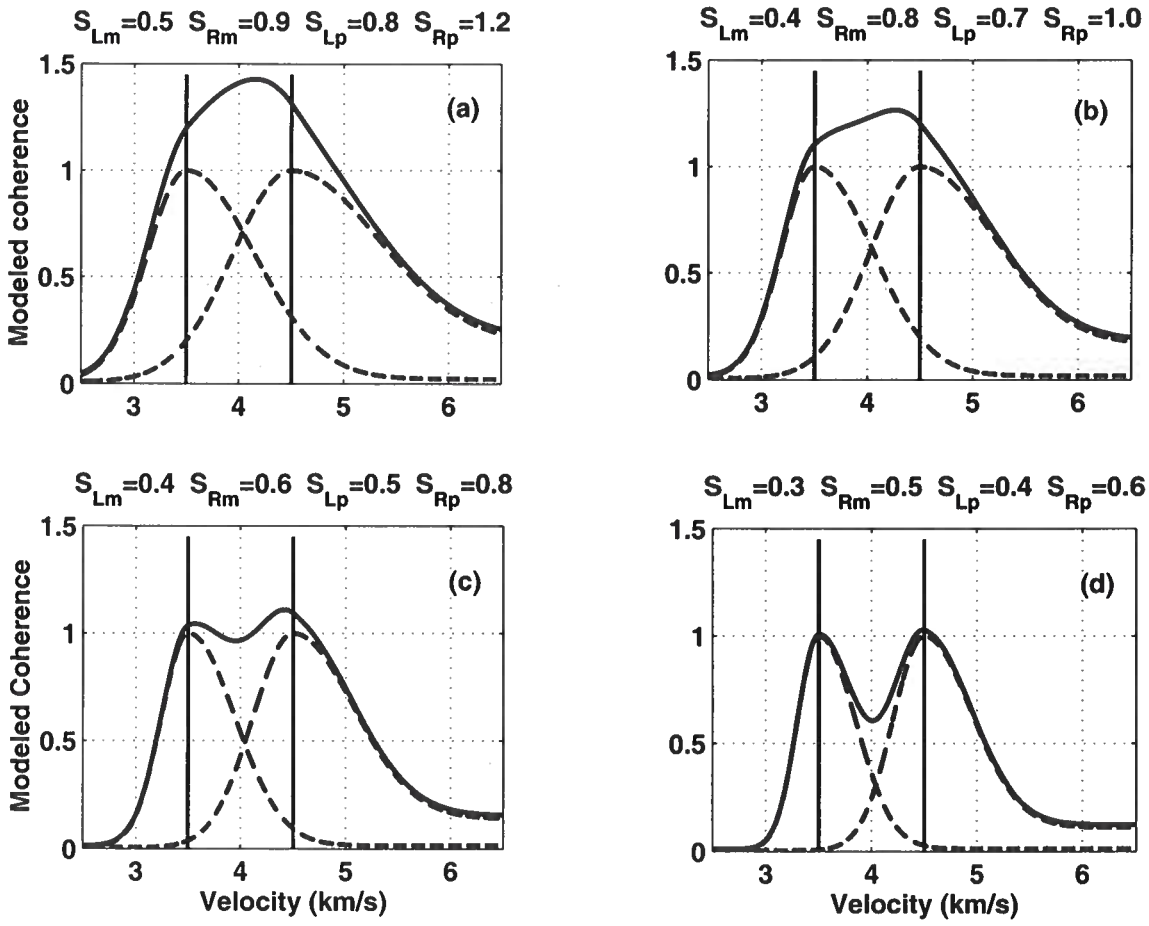

FIG. 4.6. Simulated coherence curves for interfering primary and multiple with $v_p = 4.5$ km/s and $v_m = 3.5$ km/s, respectively. The dashed curves are the modeled curves for the isolated primary and multiple, while the solid one is the sum of two dashed curves. The parameters that represent the widths of the curves, S_L and S_R, decrease in the order of plots (a), (b), (c), and (d).

scripts p and m will be used to refer to modeled primary and modeled multiple parameters. Figure 4.6 shows the coherence curves, modeled with superposition, for different values of S_{Lm}, S_{Rm}, S_{Lp}, and S_{Rp}. The values $K_{Lm} = 0.01$, $K_{Rm} = 0.02$, $K_{Lp} = 0.01$, and $K_{Rp} = 0.2$ are kept fixed for all the following examples. The dashed curves represent the coherence curves of single reflection events, those with peak at 3.5 km/s correspond to the multiple and those with peak at 4.5 km/s to the primary. The vertical lines at 3.5 km/s and 4.5 km/s show the modeled correct stacking velocities. The solid curves, which are the sum of the dashed curves, represent the coherence curves for data containing both primary and multiple events.

Figure 4.6a shows curves that could be associated with a relatively low frequency content in the data. Note that the modeled resultant coherence curve, C_{p+m}, has only one peak, biased to a velocity lower than the true velocity of the primary at 4.5 km/s. Decreasing the values S_L and S_R for the modeled primary and multiple coherence curves is equivalent to increasing frequencies of the data; this is observed in Figures 4.6b, 4.6c, and 4.6d. Figure 4.6b is particularly interesting because of its similarity with the coherence curve of the example of Figure 2.12 and Figure 4.3, when using the conventional crosscorrelation sum method (solid curves). Although in our modeling (Figure 4.6b), both component coherence curves — primary and multiple — have the same peak amplitude, the resultant curve (solid) reaches its peak closer to correct stacking velocity of the primary and has lower values toward the multiple velocity, with no peak associated with the multiple. Two distinct peaks occur in the example of Figure 4.6c, but note that the locations of both peaks are biased away from the correct velocities and toward each other. As in Figure 4.6b, the peak associated with the primary is higher than that associated with the multiple. When the frequencies in the data are high, the coherence curves show no biasing of the peak locations. This modeling is achieved with relatively small S_L and S_R values. In Figure 4.6d the peaks of the modeled resultant coherence curve are in their correct positions, and, unlike the actual coherence curves, both peaks have the same amplitude (compare with those in Figures 3.6 and 3.7). The difference in amplitude in the coherence curves diminishes with increasing peak frequency in the data, or when applying selective-correlation sum method to compute the curves. In the examples shown in Chapter 3, however, the peak of the event with lower velocity (which I have called a multiple) always has a lower amplitude. This may be related to the larger stretching of data when lower velocity is used for NMO correction. The stretching causes the wavelet to change with offset.

With this modeling of coherence curves, let us study the biasing of peak locations, in presence of interfering events, as a function of the breadth of the curves. The bias, here, is the difference between the location of peak of the primary event in the modeled curve and the correct primary stacking velocity, which in the next examples is $v_p = 4.5$ km/s. Parameters S_L and S_R are proportional to the breadth of the curves. To make the study of bias general, I plot dimensionless quantities: bias $\equiv v_p - v$ versus $\Delta v/\bar{S}$, where

$$\Delta v = v_p - vm, \tag{4.2.8}$$

$$\bar{S} = \frac{S_{Rm} + S_{Lp}}{2}, \tag{4.2.9}$$

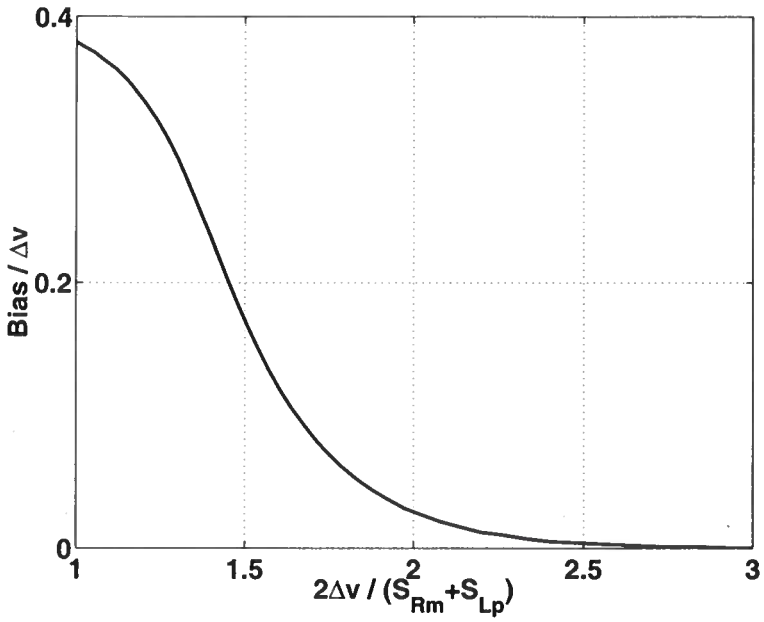

FIG. 4.7. Dimensionless bias in the velocity of the primary event versus dimensionless breadth of the modeled coherence curves.

and v is the velocity associated with the peak in the coherence curve closest to v_p. The quantity $\bar{S}$ is the average of the breadth parameters for the interfering Gaussian shapes associated with the primary and multiple events. This average breadth varies inversely with the frequency content in the data.

Figure 4.7 shows the curve of dimensionless bias in the location of the peak associated with primary velocity versus the dimensionless separation of the peaks. This curve was obtained from the modeled coherence curve by varying the primary velocity from 3.9 to 4.7 km/s, consequently, $\Delta v = v_p - v_m$ varies from 0.4 to 1.2 km/s, for fixed multiple velocity of 3.5 km/s and fixed values of the breadth of the modeled curves of $S_{Lm} = 0.3$, $S_{Rm} = 0.5$, $S_{Lp} = 0.4$, and $S_{Rp} = 0.6$. (Fixing the values of S_L and S_R is equivalent to fixing the dominant frequency in the data). Equivalent curves for dimensionless bias can be also drawn by fixing the difference between primary and multiple velocities Δv, and varying the values of S_L and S_R for both primary and multiple. Figure 4.7 shows that bias decreases rapidly with decreasing breadth of the curve, or equivalently, with increasing dominant frequency in the data. Note that the bias is always positive because the biased peak of the primary in the modeled curves is always located at a lower velocity than $v_p = 4.5$ km/s (i.e., between v_p and v_m).

Under the approximate assumption that the coherence curve for interfering primary and multiple is the superposition of the coherence curves for each of the events, the tendency will be for the locations of the peaks in the summed curve to be shifted from the correct velocities v_m and v_p. Moreover, if Gaussian shapes are used to approximate the coherence

curves for each of the isolated events, the shifts of both peaks will be toward the mean of v_m and v_p. Figure 4.8 illustrates the underlying reason. Suppose curve 1 (Gaussian) is added to curve 2, which is a straight line. The peak in the summed curve, 1+2, will be shifted in the direction of increasing amplitude of curve 2; that is toward decreasing value y in this figure. The amount of shift depends on the slope of the curve 2 and the breadth of the peak region in curve 1. The shift is larger for larger slope and for broader peak region.

Now consider the summation of two laterally separated Gaussian curves. Since each one slopes toward the other, summation will draw the peaks toward one another. Where the primary and multiple velocities are well separated relative to the breadths of the two peak regions, the shifts of the peaks is small. Where they are close to one another, the two peaks merge into a single unresolved peak region. The breadth the individual peak regions (and thus the amount of shifting of the peaks) are governed by a combination of reflection time, spreadlength, stacking velocities of the events, and the frequency content of the data. Also, pertinent to this thesis, the shift (or bias) of peaks is reduced when selective-correlation approach is used for velocity analysis.

Similar curves of bias, computed using conventional and selective methods for the velocity estimation rather than by modeling of superimposed Gaussian curves, are shown in Figure 4.9. The horizontal axis here is also a dimensionless quantity that relates peak frequency of the Ricker wavelet f_p, difference in primary and multiple velocities Δv, and the group interval Δx. The number 0.4 in the denominator scales this dimensionless quantity to the same range of values of Figure 4.7. The Ricker-wavelet peak frequency in the CMP data used here is 18 Hz, the spreadlength is 2.5 km, and zero-offset reflection time is 2 s.

The general shape of the curves in Figure 4.9 is similar to that of the curve shown Figure 4.7, but the latter is smoother because in the modeling I could readily use many values of primary velocities inside the range between 3.9 and 4.7 km/s. I evaluated more than 40 values in this range in modeling using Gaussians, while I computed only seven using the coherence measures. Note that the selective-correlation approach produces unbiased values of the primary velocity for smaller values of the dimensionless difference between primary and multiple velocity than does the conventional approach, implying greater resolving power.

Recall that while Gaussian shapes may model coherence curves computed using conventional methods, it is not a good model for the selective-correlation sum method. In the selective approach, the negative side lobe of the multiple toward higher velocities that are beneath the primary velocity peak can influence the position of the primary peak in different ways depending on the lateral position of the peak with respect to that of the lobe. Near the minimum of the lobe, the slope of the curve for the multiple event changes from being negative, to zero, to positive. Assuming that superposition holds, this time not for Gaussians but for these curves with negative side lobes as in Figure 4.4, the primary peak will be biased toward lower velocities if its location is within the negative slope region of the lobe, toward higher velocities if is within the positive slope region of the lobe, and simply be pulled down if its position coincides with the zero-slope region in the center of the lobe. This can partially explain the behavior of coherence curves computed using the selective approach in presence of interference events. In many tests with synthetic data,

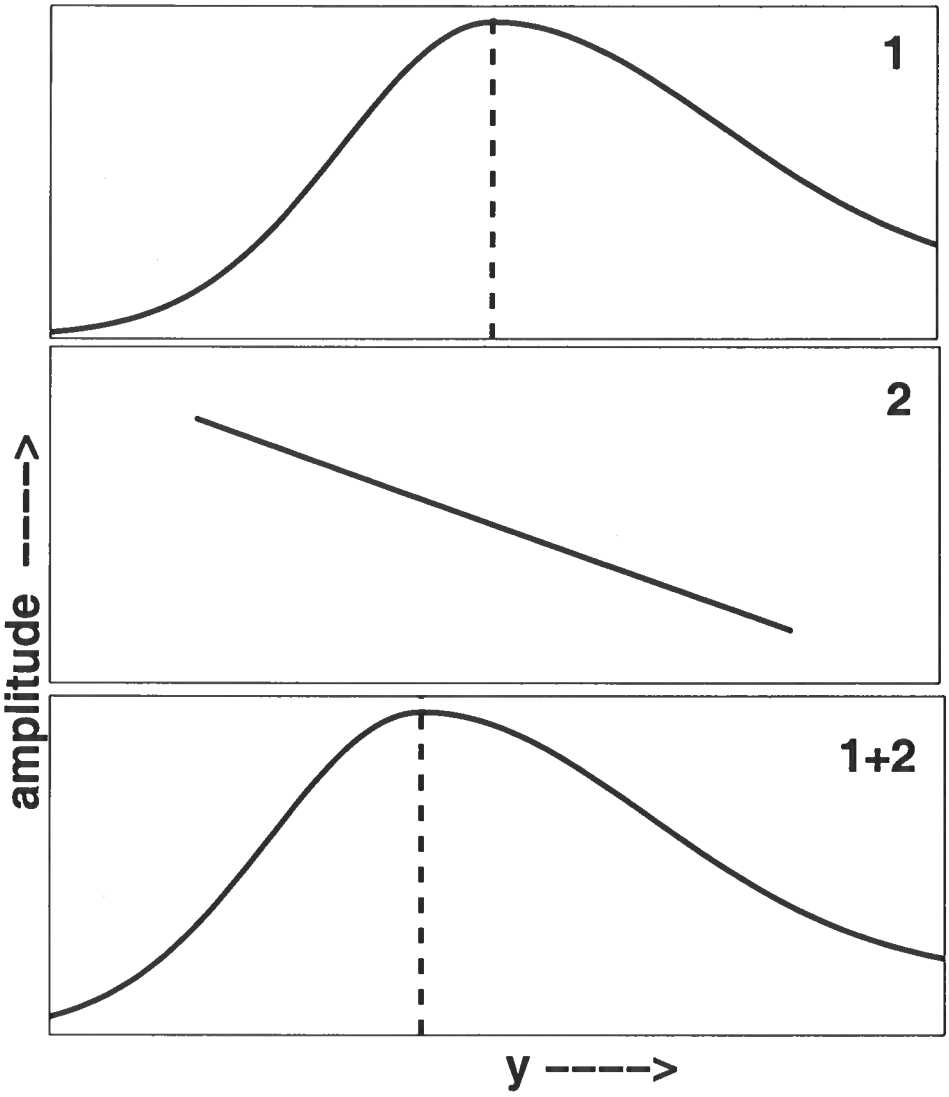

FIG. 4.8. Cartoon illustrating (1) a Gaussian-shaped curve, (2) straight line, representing the local slope of an interfering event, and (1+2) the superposition of curves (1) and (2). The vertical dashed lines show the peak locations before and after superposition of (1) and (2).

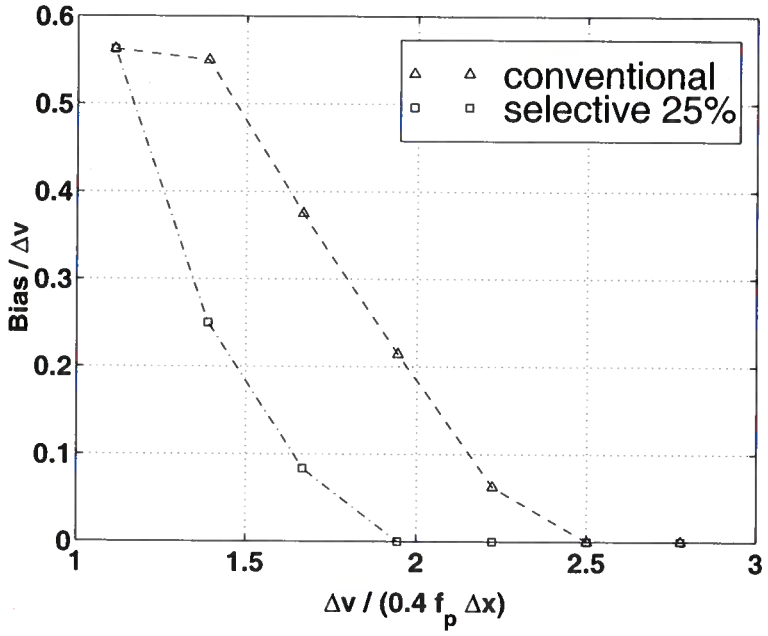

FIG. 4.9. Similar plot to that in Figure 4.7, using selective-correlation sum and conventional crosscorrelation sum instead of the Gaussian modeling. The synthetic model data used here has zero-offset reflection time 2 s, Ricker-wavelet peak frequency 18 Hz, and spreadlength 2.5 km.

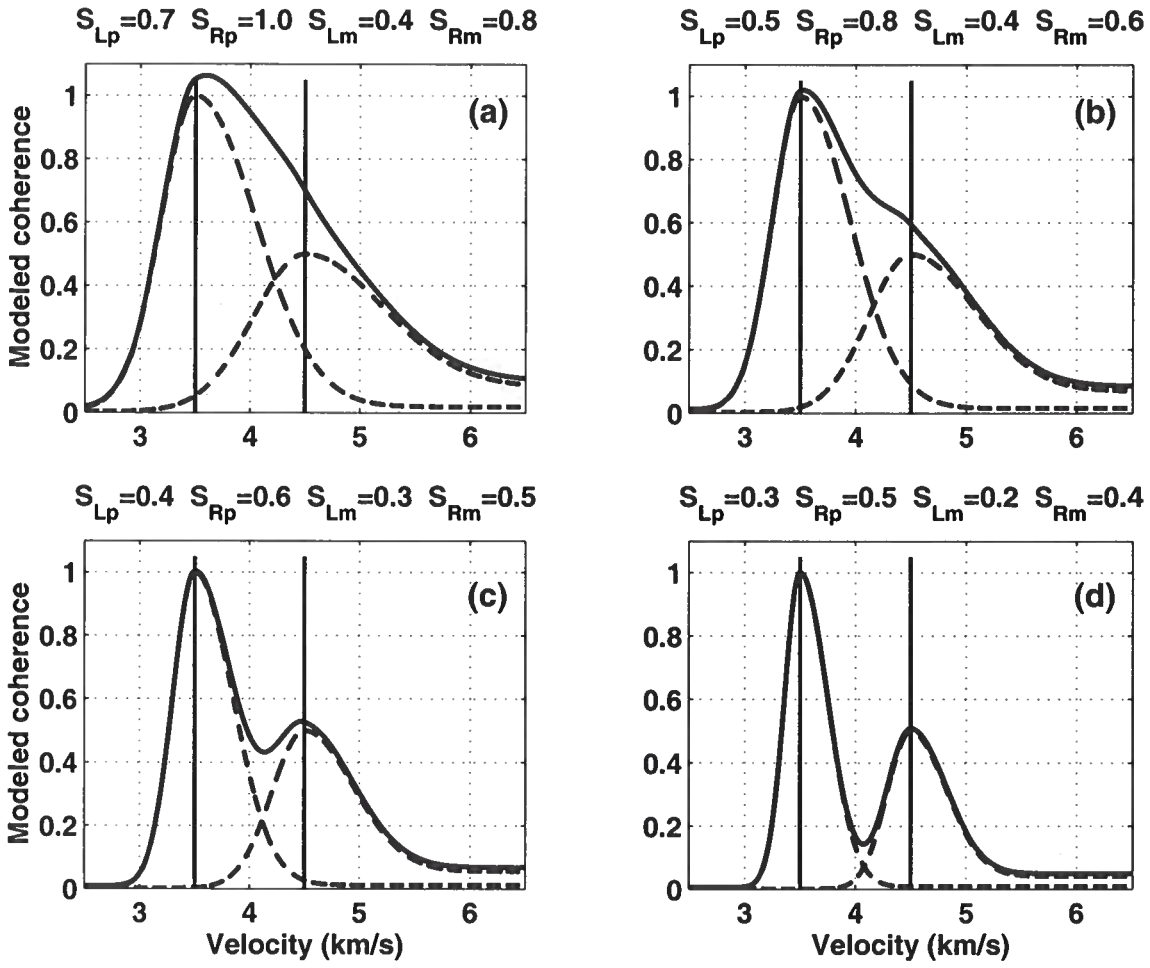

FIG. 4.10. Simulated coherence curves for a primary and a strong multiple interfering with $v_p = 4.5$ and $v_m = 3.5$, respectively. The dashed curves are the Gaussian-shaped modeled curves of the isolated primary and strong amplitude multiple, while the solid one is the sum of the dashed ones. The parameters that represent the width of the curve, S_L and S_R, decrease in the order of plots (a), (b), (c), and (d).

for given spreadlength, frequency content in the data, and SNR, using percentages of the crosscorrelations included in the sum less than 50%, the selective approach produced results that were unbiased or had substantially less bias than that of conventional methods.

All examples above are based on the assumption that the primary and multiple coherence curves have equal amplitude. Now, using modeled curves, let us consider a multiple that generates a coherence curve with twice the amplitude of that of the primary. Such a situation might arise when the amplitude of the multiple on the data traces is $\sqrt{2}$ times that of the primary. Figure 4.10 shows a series of plots, similar to those shown in Figure 4.6, but now with this disparity in amplitudes. The solid curves, again, are the result of summing the dashed curves that correspond to primary and multiple separately. The values related to the breadth of the curves, S_L and S_R, decrease from Figure 4.10a to Figure 4.10d. For relatively large values of S_L and S_R (Figure 4.10a and Figure 4.10b), implying broader curves, only one peak — that of the multiple — appears in the modeled resultant coherence curves. Note, that in order to even identify a peak associated with the primary, values of S_L and S_R corresponding to curves as narrow as those shown in Figure 4.10c are required. This implies that, for a given difference between primary and multiple velocities, relatively high frequency content in the data is needed to resolve the velocity of a primary in the presence of a strong multiple.

Now let us consider for the selective-correlation approach the behavior of coherence curves for a primary event in the presence of a strong multiple. The coherence curve for just the strong multiple will have negative side lobes more pronounced than those of the primary. Even where the selective method shows two separate peaks with no shifting (such as the dashed curve in Figure 3.11), the pull down created by the multiple side lobe will reduce the amplitude of the primary peak. Although no pull down and consequent amplitude diminishing happens in the coherence curves modeled with Gaussians or in those computed using a conventional method (solid curve in Figures 4.10 and 3.11, respectively), the weakened-amplitude primary peak still could be identifiable in the coherence curve for the selective method, while no primary peak is distinguishable in the coherence curve for the conventional method.

Chapter 5

FIELD DATA APPLICATIONS

Picking stacking velocity on velocity panels is an interpretation process that depends mainly on two factors: the quality of the data and the experience of the interpreter. The material to this point in this thesis indicates that for given data and interpreter, selective-correlation velocity analysis should help in reducing uncertainty in the velocity picking.

Even though the preceding tests on synthetic CMP gathers exhibit some of the problems that arise in seismic data they do not come close to capturing all the complexity of field data. Here, I present applications to land and marine CMP gathers, using semblance coefficient, unnormalized and normalized conventional crosscorrelation sum, and unnormalized and normalized selective-correlation sum. We shall see that, for both datasets, use of selective-correlation sum (either normalized or unnormalized) indeed enhances resolution in the velocity analysis.

5.1 Land CMP gather

These data, from eastern Venezuela are split spread, with offsets ranging from -6.6 to 6.6 km, and offset increment of 200 m (Figure 5.1). This CMP gather is the result of averaging five neighboring CMP's to increase the signal-to-noise ratio. The dominant frequency at 3 s is around 25 Hz.

Figure 5.2 shows the velocity spectra of these data using semblance coefficient (Figure 5.2a), unnormalized crosscorrelation sum (Figure 5.2b), and unormalized selective-correlation sum - 25% - (Figure 5.2c). The semblance coefficient was computed using the Seismic Un*x (SU) program (Cohen and Stockwell, 1999), **suvelan**. Where reflections are strong, conventional crosscorrelation sum and selective-correlation sum (Figures 5.2b and 5.2c, respectively) show a better standout of the velocity maxima than that of semblance coefficient (Figure 5.2a); however, where the signal is weak, especially in the shallow part of the data, the semblance coefficient shows higher values. The velocity maxima are sharper in the velocity panel computed using selective-correlation sum (Figure 5.2c). Figure 5.3 is a detail of Figure 5.2. The velocity values picked for the two events in the panels of semblance coefficient and conventional crosscorrelation sum marked with the arrows are essentially the same. In the panel computed using the higher-resolution selective-correlation method, however, these two events have an observable velocity difference that can be important for stratigraphic study and other purposes.

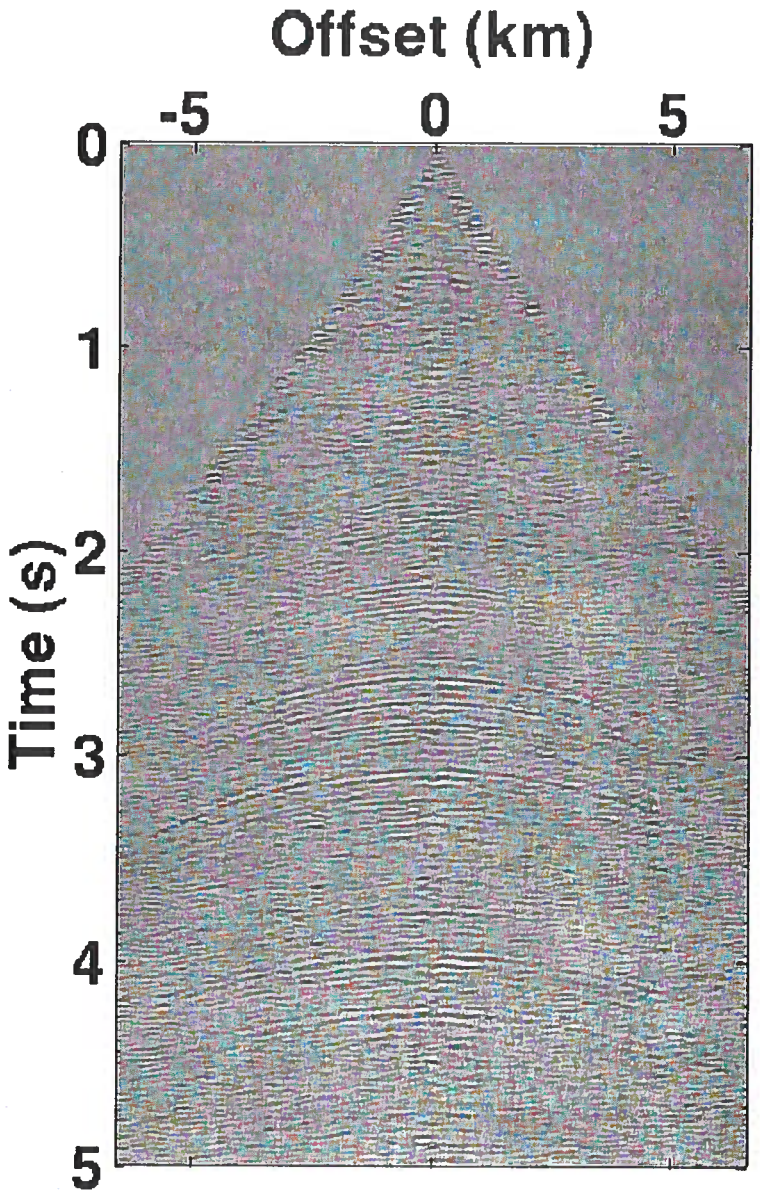

FIG. 5.1. Land CMP gather in which five neighboring CMPs have been averaged to increase the signal-to-noise ratio.

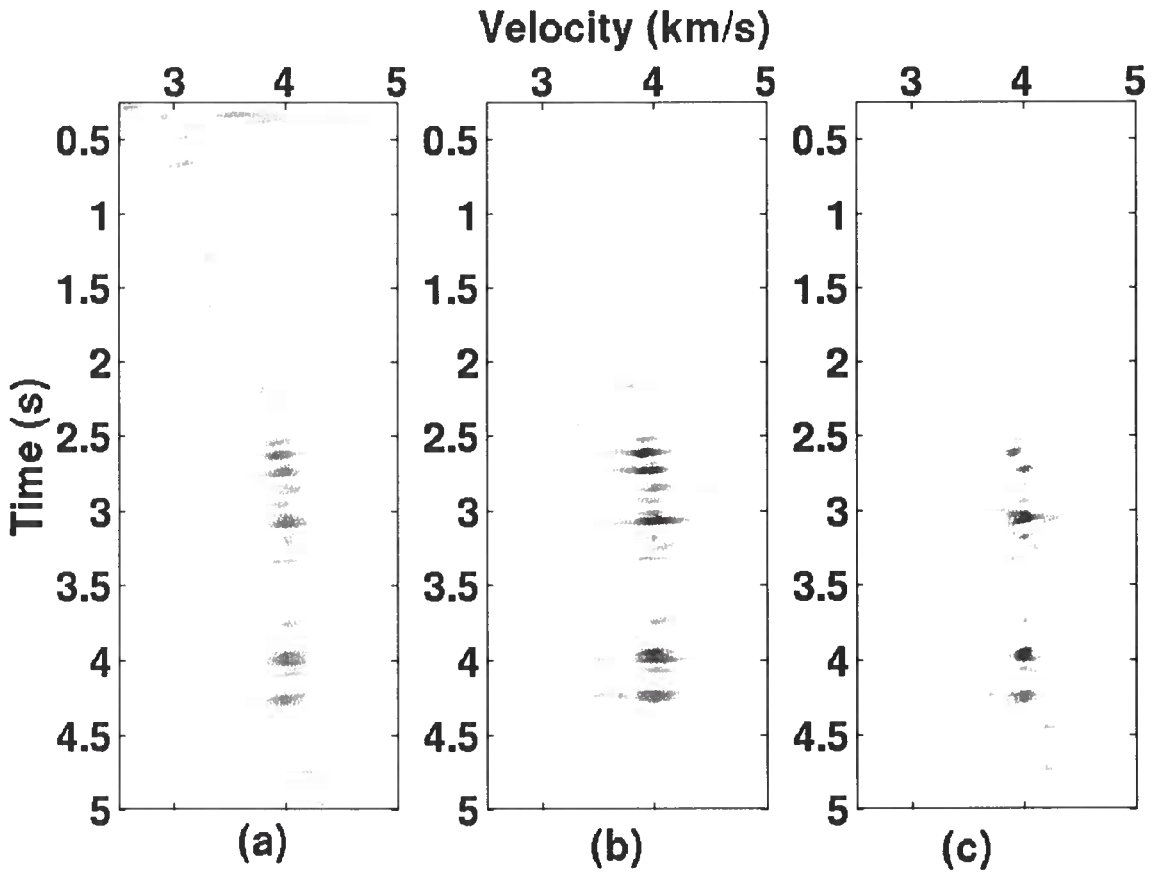

FIG. 5.2. Velocity panels for the CMP gather in Figure 5.1 computed using (a) semblance coefficient, (b) unnormalized crosscorrelation sum, and (c) unnormalized selective-correlation sum (25%).

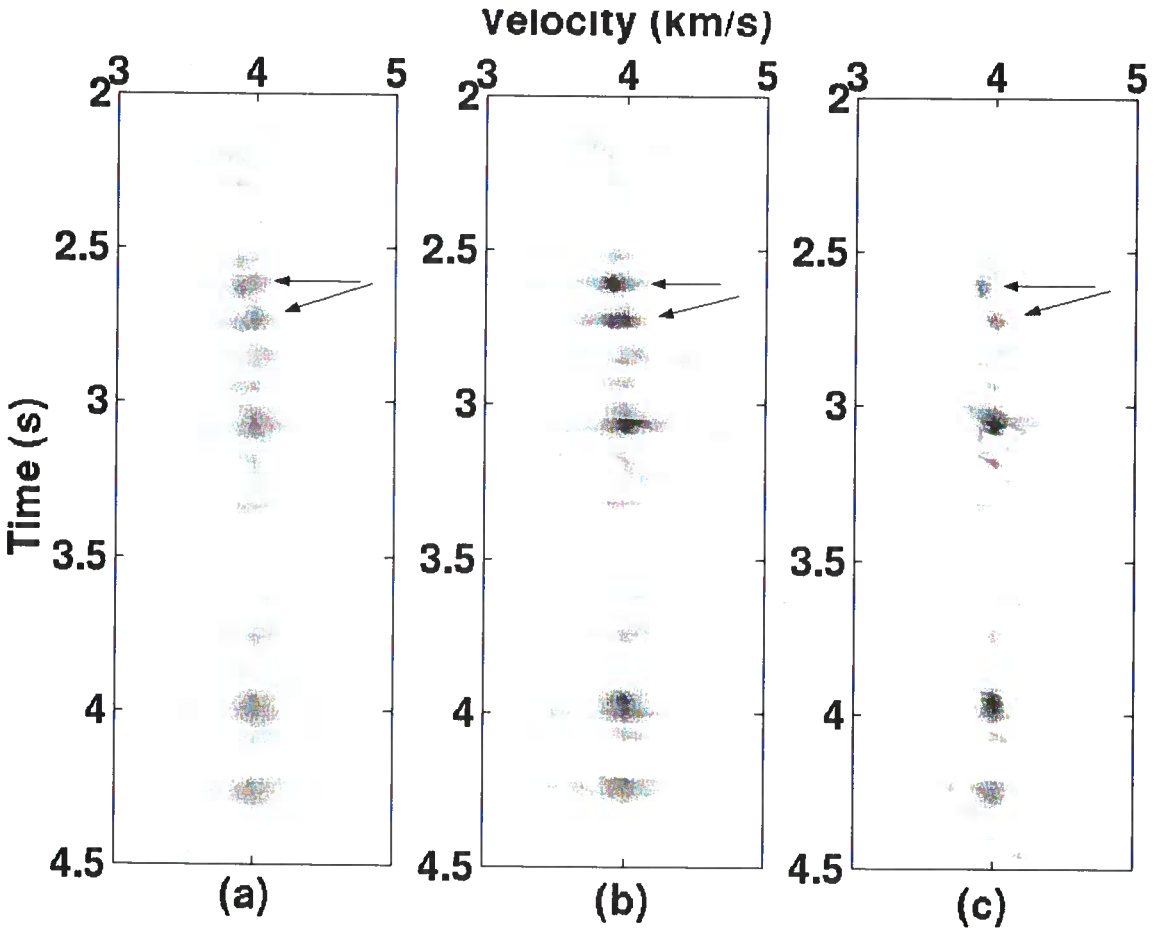

FIG. 5.3. Detail of Figure 5.2 showing the higher resolution achieved by selective-correlation sum (25%) in the events marked by arrows, compared to that achieved by the other two methods.

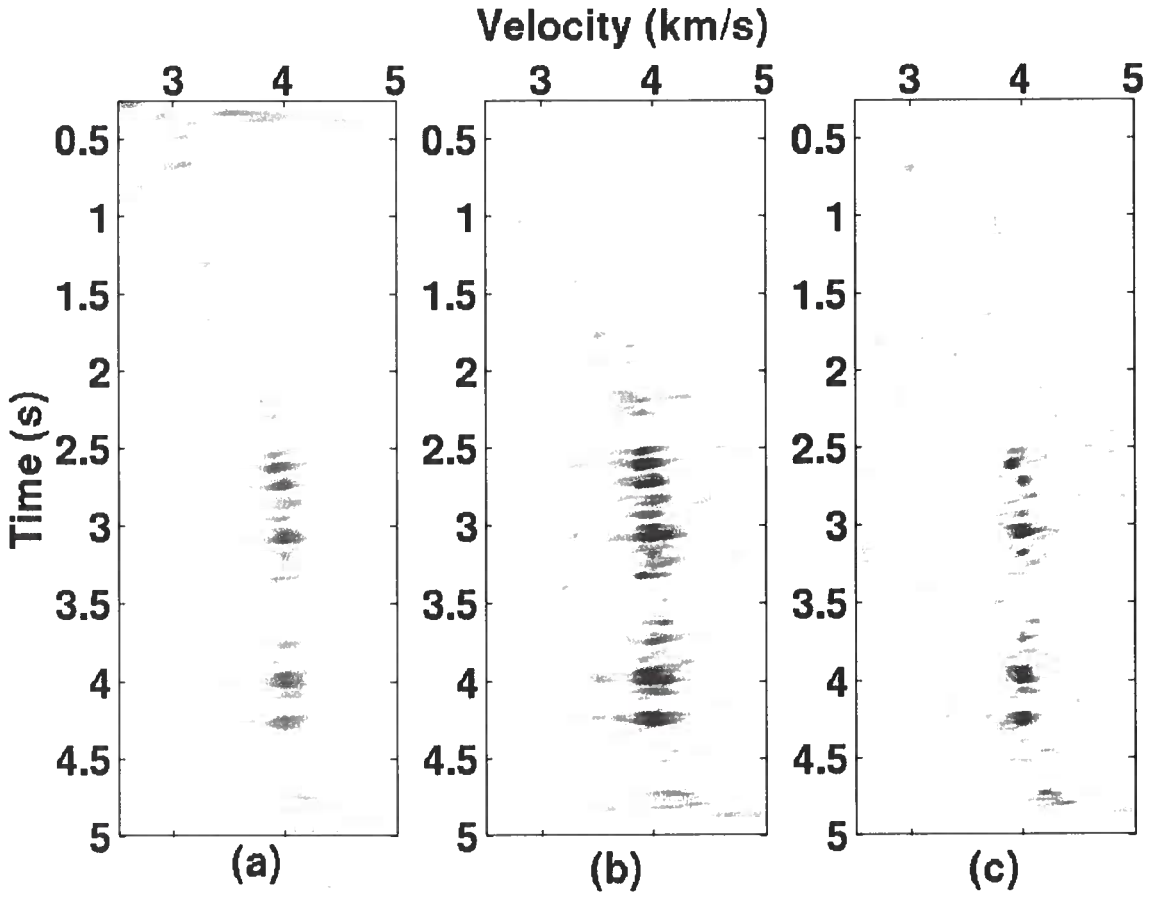

FIG. 5.4. Similar plot to that in Figure 5.2, now using in the velocity panels (b) and (c), normalized crosscorrelation sum and normalized selective-correlation sum.

Figure 5.4 shows a set of velocity panels similar to those shown in Figure 5.2, now using normalized coherence measures for conventional crosscorrelation sum and selective-correlation sum (Figures 5.4b and 5.4c). Again, the normalized version of the selective approach shows sharper velocity maxima than those in velocity panels computed using the semblance and the normalized conventional crosscorrelation sum (Figures 5.4a and 5.4b, respectively). Velocity panels (b) and (c), which seem noisier than those corresponding to the unnormalized measures shown in Figures 5.2b and 5.2c, bring out weak spectral amplitudes that may or may not correspond to velocities of primary events.

In this example, selective-correlation allows us to pick more precisely features that already were present in the velocity panels of the other two coherence measures. In the next example, the selective-correlation method brings out features with velocity for primary events that were not evident in the panels based on conventional coherence measures.

5.2 Marine CMP gather

Figure 5.5 shows a CMP gather with strong water bottom multiples indicated by the arrows. These data were recorded with a spreadlength of 3 km and offset increment of 50 m, and approximately 40-Hz dominant frequency at 3 s.

Figure 5.6 shows velocity panels for the data in Figure 5.5 computed using semblance coefficient, unnormalized conventional crosscorrelation sum, and unnormalized selective-correlation sum (Figures 5.6a, 5.6b, and 5.6c, respectively). The panels corresponding to semblance coefficient and conventional crosscorrelation sum are largely dominated by the velocity of the multiples, with little evidence of primary velocity. The velocity panel computed using selective-correlation sum – 25% – (Figure 5.6c) shows features with a better chance of being associated with primaries. These features are best evidenced in the velocity panel computed using normalized selective-correlation sum - 25% - (Figure 5.7c). Some of these features also appear to some extent in the panel for the normalized conventional crosscorrelation sum (Figure 5.7b). The difference between these velocity panels is more clearly seen in the enlargement shown in Figure 5.8. The event at 3.5 s, marked with the arrows in the three panels, appears more clear in the panel computed using selective-correlation sum (Figure 5.8c), while the event around 3.5 s is present only in this velocity panel. The later two events at around 4.2 and 4.7 s, indicated by the arrows, are present in all panels but with higher resolution in the panel corresponding to selective-correlation sum (Figure 5.8c).

Other interpretations can be made from these velocity panels. The higher resolution achieved by the selective-correlation sum, however, can reduce uncertainty in the velocity picking, allowing the analyst to deal with the tradeoff between resolution and effectiveness in attenuating noise.

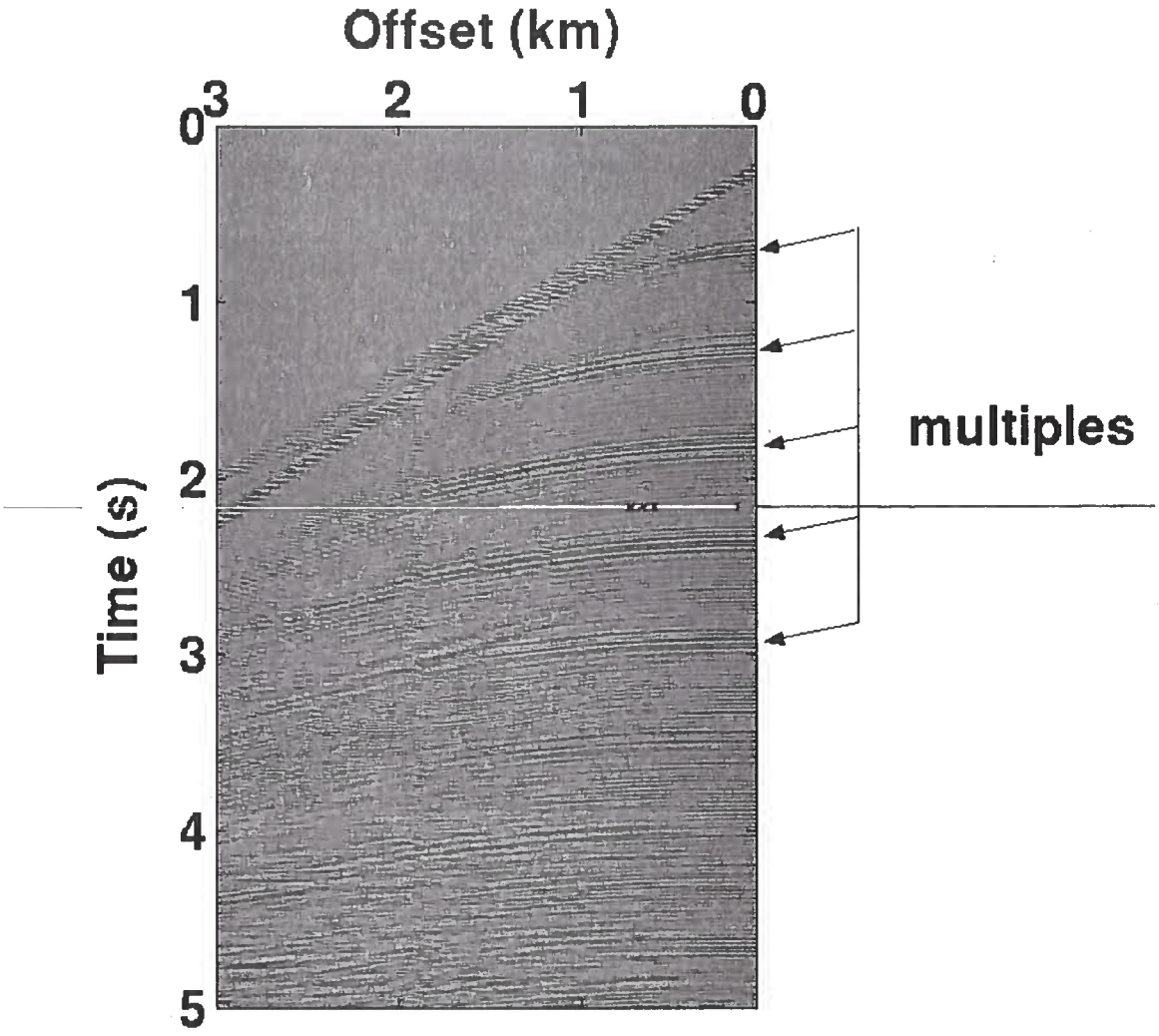

FIG. 5.5. Marine CMP gather with strong water-bottom multiples indicated by the arrows.

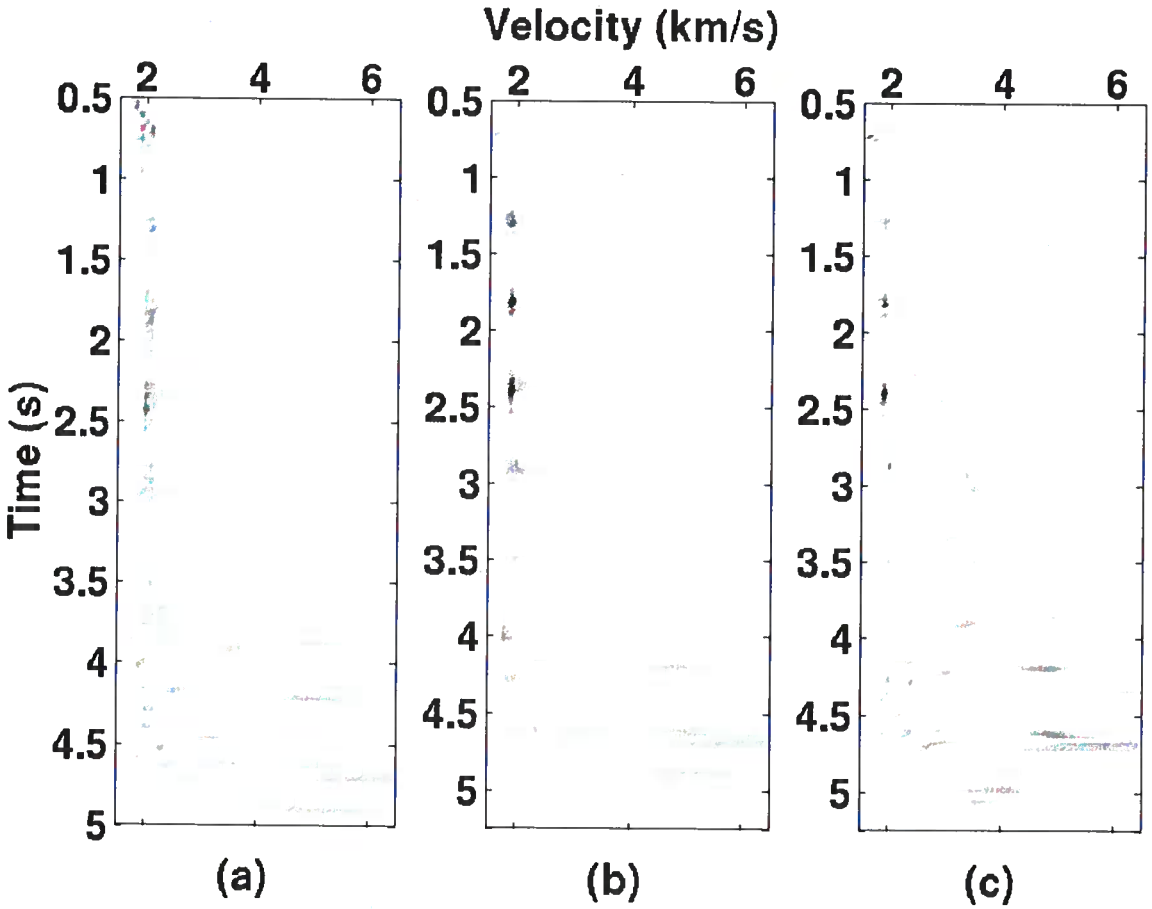

FIG. 5.6. Velocity panels for the CMP gather in Figure 5.5 computed using (a) semblance coefficient, (b) unnormalized crosscorrelation sum, and (c) unnormalized selective-correlation sum (25%).

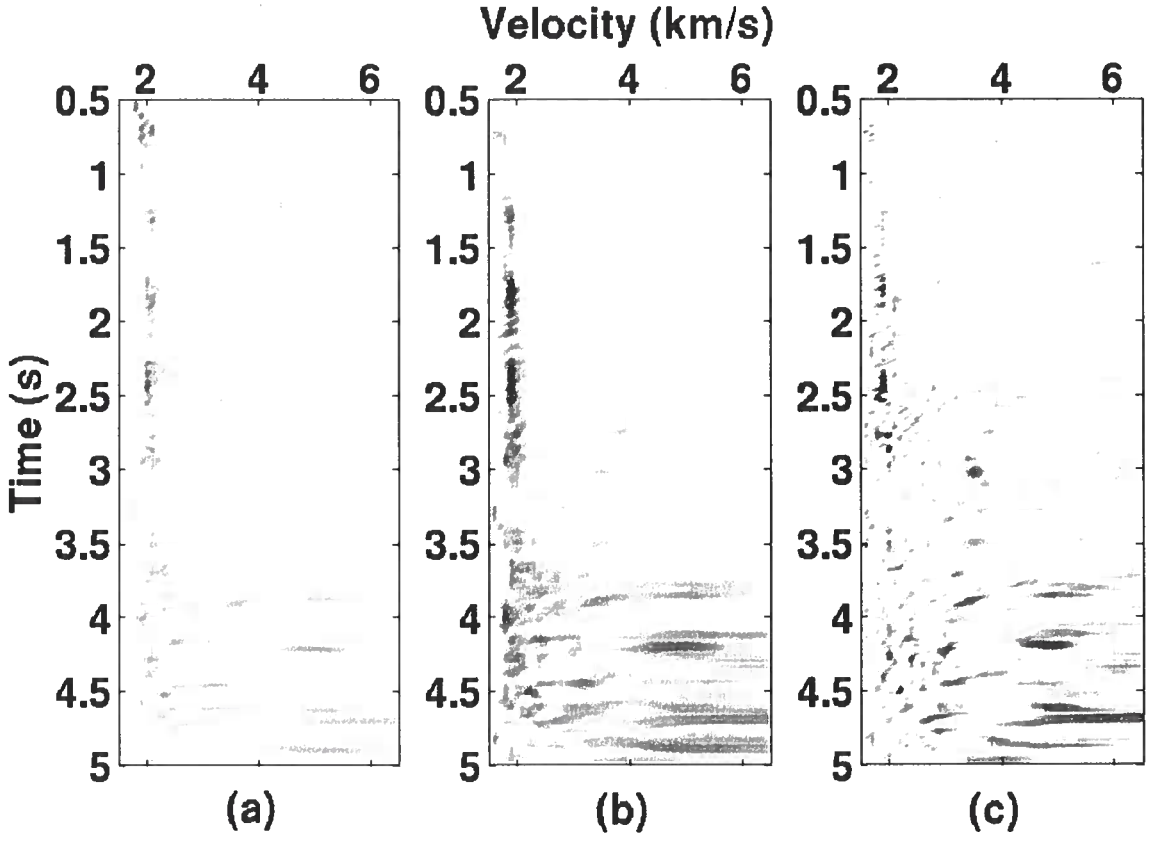

FIG. 5.7. Velocity panels for the CMP gather in Figure 5.1 computed using (a) semblance coefficient, (b) normalized crosscorrelation sum, and (c) normalized selective-correlation sum (25%).

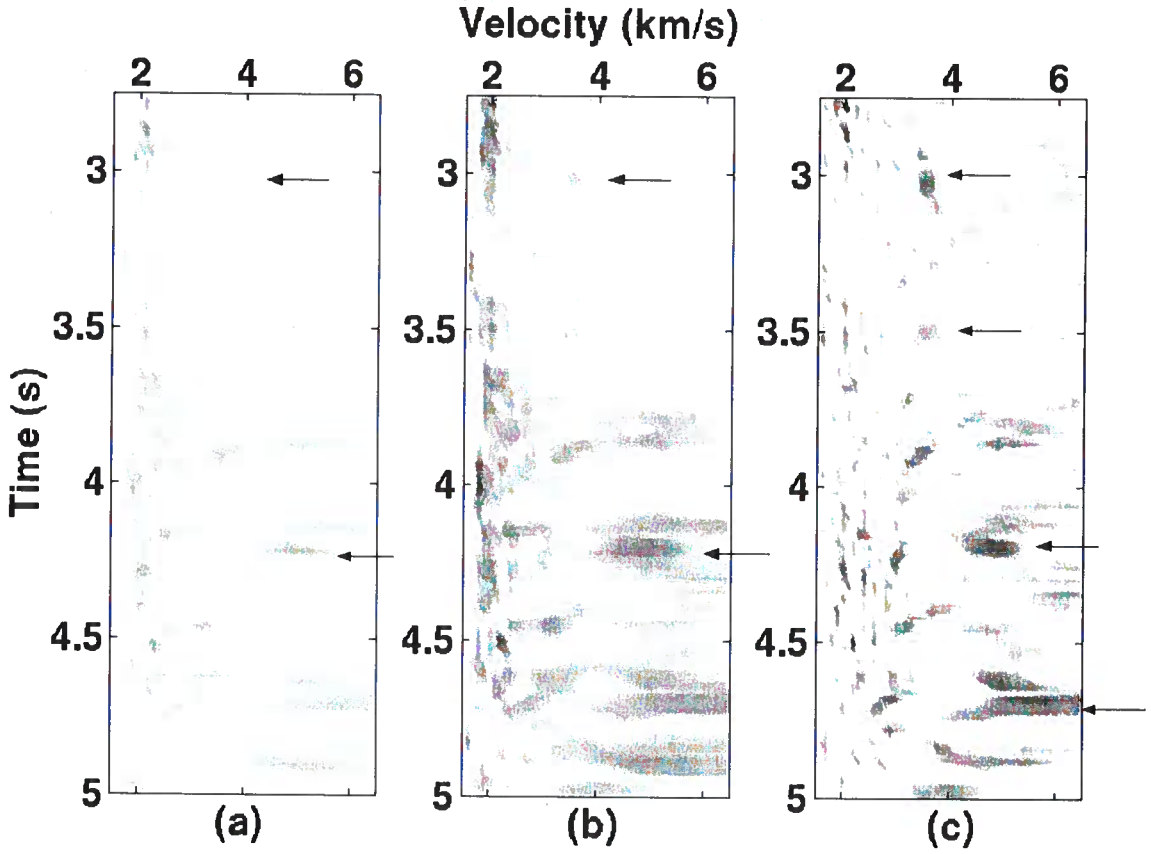

FIG. 5.8. Enlargement of Figure 5.7 showing the higher resolution achieved by selective-correlation sum (25%), in the events marked by arrows, compared to that achieved by the other two methods.

Chapter 6

DISCUSSION AND CONCLUSIONS

6.1 Summary

By including in the sum of crosscorrelations used in velocity analysis only those crosscorrelations with relatively high resolving power, one can increase velocity resolution for data with both isolated and interfering events, including data contaminated with multiple reflections, added Gaussian noise, and static time distortions.

I compared results of the selective-correlation sum method with those of several other methods for computing velocity spectra: conventional crosscorrelation sum, semblance coefficient, and conventional crosscorrelation sum using weights designed for optimum enhancement of primary-to-multiple ratio in CMP stacking. In all tests, for percentages of crosscorrelation 50% or less, selective-correlation sum yielded improved velocity resolution relative to that achieved by the other methods. Selective-correlation sum provides a new parameter – the percentage of crosscorrelations included in the sum – that controls a tradeoff between increasing resolution and effectiveness in attenuating random noise.

Tests on synthetic data show that in the presence of static distortions and additive random noise, selective-correlation velocity analysis has accuracy for estimating the stacking velocity that is comparable to that of conventional crosscorrelation sum. An interesting observation in our tests is that the error that statics time distortions and random noise introduce in picked stacking velocity is quite independent of the percentage used in the selective-correlation method, for percentages from about 20% up to 100%. The peak in velocity spectra for both selective-correlation velocity analysis and conventional velocity analysis is determined largely by crosscorrelations of trace pairs with relative large differential moveout.

The implementation of selective-correlation sum described here entails only a simple modification of conventional velocity analysis and thus achieves its increase in velocity resolution at computational cost that is comparable to that of conventional velocity analysis.

6.2 Discussion

In this thesis, I have addressed the issues of resolution and uncertainty in velocity analysis for data contaminated by additive noise, statics distortions, and interfering events.

The analysis of propagation of errors in Chapter 4 gives support to intuition that selecting crosscorrelation pairs with relatively large differential moveout can improve the accuracy and resolution of velocity analysis. We saw that the magnification of traveltime errors into velocity-estimation errors is least for trace pairs with relatively large differential moveout; also, these trace pairs have the largest influence velocity resolution.

The resolving power of any method for computing velocity spectra is limited by SNR, spreadlength, and frequency content in the data. Conventional methods provide good velocity estimates for CMP gathers with well separated reflections for given values of SNR, spreadlength, and frequency; the only gain in applying selective-correlation sum to such data would be the sharpening of the peaks in the same location already indicated by the conventional methods. The additional benefit of using selective-correlation sum is when applied to CMP gathers containing closely interfering events relative to the dominant period in the data, for which conventional methods generally fail. This is the reason why throughout this thesis I have emphasized study of interfering events, both in tests with synthetic CMP gathers and in the modeling of coherence curves using modeling with Gaussian shapes.

In Chapter 4, I showed that a reasonable approximation of coherence curves for interfering events is a superposition of Gaussians. We saw that the location of the peaks tend to be shifted or biased toward the mean value of the interfering primary and multiple velocities. For given values of stacking velocities, reflector time, spreadlength, and frequency content of the data, the amount of shifting of the primary peak depends on the local slope in the portion of the multiple coherence curve that overlaps the region near the primary peak.

This approximation of superposition of Gaussian curves, however, is no longer applicable to coherence curves generated with selective-correlation sum. The pattern of the curves for isolated events is more complicated than Gaussians since these curves have negative side lobes. Under the assumption that superposition holds, for curves that differ from Gaussian shape these negative side lobes could potentially bias the location of the peaks. Unlike the Gaussians form, however, they can have zero slope at the peak locations, in which case they would reduce the amplitudes of the primary peaks in the presence of strong multiples. Many tests with synthetic model data, however, show that the bias of the peaks is reduced when the selective-correlation sum approach is used for velocity analysis.

For a given CMP gather, the resolving ability of computed velocity spectra can be increased by previously applying to the data processes such as statics corrections, deconvolution, and bandpass filter, which can increase the frequency content in the data. Here, I have assumed identical conditions in the processing of the CMP gathers used for the computation of the velocity spectra in both the conventional and selective approaches. For CMP gathers pre-processed using the same processing sequence, with both synthetic (Chapter 3) and field data (Chapter 5), the selective-correlation sum method succeeded in increasing the resolving power of the velocity spectra and allowing picks that yielded more accurate stacking velocity estimates than those based on picks using a conventional method.

As with many parameters in seismic data processing, the new parameter introduced

in this thesis — percentage of crosscorrelations included in the sum — needs to be chosen. One way would be for the analyst to visually study velocity panels for different values of the parameter taking the trade off between resolution and possible artifacts into account. Fortunately, keeping this parameter within the confortable range 20% — 50% will increase velocity resolution while avoiding undesirable artifacts.

I have demonstrated through field data examples the applicability of the method and also that it can reduce uncertainty in interpreting stacking velocity (specifically, in the marine CMP gather example), not only by increasing the resolution of the velocity spectra but also uncovering primary peaks in the presence of strong multiples.

6.3 Future work

I have tested the method developed here on synthetic and field data under different conditions of random noise, statics distortions, frequency content of the data, and interfering events. Much work remains, however, in the understanding of the behavior of coherence measures, including selective-correlation sum, when, for instance, anisotropy or amplitude variation with offset (AVO) is present in the data. Sarkar et al. (2000) study the sensitivity of semblance coefficient to AVO and compared to that of others coherence measures that account for AVO. Also, Yilmaz (2001) shows, with a simplistic example, that different coherence measures have different sensitivity to AVO. A wider study involving other coherence measures, specially those based on sum of crosscorrelations, would help understanding AVO sensitivity of both unnormalized and normalized selective-correlation sum.

As the spreadlength increases, reflection traveltimes depart from hyperbolic trajectories, degrading rms velocity estimates based on the hyperbolic moveout assumption. Depending on the objective, coherence measures (including selective-correlation sum) are designed to search for coherence along predetermined trajectories that can be linear, parabolic, hyperbolic, or nonhyperbolic, as when the subsurface is anisotropic. Although possibly computationally more costly, an extension of selective-correlation sum that accounts for nonhyperbolic moveout can be achieved just by replacing the hyperbolic trajectory by that of nonhyperbolic moveout. However, the parabolic approximation of differential moveout, presented here, to compute the significance values still can be used on CMP data with nonhyperbolic moveout as long as the traveltimes increase with offset and do not have inflection points, as in turning waves.

One might consider implementing in the selective approach some method for optimizing the choice of the percentage of crosscorrelations included in the sum. For instance, one might minimize the expected mean-squared-error (MSE) in sums of specific combinations of crosscorrelations pairs. The procedure, however it might be done, cannot be based solely on differential moveout of reflections, since as seen in Chapter 4 the MSE (bias squared plus variance) tends to decrease with increasing differential moveout.

Another alternative to the selective method is to generate an optimized set of weights

that multiply each crosscorrelation pair considered in the conventional method. If M is the number of traces in the CMP gather, $M(M-1)/2$ weights need to be produced for each trial velocity and each zero-offset two-way traveltime, with the goal of increasing the resolving power of velocity spectra. Based on ideas presented in this thesis, I infer that these optimized weights will be higher for crosscorrelations pairs with relatively large differential moveout. A major shortcoming of applying weights to each individual crosscorrelation is that the number of operations required will increase from order M achieved in the conventional method (and in the selective method) to order M^2.

In general the basic idea presented in this thesis, that of summing crosscorrelations with the largest resolving power, can be extended to and tested on any process to enhance resolution of a measured parameter that depends on the coherence of signal along a predetermined path in multichannel data. A trivial extension, for example, is to use selective-correlation sum for residual velocity analysis either before or after migration. Another example is in searching for local dip in data.

REFERENCES

Biondi, B. L., and Kostov, C., 1989, High-resolution velocity spectra using eigenstructure methods: Geophysics, **54**, 832-842.

Cohen, J.K. and Stockwell, Jr J. W., 2002, CWP/SU: Seismic Un*x release 35: a free package for seismic research and processing, Center for Wave Phenomena, Colorado School of Mines.

Davidson, A.C., and Hinkley, D.V., 1997, Boothstrap methods and their applications: Cambridge University Press.

De Vries, D., and Berkhout, A. J., 1983, Velocity analysis based on minimum entropy: Geophysics, **49**, 2132-2142.

Garotta, R., and Michon, D., 1967, Continuous analysis of the velocity function and the moveout corrections: Geophys. Prosp., **15**, 584-597.

Gelchinsky, B., Landa, E., and Shtivelman, V., 1985, Algorithms of phase and group correlation: Geophysics, **50**, 596-608.

Key, S. C., Kirlin, L., and Smithson, S. B., 1987, Seismic velocity analysis using maximum-likelihood weighted eigenvalue ratios: 57th Ann. Internat. Mtg., Soc. Expl. Geophys., Expanded Abstracts, 461-464.

Kirling, R. L., Dewey, L. A., and Bradley, J. N, 1984, Optimum seismic velocity estimators: Geophysics, **49**, 1861-1868.

Lord Rayleigh, F.R.S, 1874, On the manufacture and theory of diffraction-gratings: Philosophical Magazine and Journal of Science, Feb. 4th series, V.47, No. 310.

Neidell, N. S., and Taner, M. T., 1971, Semblance and other coherency measures for multichannel data: Geophysics, **36**, 498-509.

Sarkar, D., Baumel, B., and Larner, K., 2002, Velocity analysis in the presence of amplitude variation: Geophysics, in press.

Schoenberger, M., 1996, Optimum weighted stack for multiple suppression: Geophysics, **61**, 891-901.

Sherwood, J. W., and Poe, P. H., 1972, Continuous velocity estimation and seismic wavelet processing: Geophysics, **37**, 769-787.

Taner, M. T., Koehler, F., and Sheriff, R. E., 1979, Complex seismic trace analysis: Geophysics, **44**, 1041-1063.

Taner, M. T., and Koehler, F., 1970, Velocity spectra: digital computer derivation and applications of velocity functions: Geophysics **34**, 859-881.

Toldi, J. L., 1989, Velocity analysis without picking: Geophysics, **54**, 191-199.

Yilmaz, Ö., 2001, Seismic data analysis: V.1, Society of Exploration Geophysicists.

APPENDIX A

A.1 Derivation of index limits for selective-correlation sum

For a CMP gather, I derive here the summation limits, $j_{0\tau}$ and $k_\tau(j)$, for expression (2.3.19) in the selective-correlation sum method. Suppose that τ is the threshold imposed on the significance values such that only trace pairs for which $S_{jk} > \tau$ are used in the summation. Also, consider offset geometry such that shortest offset is a multiple L of the trace increment Δx, so $x_0 = L\Delta x$. Then, $x_{\max}$, x_j, and x_k can be expressed as a function of the number of traces M, the trace indexes j and k, and L, giving

$$\begin{aligned} x_{\max} &= (M+L-1)\Delta x, \\ x_j &= (j+L-1)\Delta x, \\ x_k &= (k+L-1)\Delta x. \end{aligned}$$

Substituting these expressions into expression (2.2.18) gives expressions for the indexes j and k, along the curve $S_{jk} = \tau$, as functions of one another;

$$j = \left\{\tau\left[(M+L-1)^2 - L^2\right] + (k+L-1)^2\right\}^{1/2} - L + 1, \tag{A.1.1}$$

and

$$k = \left\{(j+L-1)^2 - \tau\left[(M+L-1)^2 - L^2\right]\right\}^{1/2} - L + 1. \tag{A.1.2}$$

Based on these expressions, we can determine the range of values of j and k inside the region in bricked pattern in Figure 2.4. The abscissa index j varies between $j_{0\tau}$ and M, where $j_{0\tau}$ is just expression (A.1.1) evaluated at $k = 1$ plus unity,

$$j_{0\tau} = \left\{\tau\left[(M+L-1)^2 - L^2\right] + L^2\right\}^{1/2} - L + 2, \tag{A.1.3}$$

and the ordinate index k, which depends on the index j, varies from 1 to $k_\tau(j)$ minus unity, giving

$$k_\tau(j) = \left\{(j+L-1)^2 - \tau\left[(M+L-1)^2 - L^2\right]\right\}^{1/2} - L. \tag{A.1.4}$$

Then, the selective-correlation sum CC_{sc}, is given by

$$CC_{sc}(v_{trial}, t_0) = \sum_{j=j_{0\tau}}^{M} \sum_{k=1}^{k_\tau(j)} \sum_{w} f_{j,t(j)}\ f_{k,t(k)}. \tag{A.1.5}$$